SEDIMENTOLOGY AND DEPOSITIONAL HISTORY OF THE MIOCENE – PLIOCENE SOUTHERN BOUSE FORMATION, ARIZONA AND CALIFORNIA

by

BRENNAN O'CONNELL

A THESIS

Presented to the Department of Earth Sciences
and the Graduate School of the University of Oregon
in partial fulfillment of the requirements
for the degree of
Master of Science

December 2016

THESIS APPROVAL PAGE

Student: Brennan O'Connell

Title: Sedimentology and Depositional History of the Miocene–Pliocene Southern Bouse Formation, Arizona and California

This thesis has been accepted and approved in partial fulfillment of the requirements for the Master Science degree in the Department of Earth Sciences by:

Dr. Rebecca J. Dorsey	Chairperson
Dr. Eugene D. Humphreys	Member
Dr. James Watkins	Member

and

Scott L. Pratt	Dean of the Graduate School

Original approval signatures are on file with the University of Oregon Graduate School.

Degree awarded December 2016

THESIS ABSTRACT

Brennan O'Connell

Master of Science

Department of Earth Sciences

December 2016

Title: Sedimentology and Depositional History of the Miocene–Pliocene Southern Bouse Formation, Arizona and California

The Miocene to Pliocene southern Bouse Formation preserves a record of depositional environments immediately prior to and during integration of the Colorado River to the Gulf of California. Uncertainty over Bouse paleoenvironments obscures our understanding of the timing and magnitude of regional uplift, as well as the conditions and processes that were active during integration and early evolution of the Colorado River. Prior studies over the past 20 years have concluded that the southern Bouse Formation accumulated in chain of lakes isolated from the ocean. Sedimentologic analyses presented here aid interpretation of depositional environments and provide evidence for a strong tidal influence on deposition, consistent with a marine interpretation of other prior studies. This interpretation places a critical constrain on the elevation of these deposits at ca. 5 Ma, and suggests post-Miocene uplift of the Lower Colorado River corridor.

This thesis includes previously published coauthored material.

CURRICULUM VITAE

NAME OF AUTHOR: Brennan O'Connell

GRADUATE AND UNDERGRADUATE SCHOOLS ATTENDED:

University of Oregon, Eugene, Oregon
Colorado College, Colorado Springs, Colorado

DEGREES AWARDED:

Master of Science, Geological Sciences, 2016, University of Oregon
Bachelor of Arts, Geology, 2013, Colorado College

AREAS OF SPECIAL INTEREST:

Sedimentology
Geologic mapping
Sedimentary geochemistry
Desert Tortoises
Tides

PROFESSIONAL EXPERIENCE:

Graduate Teaching Fellow, University of Oregon, 2014 to present

Exploration Geologist, Cripple Creek and Victor Gold Mine, AngloGold Ashanti, 2013

Exploration Geologist Intern, Cripple Creek and Victor Gold Mine, AngloGold Ashanti, 2012

Geologic Field Mapping Assistant, AngloGold Ashanti, 2011

GRANTS, AWARDS, AND HONORS:

Research Recognition Award, University of Oregon, 2016

Graduate Student Research Grant, Geological Society of America, 2015

Student Research Grant, Society of Sedimentary Geology, 2015

Donald B. Gould Scholarship Award in Geology, Colorado College, 2013

Darrel M. Putman Scholarship Award in Geology, Colorado College, 2013

PUBLICATIONS:

O'Connell, B., Dorsey, R.J., Humphreys, E.D., Tidal Rhythmites in the Southern Bouse Formation as Evidence for Post-Miocene Uplift of the Lower Colorado River Corridor: In press, *Geology*

Gootee, B.F., Pearthree, P.A., House, P.K., Youberg, A., Spencer, J.E., and **O'Connell, B.,** 2016, Geologic Map of the Cibola 7 ½ Quadrangle and the northwestern part of Cibola SE 7½ Quadrangle, LA Paz County, Arizona, and Imperial County, California. Arizona Geological Survey Digital Map DGM117, Scale 1:24000, with text

ACKNOWLEDGEMENTS

I wish to express sincere appreciation to my advisor Becky Dorsey for providing necessary funding and for making numerous and detailed reviews of my work throughout my M.S. I've never met a more enthusiastic human. Her guidance, excellence, patience, and genuine care was instrumental to my success in this program, for which I am grateful. I thank my committee members Gene Humphreys for his contribution to my *Geology* paper, and Jim Watkins for teaching me how to code in Matlab.

I would like to express thanks to my wonderful field assistants Logan Wetherell, Avery Maverick, and Jordan Lanni. True American heroes. Special thanks to Kristin Franks who shared a particularly hideous experience with me stuck in sand in Milpitas Wash. Thanks to Border Patrol and Ramsey Towing for pulling us out of the sand while laughing the whole time because they were expecting El Chapo, and instead found two crusty stranded geologists.

I thank financial support from the University of Oregon Department of Earth Sciences, National Science Foundation, Society of Sedimentary Geology, and Geological Society of America.

I gratefully acknowledge the following people for support and friendship; Stephen Meigher; Devon Cole for sharing graduate school, geology, and weightlifting successes and (more often) fails, and all the plundered treasures of the internet; Anna Moore, Angie Seligman, Ellen Aster, Randy Krogstad, and Kayak for great times at the Riverview House; my wonderful Slytherin Dungeon officemates David Zakharov, Marisa Acosta, and Genevieve Perdue.

I thank my weightlifting team for providing a non-academic support system and friend group, especially Mary Pond for pre-training bakery runs and for visiting me in the desert and Delina Whidden for training carpools full of giggles and snacks (snakes). I sincerely thank my weightlifting coach Tom Hirtz for getting me involved with the Heavy Athletics program at the jail, and for teaching me about the mental aspects of sport and life. You have had a profound impact on my life.

Most importantly, I am particularly grateful for the love and support of my family.

TABLE OF CONTENTS

Chapter Page

LIST OF FIGURES

CHAPTER I

INTRODUCTION

The upper Miocene to lower Pliocene Bouse Formation, exposed discontinuously along the lower Colorado River corridor in California and Arizona, preserves a record of depositional environments that existed in the Colorado River valley south of Blythe, CA, immediately prior to and during the integration of the Colorado River to the Gulf of California. This study is focused on the basal carbonate member of the southern Bouse Formation southeast of Cibola, AZ, which provides insights into conditions that existed prior to integration of the Colorado River system.

Paleoenvironments recorded in the Bouse basal carbonate member are widely debated because of conflicting data and incompatible models. Specifically, the southern Bouse has been interpreted to record deposition in either (1) a marine-embayment at the north end of the Gulf of California oblique-rift basin; or (2) a large inland lake with no connection to the ocean. An understanding of depositional environments is important for constraining the timing and magnitude of uplift along the lower Colorado River corridor, as well as understanding the conditions and processes that were active during integration of the Colorado River to the Gulf of California. If the Bouse accumulated at sea-level, it would suggest ~330 m of post-Miocene uplift, whereas deposition in a lake isolated from the ocean would place no constraint on uplift of the region.

In this thesis I present new sedimentologic and quantitative data from the basal carbonate member of the southern Bouse Formation, and use the data to interpret depositional processes and paleoenvironments of this unit. I then discuss the tectonic

implications of these results. Specifically, in Chapter II, I integrate process-based sedimentology and fast Fourier transform (FFT) analysis of rhythmite layers to infer a tidal origin for the Bouse basal carbonate member. In Chapter III I explore the process sedimentology of these deposits in more detail to reconstruct the depositional paleoenvironments and basin hydrodynamics, and propose facies models based on comparison to published studies of similar mixed-carbonate siliciclastic tidalites.

This thesis is primarily a field-based study, with particular emphasis on detailed description and interpretation of lithofacies exposed in outcrops. Fieldwork was carried out during two winters (January-February) in 2015 and 2016. Stratigraphic sections were measured at outcrops in the Trigo Mountains, Palo Verde Mountains, and Milpitas Wish areas in California and Arizona. This study is focused on outcrops west of the Trigo Mountains, southeast of Cibola, AZ, where thick relatively continuous exposures are readily accessible. Chapter II is presented in manuscript form for the journal *Geology,* and is co-authored with Dr. Rebecca Dorsey and Dr. Eugene Humphreys. Chapter III is presented as an extended abstract.

CHAPTER II

TIDAL RHYTHMITES IN THE SOUTHERN BOUSE FORMATION AS EVIDENCE FOR POST-MIOCENE UPLIFT OF THE LOWER COLORADO RIVER CORRIDOR

From O'Connell, B., Dorsey, R.J., Humphreys, E.D., Tidal Rhythmites in the Southern Bouse Formation as Evidence for Post-Miocene Uplift of the Lower Colorado River Corridor: *Geology*, 2017

INTRODUCTION

Our understanding of the conditions and processes that were active during integration and early evolution of the Colorado River, as well as models for post-Miocene tectonic uplift of the western Colorado Plateau region (western United States), depend on interpretation of depositional environments of the uppermost Miocene to lower Pliocene Bouse Formation (Fig. 1.1). The southern Bouse Formation is interpreted to have formed in either a marginal-marine setting at the north end of the late Miocene Gulf of California oblique rift, as suggested by marine and brackish-water fossils and sedimentary structures (Buising, 1990; Turak, 2000; McDougall, 2008; McDougall and Martínez, 2014), or a large inland lake isolated from the ocean, as suggested by Sr isotopes, stable isotopes, and elevation data (Spencer and Patchett, 1997; House et al., 2008; Spencer, et al., 2008, 2013; Bright et al., 2016). The isolated-lake hypothesis explains the presence of marine fossils by introduction of marine organisms by birds.

Although Sr isotopes have been used to suggest a lacustrine origin for the Bouse Formation, a recent modeling study shows that the observed Sr-isotope values could have resulted from mixing of marine-water, freshwater, and radiogenic spring-water components (Crossey et al., 2015). Thus Sr values slightly more radiogenic than seawater do not preclude a marine influence. Deposition of the southern Bouse Formation at sea

level would require ca. 330 m of post-depositional tectonic uplift in the western Colorado Plateau region to explain the modern elevations of known outcrops, whereas accumulation in an isolated lake would place no constraint on post-Miocene uplift.

In this paper we present new sedimentologic and layer-thickness data to interpret the depositional paleoenvironment of the southern Bouse Formation. We focus on the basal carbonate member of the Bouse Formation exposed south of Blythe, CA (Fig. 1), a mixed carbonate-siliciclastic unit that rests on Miocene conglomerate and volcanic rocks (Fig. 2A). Sedimentary lithofacies and quantitative analysis presented below provide new evidence for deposition under the influence of tidal currents, consistent with a well-documented marine to brackish-water fauna in the southern Bouse Formation.

RESULTS

Sedimentary Lithofacies

The basal carbonate member of the southern Bouse Formation includes: matted silty lime mudstone with reed and grass imprints; heterolithic facies comprising wackestone, grainstone, and bioturbated lime mudstone with horizontal, flaser, wavy, and lenticular bedding; and crossbedded barnacle-oncoid grainstone. These lithofacies contain sedimentary structures that are commonly attributed to a tidal origin, including (Fig. 2): (1) well-sorted and segregated carbonate-siliciclastic couplets that display systematic alternation of thin and thick mm- to cm-scale layers; (2) distinctive sigmoidal bundles; (3) crossbed foresets that pass laterally into stacked wavy, lenticular, and flaser heterolithic bedding; (4) lateral variations in thickness of crossbed and sigmoidal bundle foresets and bottomsets; (5) common reactivation surfaces; (6) cross-lamination that records reversing currents and migration of ripples up meter-scale foresets; (7)

Thalassinoides burrows; and (8) bimodal-bipolar crossbedding (e.g., Nio and Yang, 1991; Longhitano, 2012; Davis, 2012). Lime mud is a common component of these deposits, and is ubiquitous in other carbonate depositional systems.

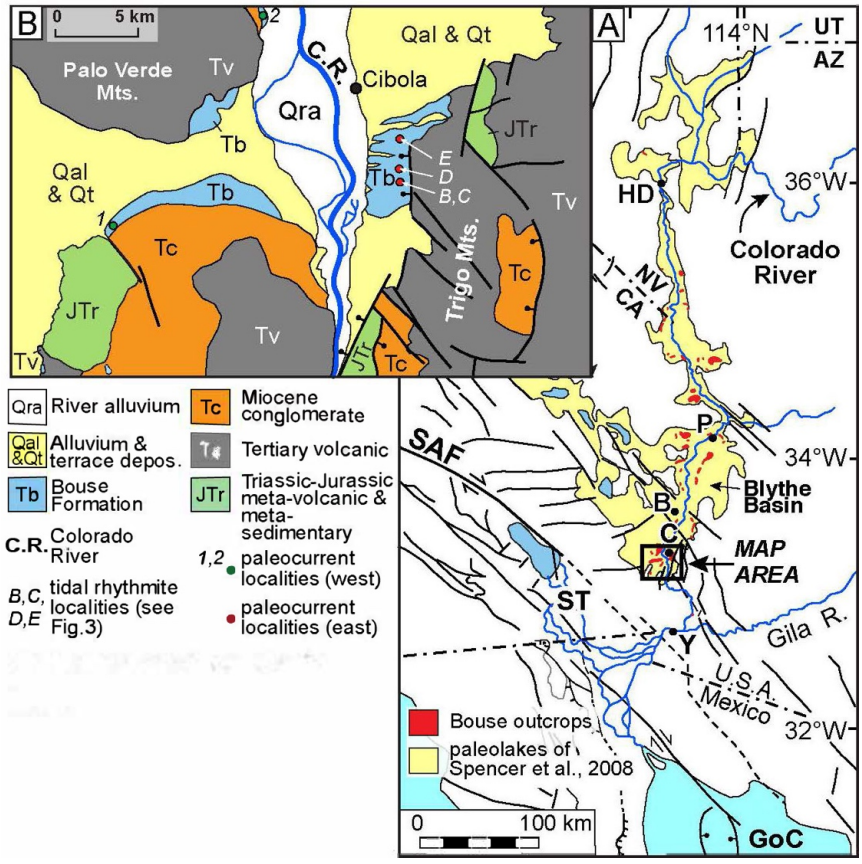

Figure 1 A: Map of lower Colorado River (western USA) regional major faults, exposures of Bouse Formation (red), and Bouse paleolakes of Spencer et al. (2008) (yellow). State abbreviations: AZ—Arizona; CA—California; NV—Nevada; UT—Utah. Other abbreviations: B—Blythe; C—Cibola; GoC—Gulf of California; HD—Hoover Dam; P—Parker; SAF—San Andreas fault; ST—Salton Trough; Y—Yuma. B: Simplified geologic map of study area, compiled from Sherrod and Tosdal (1991). depos.—deposits.

Lateral and vertical transitions and complex interbedding geometries are abundant in the southern Bouse basal carbonate. For example, foreset strata of crossbedded barnacle-oncoid grainstone pass laterally into flat-lying bottomsets of well-sorted sandy grainstone with small-scale bidirectional ripples, reactivation surfaces, and lime mud drapes, which pass laterally into stacked flaser, wavy, and lenticular bedding of the heterolithic facies association.

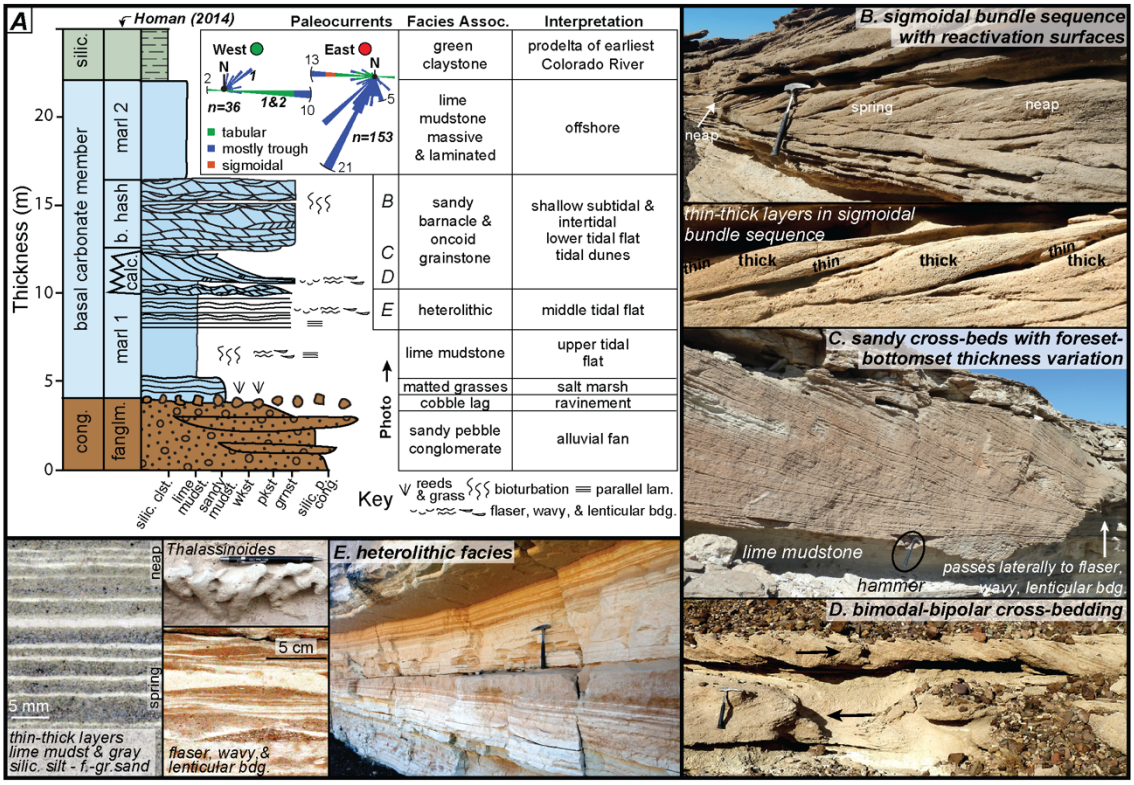

Figure 2. A. Representative stratigraphy of the southern Bouse Formation (western USA) after Homan (2014), sedimentary lithofacies examined in this study, and environmental interpretations. Paleocurrent locations in Fig. 1B. B. Sigmoidal bundle sequence with reactivation surfaces and thin-thick couplets. C. Crossbedded grainstone passing laterally into flat bottomsets to flaser, wavy, and lenticular bedding. D. Bimodal-bipolar cross-bedding in bioclastic grainstone. E. Heterolithic facies with Thalassinoides burrows, horizontal couplets, and flaser, wavy, and lenticular bedding. Hammer is 32.5 cm and pencil is 13 cm. AbbreviationsAbbreviations: silic.—siliciclastic; clst.—claystone; mudst.—mudstone; wkst.—wackestone; pkst.—packstone; grnst.—grainstone; p. cong.—pebble conglomerate; b. hash—barnacle hash; calc.— calcarenite; fanglm.—fanglomerate; bdg.—bedding; lam.—lamination; f.-gr.—fine-grained.

Layer-Thickness Analysis

Layer-thickness and Fourier analyses of rhythmites are used extensively to test for and establish a tidal influence on sedimentation (e.g., Kvale et al., 1999; Williams, 1989; Hovikoski et al., 2005). The most distinctive sequences form in mixed diurnal and semidiurnal tidal systems where the semidiurnal signal is relatively strong (De Boer et al., 1989; Williams, 2000). This type of tidal environment creates systematic alternation of thick and thin layers where each couplet is deposited in one tidal cycle. Preservation of daily couplets is enhanced by hydraulic sorting and segregation in mixed bioclastic-siliciclastic tidal systems (Longhitano, 2011). Where a layering sequence is nearly complete, Fourier analysis reveals daily to monthly cyclicity. Rhythmite sequences commonly are incomplete due to the influence of non-tidal processes such as storms, waves, and partial submergence or emergence of tidal flats (e.g., Kvale et al., 1995). Deposition of tidal rhythmites typically is dominated by short-term very fast accumulation rates.

Data for modern tides from the northern Gulf of California express a semi-diurnal oscillation superposed on the monthly spring-neap tidal cycle (Fig. 3A), and are used for comparison to the southern Bouse Formation rhythmite layers. Bouse rhythmites analyzed for this study include laminae, thin beds, and thin-thick couplets in horizontal layers, sigmoidal bundles, and crossbed foresets. Fourier transformed layer-thickness series show well-defined peaks at 0.96 and 1.91 cycles/couplet (Fig. 3B), similar to the Fourier components of modern tides in the northern Gulf of California which display weighted-average diurnal and semidiurnal frequencies at 0.92 and 1.92 cycles/day (Fig. 3A). This bimodal signal is characteristic of a dominantly semidiurnal mixed-tidal marine

setting (De Boer et al., 1989; Archer and Johnson, 1997; Williams, 2000). Apparent neap-spring long-wavelength tidal cyclicity is present in thickness series of horizontal rhythmites, crossbed foresets, and sigmoidal bundle sequences with prominent fast Fourier transform (FFT) peaks at periods of 4–10 couplets/cycle (8–20 layers/cycle) (Figs. 3C, 3D, 3E), as is commonly seen in tidal flat sequences (Kvale et al., 1995). We interpret segregation of siliciclastic and bioclastic sediment to record hydraulic sorting due to regular changes in tidal current energy and contrasting entrainment potential of the two grain types (e.g., Longhitano, 2011).

DISCUSSION AND CONCLUSIONS

We find that the basal carbonate member of the southern Bouse Formation was deposited in a tide-dominated marginal-marine setting based on: (1) Fourier analysis of rhythmite successions that record daily and neap-spring tidal cyclicity; (2) remarkable continuity, sorting, and lithological segregation of thin-thick couplets; (3) distinctive sigmoidal bundle sequences and non-random tidal bundling; and (4) abundance and variety of tidal sedimentary structures, lateral relationships, and vertically stacked tidal facies assemblages (e.g., Dalrymple, 2010). Our data and interpretation are in agreement with a moderately diverse marine to brackish-water faunal assemblage documented from south of Blythe, CA, to Parker, AZ (Fig. 1; McDougall, 2008; McDougall and Martínez, 2014). Collectively, these new observations and existing paleontology are best explained by deposition in a marine tidal environment.

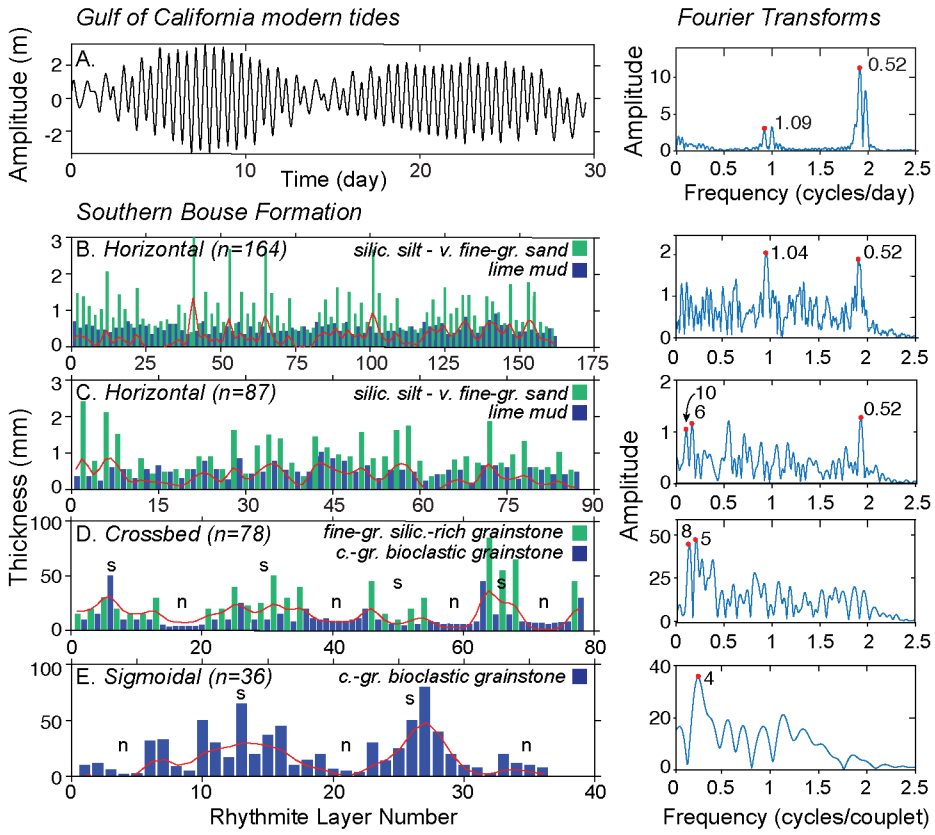

Figure 3. (A). One month (March, 1993) of modern tide record at San Felipe, northern Gulf of California (http://sanfelipe.com.mx/weather/tide-calendars), and its fast Fourier transform (FFT). Note the strong semidiurnal signal with two cycles per day, and the longer-wavelength oscillating constructive-destructive interference between the solar and lunar tides. B–E: Layer-thickness data and FFTs for southern Bouse Formation rhythmites. Red curve superimposed on rhythmite data indicates a five-point moving average (1, 4, 6, 4, 1). Red dots corresponding numbers indicate period (couplets per cycle). (B). Horizontal lamina with clear thin-thick alternations of lime mudstone (blue) and siliciclastic (silic.) silt – to v.f.-gr. sand (green). The FFT has strong peaks at frequencies of 0.96 and 1.91 cycles/couplet. (C). Another example with strong peak at 1.92 cycles/couplet. Neap-spring cyclity is inferred from low-frequency peaks with periods (inverse of frequency) at 10 and 6 couplets/cycles (D). Cross-bedded grainstone showing a strong alternation sequence during inferred spring tides (s) but no alternation during inferred neap tides (n) with strong peaks at a period of 8 and 5 couplets/cycle (c.-gr.)—coarse-grained.. (E). Sigmoidal rhythmites with a peak at 4 couplets/cycle. Abbreviations: n, neap; s, spring. See Appendix A for rationale, FFT methods, and Matlab code.

Long series of thin-thick layer alternations (Fig. 3B–D), and apparent neap-spring cyclicity in heterolithic and grainstone facies (Figs. 3C-E), are predicted for a mixed-tidal marine setting and are inconsistent with deposition in an isolated lake. While some of the observed sedimentary structures are found infrequently in non-tidal environments, deposition in a lake would produce non-cyclic layering due to random variations in flow velocity and direction (Ainsworth et al., 2012). The cyclic periodic thickness variations and regular lithologic alternations in the southern Bouse Formation are not formed by non-tidal processes such as tributary river floods, storms, wind-generated lake currents, or biochemical varve deposition (Ainsworth et al., 2012; Dalrymple and Choi, 2007; De Boer et al., 1989). Tidal sedimentary structures are generally preserved only in macrotidal, mesotidal, or highly microtidal settings with a strong asymmetry between daily high and low tides (Archer, 1998). Proposed modern analogues for the Bouse isolated-lake model, such as the Great Lakes, Black Sea, and Caspian Sea, are essentially non-tidal (Eisma et al., 1998; Fraser et al., 1991) and could not produce the rich assortment of tidal facies with cyclicity documented in this study. These results show that the southern Bouse Formation accumulated in a marine embayment at the north end of the Gulf of California with a mixed tidal regime similar to that of the modern Gulf of California. Consistent basinward dips of foreset strata (Fig. 2A) indicate that bedform migration and deposition were dominated by ebb-tide currents.

During the past ~20 years, radiogenic (Sr; e.g., Spencer & Patchett, 1997) and stable isotopes (C, O; e.g., Bright et al., 2016) have played a major role in interpretation of the Bouse Formation. Importantly, however, these data sets could be influenced by mixing of river and marine waters with radiogenic spring waters (Crossey et al., 2015), or

by post-depositional alteration resulting in open-system isotopic behavior (Crow et al., 2016). This concern is particularly relevant for carbonate material where poorly buffered trace metal systems such as Sr are commonly altered by diagenesis and other post-depositional influences (e.g., Brand and Veizer, 1980). These complexities require an integrated petrographic-geochemical approach and careful sample screening for trace metal-based carbonate geochemistry (Hood et al., 2016). Process sedimentology and the quantitative analyses presented here provide unique insights into physical processes that are not subject to the concerns and ambiguities of potential post-depositional alteration.

Our conclusion of a tide-influenced marine setting for the southern Bouse Formation supports significant post-Miocene uplift in the western Colorado Plateau region (e.g., Karlstrom et al., 2012; Crow et al., 2014), and suggests activity of young (post-subduction) crustal and upper-mantle deformation processes that remain incompletely understood.

CHAPTER III

AN ANCENT MIXED CARBONATE-SILICICLASTIC TIDAL ENVIRONMENT FOR THE CA. 5.0-MA SOUTHERN BOUSE FORMATION

INTRODUCTION

Tidalites

Tidalites are deposits of tide-influenced carbonate, siliciclastic, and mixed carbonate-siliciclastic settings that are characterized by distinctive sedimentary textures, structures, lithologies, and lateral and vertical facies variations that reflect deposition in supratidal, intertidal, and shallow subtidal environments (e.g. Klein 1971, 1998). Tides are effective agents of sediment transport, sorting, and deposition. Their effectiveness and resulting sedimentary deposits are directly related to tidal range and resulting tidal current velocity (FitzGerald and Nummedal, 1983; Boothroyd, 1985; Williams, 2000). Tidal successions can be deposited and preserved as horizontally laminated (vertically accreted) rhythmites (e.g., Williams, 1989, 2000; Dalyrmple et al., 1991; Chan et al., 1994; Tessier et al., 1995; Mueller et al., 2002), laterally accreted foresets (e.g., Visser, 1980; De Boer et al., 1989; Deynoux et al., 1993; Bose et al., 1997; Eriksson and Simpson, 2000, 2004; Mueller et al., 2002; Tape et al., 2003; Mazumder, 2004; Longhitano, 2011), or laterally accreted sigmoidal bundles (e.g., Kreisa and Moila, 1986).

A diverse array of tidal sedimentary environments are recognized in the literature and range from the upper reaches of tidal marshes and inlets in river deltas, to upper and lower tidal flats, intertidal channel complexes, and subtidal continental shelves. The shelf/platform marine environment is one of the most complex settings because of the

many complicated interactions among currents produced by tides, waves, storms, salinity variations, platform currents, sediment input, and biogeneic activity.

Mixed Carbonate-Siliciclastic Tidal Environments

Our present understanding of hydrodynamic influences on mixed carbonate–siliciclastic (also known as "silici-bioclastic") sedimentation in tidal environments is still in a formative stage and requires more detailed observations. Indeed, facies models in mixed carbonate–siliciclastic systems have received little attention in comparison to their siliclastic and carbonate counterparts. Few examples of modern mixed tidal flats and mixed tide-influenced lagoons are documented (e.g. Larsonneur, 1975, and Flemming, 1976), and much recent work has been focused on the mixed silici-biolclastic deposits of the Pliocene–Pleistocene tidal bay-fill successions and ancient tectonically confined straights of the Southern Italy (e.g. Di Stefano and Longhitano, 2009; Longhitano, 2011; Chiarella and Longhitano, 2012). In siliciclastic tidal systems, grain size depends on distance to the source area, and lithofacies zonations are dependent on hydrodynamic energy (Eisma et al., 1998). In carbonate tidal systems, conversely, biogenic and in-situ production of carbonate material controls grain-size and facies zonations in addition to the hydrodynamic regime (Eisma et al., 1998).

Once in the basin, in-situ carbonate and extra-basinal siliciclastic components are subject to the same hydrodynamic forces, but they behave differently because their response to changes in hydrodynamic forcing is affected by differences in relative density and shape (e.g. Prager et al., 1996). Because tidal environments record perhaps the shortest cyclicity recognizable in the rock record, careful sedimentologic study of mixed

carbonate–siliciclastic deposits can improve our understanding of short-term processes that control tidal sedimentation.

Tidal Amplification

The strength of tidal currents in coastal embayments can be amplified considerably when the length and depth of the bay produces local amplification of the tidal wave (Pugh, 1987). High tidal ranges are produced by embayment funneling effects, in particular when the tides and the shape of the basin produce a resonance effect (e.g., Bay of Fundy; Dalrymple et al., 1990). Tidal waves may be subject to hydraulic amplification by entering into resonance with the basin or reduction of the hydraulic cross section along shallow coastal shelves, where long-wavelength tidal waves become modified in shallow marine areas due to tide-bottom interactions (Pugh, 1978; Dalrymple, et al., 1990; Stanzo and De Boer, 1995). Resonance occurs when the amount of time it takes a tidal wave to travel from the mouth of a bay to the far shore and back is about the same as the time difference between high and low tides. During this process the tidal waves become synchronized in time, which in turn amplifies the tidal effect.

'Tidal amplification window' refers to the ideal basin conditions that produce resonance or amphidromic amplification of tidal currents (Stanzo and De Boer, 1995). Amplification occurs in settings with ideal basin length:depth or width:depth ratio of the tidal embayment relative to the wavelength of the astronomical tide. Resonant amplification occurs when the length of the bay (*l)* is close to the odd multiples of the

quarter of the tidal wavelength (L), and n=0, 1, 2, 3, … etc. (Pugh, 1987):

$$l=2n+1*L/4 \quad \textit{(Equation 1)}$$

Amplification will be favorable when, for example, l=L/4, l=3L/4, or l=5L/4. The tidal wavelength (L) can be determined if average water depth *(d)* is known, where T is the period of the tide (44712 seconds), and g is gravitational acceleration (9.8 m/s^2).

$$L=T(g*d)^{1/2} \quad \textit{(Equation 2)}$$

Thus, for a 100 km long basin, water depth would have to be ~10 m to fall within the local tidal-amplification window. Importantly, tectonically controlled changes in basin dimensions can often result in a stage of basin evolution that passes through a tidal-amplification window. As such, careful sedimentological and stratigraphic study of ancient marine deposits may reveal transitions in basin bathymetry and resulting hydrodynamics (e.g. Longhitano, 2014; Anastas et al., 1997, 2006).

Our facies analysis of the southern Bouse basal carbonate member suggests that distinctive tidal facies accumulated in a tide-dominated marine embayment during a major transgression and rise in relative sea level. An increase of water depth in the embayment may have altered the tidal flow regime as the basin passed through and then out of the tidal-amplification window. Because this single transgression appears to have occurred during several cycles of glacial-interglacial eustatic change (e.g., Raymo et al.,

2009), we infer that the rise in relative sea level was controlled primarily by a period of accelerated subsidence in the basin.

Consequently, the base of the southern Bouse basal carbonate member is dominated by tidal facies that we interpret to record relatively rapid deposition when the basin was within a tidal-amplification window. These tidal deposits are abruptly overlain by open-platform lime mudstone that lacks a tidal signature, which we interpret to record relatively slow deposition below wave base as water depth increased. This shift could record the basin to passing out of the tidal-amplification window, a drowning of a carbonate platform, or rapid shift to low-energy environment such as a lagoon. The detailed facies analysis and reconstruction below are thus useful for understanding the upper Miocene to lower Pliocene depositional history and regional basin dynamics recorded in the southern Bouse Formation. In addition, this analysis provides a case study that will be useful for comparison to other mixed carbonate–siliciclastic tide-dominated depositional systems.

REGIONAL GEOLOGIC SETTING

The Bouse Formation is exposed along the lower Colorado River corridor of the southwestern United States, spanning a long reach of the river from the Lake Mead region down the Arizona and California border to Yuma, Arizona (Fig. 4). Tertiary sedimentary basins of the lower Colorado River corridor region were formed first by early to middle Miocene regional extension and detachment faulting, and later by transtensional deformation and wrench tectonic and strike-slip faulting in the dextral Eastern California Shear Zone (ECSZ) that started in late Miocene time and continues to

the present day (see summary below). The southern Bouse Formation is exposed in the Blythe Basin south of Parker, Arizona, and – in our preferred interpretation – represents the northernmost exposure of the ancient ~5-6 Ma Gulf of California marine embayment (McDougall, 2008; McDougall and Martínez, 2014; O'Connell et al., 2016).

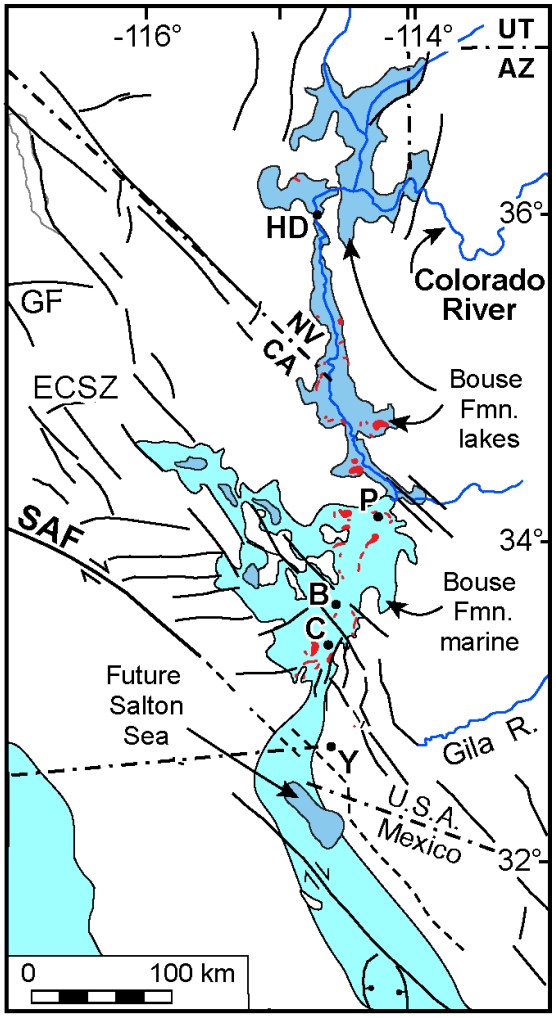

Figure 4: Map reconstruction of the Ancient Gulf of California at ~6 Ma. State abbreviations: AZ—Arizona; CA—California; NV—Nevada; UT—Utah. Other abbreviations: B—Blythe; C—Cibola; HD—Hoover Dam; P—Parker; SAF—San Andreas fault; ST—Salton Trough; Y—Yuma.

Located east of the San Andreas Fault, the eastern California shear zone (ECSZ) is a broad zone of dextral faults and related block rotations that cuts across the Lower Colorado River corridor (Fig. 2.1). From ~24 to 18.5 Ma (early Miocene), the ECSZ and lower Colorado River corridor region underwent regional extension, detachment faulting, exhumation of crystalline basement rocks, and widespread basin formation and filling that ended around 12-14 Ma (Davis and Lister, 1988; Spencer and Reynolds, 1989; Nielson and Beratan, 1990; Dorsey and Becker, 1995; Glazner et al., 2002). The low-angle detachment faults are cut and offset by a network of late Miocene (ca. 12-6 Ma) high-angle strike-slip and normal faults including the Laguna Fault system (Bartley and Glazner, 1991; Sherrod and Tosdal, 1991; Richard, 1993; Howard and Miller, 1992; Jachens and Howard, 1992; Glazner et al., 2002; Shelef and Oskin, 2010; Ricketts et al., 2011). Our recent work shows that this dextral-transtensional fault system was at least locally active during deposition of the southern Bouse Formation, and may have exerted a major control on syn-Bouse subsidence rates, transgression, and relative sea-level rise (O'Connell et al., 2017; Dorsey et al., 2016b).

Regional Stratigraphy

Southern Bouse Formation

The southern Bouse Formation is exposed from a small (debated) patch north of Yuma, Arizona, north to Parker, Arizona (Fig. 2.1). The southern Bouse is divided into three members, defined here: (1) basal carbonate member, a mixed carbonate-siliciclastic unit with a large carbonate component (focus of this chapter); (2) middle siliciclastic member, comprising Colorado River derived claystone, siltstone, and cross-bedded river

deltaic and channel sandstone; and (3) upper bioclastic member, which includes a mixed carbonate-siliciclastic unit and overlying calcareous gravel (Homan, 2014; Dorsey et al., 2016a, b). Based on results presented in Chapter II (O'Connell et al., 2017), we interpret the basal carbonate member to record deposition in a tide-dominated marine embayment at the north end of the Gulf of California oblique- rift basin. The middle siliciclastic member records the first arrival of the Colorado River to the region and has been interpreted as progradation of the Colorado River deltaic sequence and earliest through-flowing Colorado River (Dorsey et al., 2016a, b), or a deltaic sequence that does not record the through-flowing Colorado River (Gootee et al., 2016a, b). The upper bioclastic member has been interpreted as a large lake or marine estuary during re-flooding of the lower C.R. corridor due to poorly understood changes in relative sea level and river sediment supply (Dorsey et al., 2016a, 2016b), or a progressive lowering of base level at the end of a lake highstand (Gootee et al., 2016a, b). Hypothetically, the upper bioclastic member could record re-flooding of the lower Colorado River valley followed by falling base level at the end of the re-flooding phase, an explanation that could reconcile these two data sets and interpretations.

In the study area, southeast of Cibola, Arizona, the Bouse Formation typically rests uncomfortably on Miocene alluvial fan conglomerate consisting of poorly-sorted sandy conglomerate and pebbly sandstone with clasts of locally-derived volcanic, intrusive, and metamorphic rocks. Elsewhere, Bouse basal carbonate rests on older Miocene volcanic and pre-Miocene crystalline rocks. The Miocene alluvial fan conglomerate represents local basin fill that accumulated in extensional and transtensional basins prior to Bouse deposition (e.g., Buising, 1990; House et al., 2008;

Spencer et al., 2008, 2013; Homan, 2014). The Bullhead Alluvium and younger Qt terrace gravels erosionally overlie and are inset into the Bouse Formation (House et al., 2008; Howard et al., 2014). This study is focused on the process sedimentology and depositional paleoenvironments of the basal carbonate member of the Bouse Formation southeast of Cibola, Arizona.

RESULTS

Sedimentary rocks in many facies of the southern Bouse basal carbonate member display distinctive segregation of siliciclastic and bioclastic components in cross-bed foreset strata, horizontal lamination, and heterolithic ripple- to planar-laminated deposits. These mixed silici-bioclastic tidalites differ from purely siliciclastic tidal deposits in that horizontally laminated (vertically accreted) rhythmites display systematic alternations of lime mud and siliciclastic sand, and laterally accreted rhythmites such as cross-bed foresets show segregation of siliciclastic and bioclastic lithologies into alternating layers (e.g. Longhitano and Chiarella, 2009; Longhitano, 2011; Longhitano, 2012).

Sedimentary Facies Associations of the Bouse Basal Carbonate Member

Basal Cobble Lag: Ravinement Association

Well-sorted volcaniclastic cobbles commonly distributed as a single-clast horizon (lag deposit) overlying Miocene fan conlomerate (Facies A). This association is interpreted to recorded a transgressive ravinement surface formed during initial transgression that flooded the former alluvial basin (e.g., Numedal and Swift 1987; Catuneanu et al., 2011). See Appendix B for details.

Matted Calc-Siltstone: Salt Marsh Association (Plate 1)

This association includes calc-siltite with carbonate sandy lime mudstone (Facies B) and lime-mud-rich carbonate sandstone, calc-siltstone with mudcracks, and matted lenticular lamina to thin beds that drape over cobble clasts (Facies C), interpreted to record deposition by biological trapping (algae, reeds and grasses) in low-energy, shallow water or salt marsh environment. Facies coarsen upwards to wave ripple laminated calc-silt to f.g. calcarenite interpreted to reflect an increase in current energy and water depth. Marshes experienced occasional inundation during extra high (spring) high tides and/or or tidal creek floods. This facies rarely overlies the ravinement surface, and is commonly exposed at the base of the basal carbonate on Miocene conglomerate within the Marl Wash localities. See Appendix B for details.

Gravel: Gravelly Bedform Association (Plate 2)

This facies association is dominated by well-sorted, coarse siliciclastic sandstone to pebble conglomerate with lenticular geometry and tabular cross stratification (Facies D), interpreted to record locally sourced gravels transported, reworked, and deposited by migrating gravelly bedforms in wave- and tide-reworked beach ridges, Gilbert delta-front lobes, and detached nearshore bars. Tidal currents likely contributed to winnowing and sorting. See Appendix B for details.

Heterolithic: Middle and Upper Tidal Flat and Shallow Subtidal, Bottomsets of Ebb-Dominated Tidal Dunes Association (Plate 3)

The heterolithic facies association is so named because it exhibits diversity in lithofacies varieties, and includes: (1) Sandy calcarenite and calcarenitic sandstone with asymmetrical and symmetrical ripple cross lamination (Facies E); (2) interbedded lime mudstone, carbonate clay, and/or pale green siliciclastic clay (Facies F); (3) Lime mudstone with horizontal tidal rhythmites, silt–f.g. laminations to thin beds with, wavy, flaser, and lenticular bedding (Facies G). We interpret this facies association to record deposition in upper and middle tidal flat and shallow subtidal settings as the distal bottomsets of ebb-dominated tidal dunes (Grainstone Association) and gravelly bars (Gravel Association). See Appendix B for details.

Grainstone: Tidal Dune Association (Plate 4)

The grainstone facies association includes: (1) Bioclastic barnacle and oncoid sandy grainstone to grainstone hash with complex bedding, reactivation surfaces, and sigmoidal bundle sequences (Facies H); (2) v.f.g. to f.g. mixed-carbonate and siliciclastic sand (~50:50) with small scale, bimodal-bipolar, asymmetrical ripples with lime mud drapes (Facies I); (3) barnacle oncoid. wackestone and packstone (Facies J).

We interpret this association to record deposition by migrating dunes and tidal bars in tidal channels, lower tidal flat and shallow subtidal settings, with systematic hydraulic sorting of carbonate and siliciclastic sediment by tidal currents, under the influence of cyclic solar cycles. Sedimentary structures of this association display many criteria that are commonly used to identify tide-dominated deposits, including: (1) lateral bundle/bottomset thickness variation; (2) bundle thickness variation that tracks cyclic astronomical cycles; (3) common reactivation surfaces with reverse ripples; and (4)

common opposing bidirectional paleocurrents (Nio and Yang, 1991). See Appendix B for details.

Lime Mudstone: Offshore 'Marl 2' Association (Plate 5)

This association consists of massive white carbonate clay with interbedded carbonate paper shale (Facies K), interpreted to record subtidal offshore deposition by suspension settling and slow fallout of carbonate from ambient water column. See Appendix B for details.

Summary

Five facies associations in the basal carbonate member of the Bouse Formation include: (1) basal cobble lag is interpreted as forming by low to moderate energy currents along a transgressive ravinement surface; (2) the plant-rich lime siltstone and lime mudstone association reflects storm, tidal, and biological deposition in low-energy shallow water or salt marsh settings; (3) the gravel facies association is represented by golden gravel and associated bioclastic carbonate, and is interpreted as locally-sourced wave and tide worked nearshore gravels; (4) The heterolithic association includes heterolithic, silty lime mudstone with abundant wavy, flaser, and lenticular bedding, and represents upper and middle tidal flats as well as offshore subtidal bottomsets of tidal dunes, and: (5) Grainstone association likely records hydraulic sorting of carbonate and siliciclastic material during migration of large tidal dunes and bars in lower tidal flat settings; and (6) the lime mudstone offshore association consists of recessive white

carbonate clay deposited by suspension settling and slow fallout of carbonate from an ambient carbonate-saturated water column.

DISCUSSION

Tidal Depositional Model

The basin-confined distribution of southern Bouse Formation, mixed nature of deposits, and abundant tidal sedimentary structures suggest that the base of the basal carbonate member preserves the record of a tide-dominated carbonate-producing marine embayment along basin margins that provided siliciclastic detritus. Along this NNE-SSW oriented embayment (Fig. 4), tidal currents played a fundamental role in sediment distribution and accumulation of mixed-carbonate siliciclastic facies. Figure 5 *(facies model)* depicts our depositional model for the facies associations described above.

This tidal interpretation is based on sedimentary structures and facies associations such as asymmetric ripples with reactivation surfaces and lime mudstone drapes, ripple cross lamination with reactivation surfaces, sigmoidal bundle sequences, lateral thickness variations in bundles and bottomsets, and abundant flaser, wavy, and lenticular bedding (e.g., Kreisa and Moila, 1986; Nio and Yang, 1991). This interpretation is further supported by Fourier transform analysis of tidal rhythmites in the basal carbonate member (Chapter II; O'Connell et al., 2017).

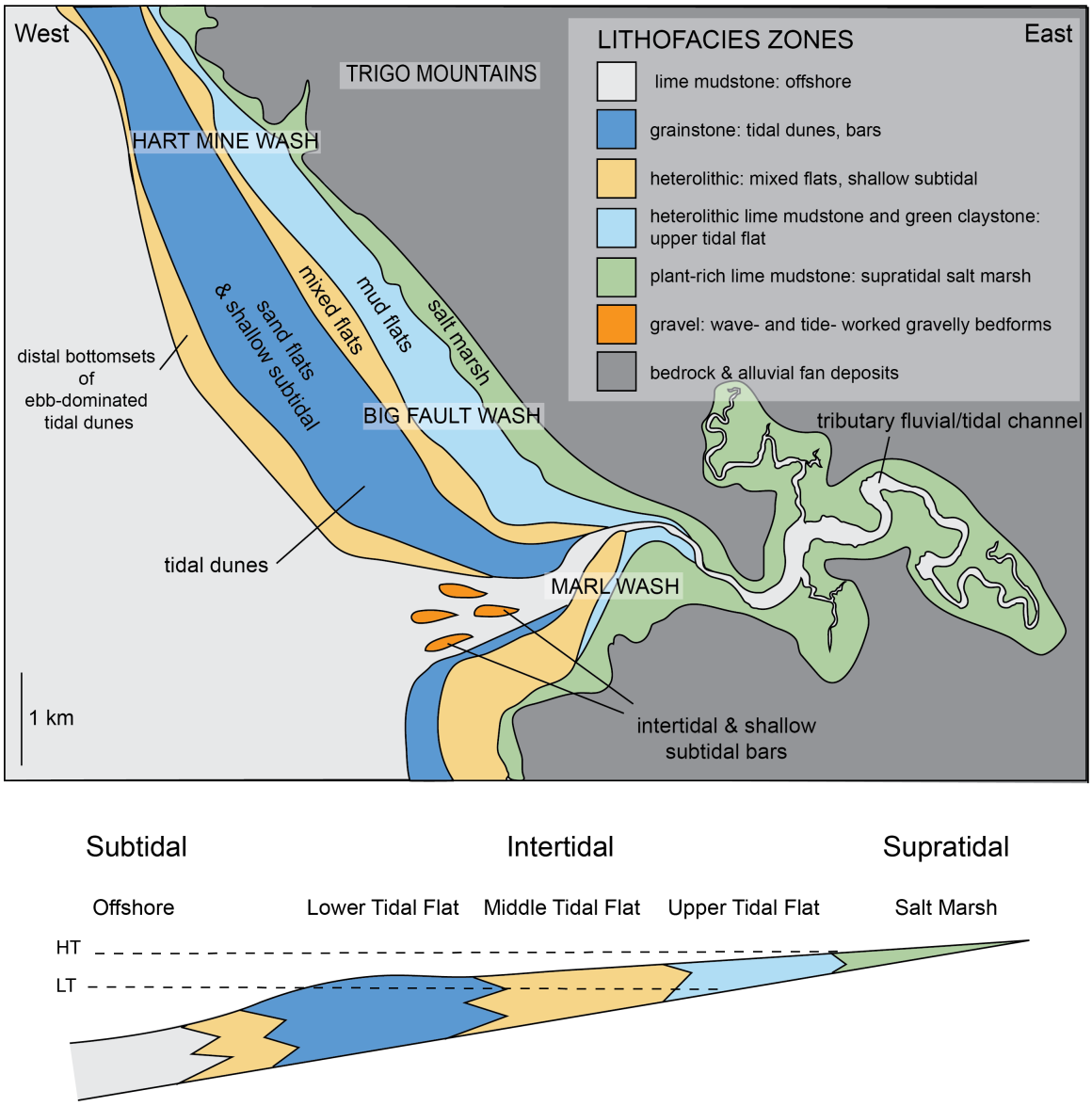

Figure 5: Depositional model and lithofacies zones of the basal carbonate member.

Many of the observed sedimentary structures match criteria for recognizing the influence of tidal currents. Other features such as mud drapes and flaser bedding are commonly observed in tidal settings though they may (rarely) also form under non-tidal conditions (Ainsworth et al., 2012; Davis Jr, 2012). Importantly however, the great abundance of characteristic and diagnostic tidal features, and their systematic lateral and vertical stacking patterns, provide compelling evidence for deposition in a tidally influenced transgressive marine embayment (O'Connell et al., 2017).

The vertical stacking of the Bouse Formation deposits records an overall deepening transgressive phase, perhaps reflecting rapid temporal change in the tidal current strength as the basin evolved prior to deposition of siliciclastic Colorado River delta and river-channel sequence. The heterolithic, grainstone, and offshore lime mudstone facies associations laterally interfinger and are locally interbedded with each other, indicating the time-transgressive nature of facies transitions. The heterolithic association represents both proximal upper and middle tidal flat deposits, as well as offshore subtidal distal bottomsets of ebb-dominated tidal dunes of the lower tidal flat and shallow subtidal environments. Mixed tidal-influenced sediment are abruptly capped by a transgressive bioturbated lime-mudstone or wackestone deposit with no apparent tidal signature (e.g. Chiarella, 2011).

The overall stratigraphic architecture records progradation of tidal flat facies over subtidal deposits, as evidenced by numerous shoaling-upward sequences from subtidal lime-mudstone to heterolithic to inferred lower tidal flat grainstone cross-bed sets. Stratigraphically above the tidal deposits, an apparent 'drowning' of the mixed carbonate-silicicasltic tide-influenced platform may have occurred when prograding tidal deposits

were outpaced by a rise in relative sea level. This is recorded in the stratigraphic shift from tidal deposits to an abrupt vertical shift to offshore, subtidal lime mudstone with no obvious tidal influence on deposition and no preserved sedimentological record of time-transgressive facies shifts at this stratigraphic interval.

This shift could reflect a 'shutting off' of the northern Gulf of California embayment tides because of changes in basin hydrodynamics accompanying a rise in relative sea level, a flooding of a carbonate platform, rapid shift to low-energy environments, or perhaps it records an abrupt landward shift in facies that are not preserved along the basin margins. A regional change in basin hydrodynamics is supported by a lack of obvious tidal deltaic features in Colorado River sediment of the middle siliciclastic member that directly overlies the offshore lime-mudstone. This question remains to be studied in more detail.

Controls on Regional Transgression

Stratigraphic analysis shows that tidal facies associations of the basal carbonate member in the Cibola area are locally interbedded and interfinger laterally with each other, and define an overall deepening-up succession that is readily correlated to the southeast Palo Verde Mountains and Milpitas wash area (Fig. 1; Homan, 2014; Dorsey et al., 2016a). The sedimentary facies thus define a stacked transgressive assemblage in which the basal cobble lag is overlain by deposits of (in ascending order) supratidal salt-marshes, beach ridges and nearshore bars, tidal flats with tidal channel bars, intertidal lower tidal flat and shallow subtidal grainstone tidal dunes, and offshore sub-wavebase environments.

The systematic, widespread facies stacking pattern shows that the basal carbonate member of the southern Bouse Formation is a regional transgressive systems tract (c.f., Van Wagoner et al., 1990; Posamentier and Allen, 1999; Catuneanu et al., 2011). The marine transgression recorded in this sequence occurred prior to earliest arrival of Colorado River delta deposits represented by the middle siliciclastic member of the southern Bouse Formation (Homan, 2014).

It is of fundamental interest to determine what controlled the rise in relative sea level that drove marine transgression during deposition of Bouse basal carbonate in the Blythe basin. The marine signal tells us that regional transgression was due to either a rise in global sea level or an increase in the rate of basin subsidence. Paleontologic and biostratigraphic studies show that the basal carbonate was deposited between about 6.5 and 5.5 Ma (McDougall and Miranda Martinez, 2014, 2016a, b; Dorsey et al., 2016b) The offshore-marl unit likely records more time than the rapidly-deposited tidal facies, though the total time represented by the basal carbonate member remains unknown. Despite this uncertainty, it is clear that the lower Colorado River valley was flooded by *one major marine transgression* during deposition of the basal carbonate member, followed by progradation of the Colorado River delta into the marine embayment during a relative sea-level highstand (Homan, 2014; Dorsey et al., 2016a, b). In contrast, the marine-isotope record reveals evidence for numerous small magnitude (20-40 m) global sea-level fluctuations during an overall *fall* in global sea level in latest Miocene time (e.g., Miller et al., 2005; Lisieki and Raymo, 2005; Raymo et al., 2009).

We therefore conclude that the small magnitude, large number, and overall *fall* of global sea-level fluctuations recorded in marine oxygen isotopes does not match the

singular, regionally extensive and implied large magnitude of relative sea-level *rise* recorded in the southern Bouse basal carbonate and overlying siliciclastic member. The lack of correlation between local and global sea-level signals suggests that regional transgression was controlled by an increase in rate of basin subsidence during Bouse basal carbonate deposition. This implies that marine transgression and deposition of the southern Bouse Formation was the result of tectonically controlled basin subsidence along the lower Colorado River corridor at the north end of the Gulf of California oblique-rift basin, which underwent rapid synchronous marine incursion over a distance of ca. 500 km along the active plate boundary at 6.5-6.3 Ma (Dorsey et al., 2007, 2011; McDougall, 2008; Bennett et al., 2016). A full discussion of this problem is beyond the scope of this study, and is the subject of ongoing investigation.

CONCLUSIONS

Six facies associations in the basal carbonate member of the Bouse Formation south of Blythe, California, are stacked in an overall transgressive vertical succession that accumulated before arrival of the siliciclastic Colorado River delta sequence. (1) The basal cobble lag is interpreted as forming by low to moderate energy currents along a transgressive ravinement surface; (2) the plant-rich lime mudstone salt marsh association reflects storm, tidal, and biological deposition in shallow water or salt marsh settings; (3) the gravel association is represented by cross-bedded golden gravel and is interpreted as locally sourced, wave and tide worked beach and nearshore gravels; (4) The heterolithic association is represented by silty lime mudstone and silt to f.g. sand with abundant wavy, flaser, and lenticular bedding. This association is interpreted to have accumulated

in intertidal tidal flat environments and in a shallow subtidal setting as the bottomsets of tidal dunes; (5) The high-energy grainstone association likely records hydraulic sorting of carbonate and siliciclastic grains during migration of large tidal dunes and bars in lower tidal flat environments; and (6) the lime mudstone subtidal offshore association consists of white recessive micrite (marl) and carbonate paper shale that was deposited in quiet water by suspension settling of carbonate through an ambient water column. The abrupt transition to subtidal offshore micrite likely records a critical shift in hydrodynamics, as water depth increased and the basin passed through the tidal amplification window.

Plate 1: Salt Marsh Association

a: Matted lime mud-rich sandstone, and sandy lime-mudstone (note sand in this context refers to carbonate sand-size grains), and gypsum layers. Stratigraphically above the Miocene conglomerate.

b: Grass and reed imprints on bedding planes of sandy beds.

c: Matted f.g. carbonate grainstone with grass imprints. Stratigraphically above the Miocene conglomerate. Note interbedded golden gravel pebble bed overlying matted facies.

d: Matted sandy facies draped over large cobble.

e: Recessive muddy facies and resistant matted sand rich facies of the salt marsh association. Note wavy character of the resistant beds.

f: ~7 cm bed of poorly sorted granules and pebbles dispersed in a recessive carbonate sand and mud matrix.

g: Matted f.g. facies and more massive beds (at base).

h: Matted f.g. facies.

Plate 1

Plate 2: Gravel Association

a: Gravel scours in underlying heterolithic beds.

b: Angular to well-rounded granules to small cobbles of the golden gravel association. Note some beds are well sorted, and others poorly sorted. Note the golden staining.

c: Horizontal beds of well-sorted golden gravel interbedded in sandy facies of the heterolithic association (Facies E). Discontinuous laterally, and overlain by lime mudstone of the heterolithic association (Facies F).

d: Cross-bedded golden gravel lense with a flat-base and conxex top geometry. Note slight green tint. Lense of golden gravel become thin pebble beds when traced laterally.

e: Interbedded golden gravel and sandy silic-rich grainstone. Note carbonate material rinds around large sub-rounded cobbles.

f: Close-up of carbonate rinds on locally derived golden gravel cobble.

G: Convex crossbedding of golden gravel and overall migration of gravelly bars toward the left. Note gravels association with facies of the heterolithic association. Also note sharp base and planar nature of gravel cross-bed foresets.

Plate 2

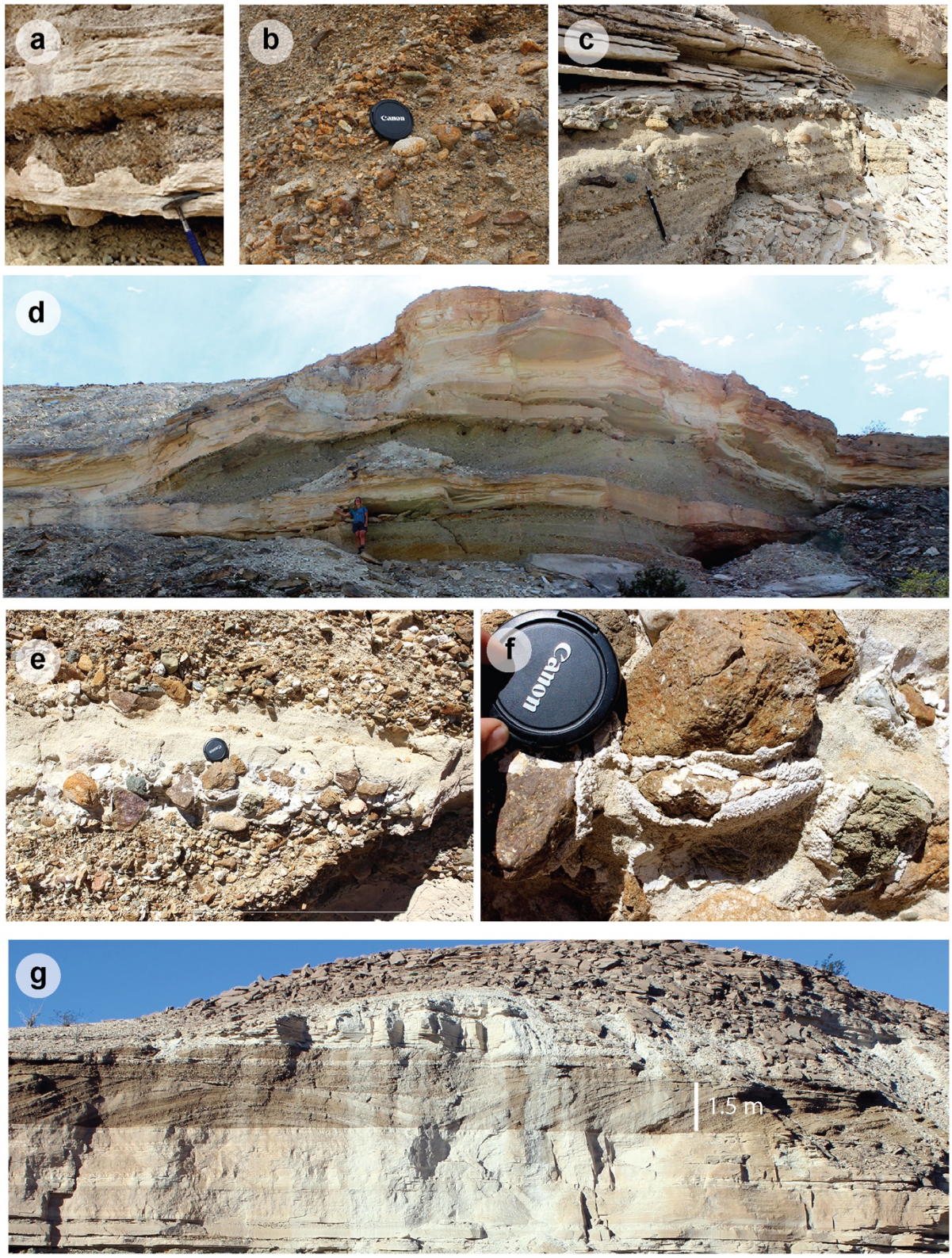

Plate 3: Heterolithic Association

a: Typical exposure of heterolithic bedding stratigraphically under the grainstone association. Interbedded lime mudstone and heterolithic f.g. sandy grainstone. Wavy, flaser, and lenticular bedding is common. Hammer is 32.5 cm long.

b: Wavy, flaser, and lenticular bedding.

c: Wavy and flaser bedding of f.g. sandy grainstone and lime mudstone.

d: Rhythmites of silic.-rich silt to f.g. sand and lime mudstone

e: Close up of silic.-rich and lime mudstone rhythmites.

f: Interbedded lime mudstone and silic.-rich grainstone.

g: Interbedded lime mudstone and green siliciclastic claystone. Mudcracks on most bedding planes. Lime mudstone commonly contains mudcracks. Hammer is 32.5 cm long.

h: Close-up of interbedded lime mudstone and green siliciclastic claystone. Note wavy character of siliciclastic clay beds.

i: Massive lime mudstone beds with wavy bedding and sparse snail, clam, bivalve shells preserved.

j: Bioturbated wackestone with abundant snail, clam, bivalve shells preserved

Plate 3

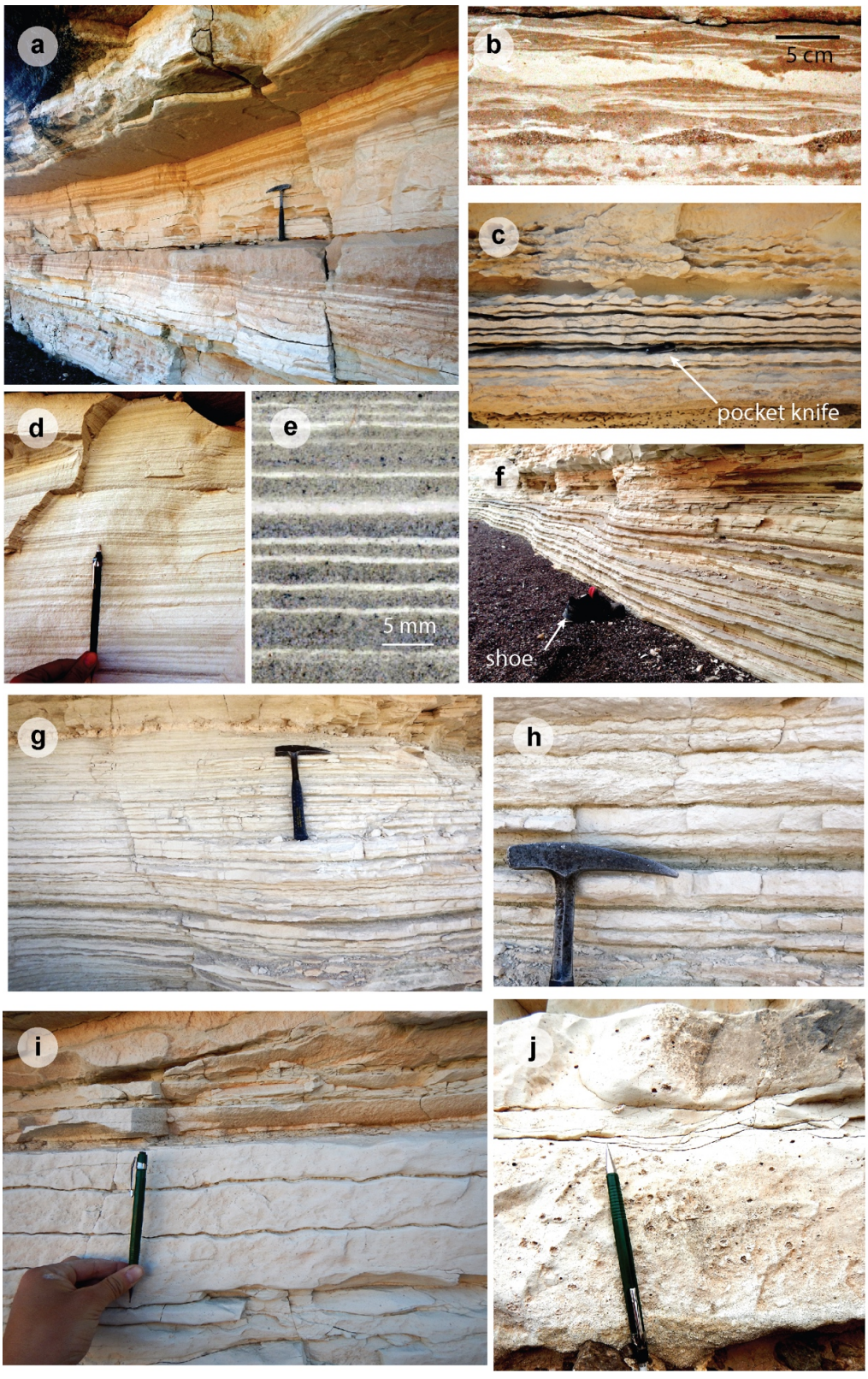

Plate 4: Grainstone Association

a: Sigmoidal bundle sequence in barnacle and oncoid grainstone.

b. Overall migration of tidal dunes toward the left. Note one bimodal bipolar paleocurrent indicator with foreset dips in the opposite direction. Distance between red circles is 30 cm. Photo by Brian Gootee.

c: Thin and thick alternations of grainstone sigmoidal bundles.

d. Possible shoaling-upward sequences from subtidal lime mudstone to intertidal grainstone tidal barss. Note lateral facies variations from grainstone to lime mudstone. A subtidal origin is inferred for the lime mudstone units because of a lack of obvious signs of periodic exposure (e.g., mudcracks).

e. Massive cross-bed sets of grainstone facies overlaying the heterolithic association. Overall migration toward the basin center. Photo by Brian Gootee.

f. Bimodal-bipolar paleocurrents.

g. Fresh, unweathered surfaces of recessive siliciclastic-rich f.g. grainstone layers (thick) interbedded with resistant bioclastic rich (thin) layers in cross-bed sets. Pocketknife is 6 cm.

h. Siliciclastic-rich f.g. grainstone layers (thick) interbedded with bioclastic rich (thin) layers in cross-bed sets. Note up-dip migration of ripples. Pocketknife is 6 cm. s = siliciclastic b= bioclastic lithologic alternations. Note recessive nature of siliciclastic layers and resistant layers of bioclastic material.

i. Mudcracks or teepee structures on grainstone bedding planes.

j. Recessive mixed carbonate and siliciclastic white-gray packstone with sigmoidal bundles with resistant mixed carbonate and siliciclastic tan grainstone. Note lateral facies changes and segregation of carbonate and siliciclastic components, similar to g and h of this association. Pencil is 13 cm long.

Plate 4

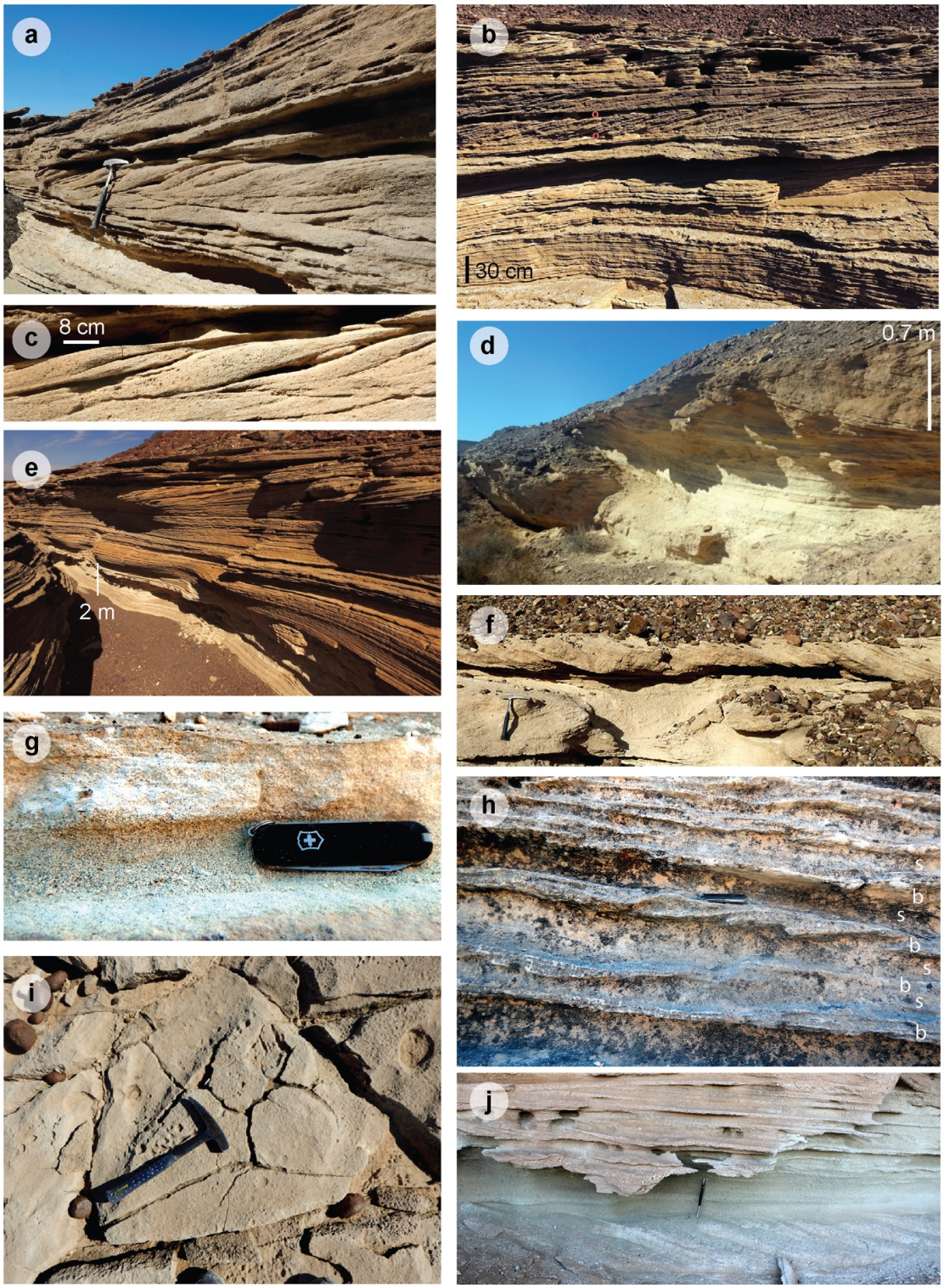

Plate 5: Offshore Association

a: Clam-rich bed in lime mudstone offshore facies. Plan view of a bedding surface.

b: Cross-section of clam-rich bed in lime mudstone offshore facies. Note slight sparry character of mudstone facies.

c: Massive, bioturbated, more resistant offshore facies with interbedded ash layer (same ash layer as indicated in d).

d: Massive lime mudstone, both resistant and recessive varieties exposed.

e. Carbonate 'paper shale'. Paper shale is often interbedded with massive recessive lime mudstone facies.

f: Offshore facies, both resistant and recessive, underneath Colorado River derived siliciclastic sediment.

g: Resistant offshore lime mudstone overlain my recessive lime mudstone and carbonate paper shale.

h. Resistant bioturbated offshore facies overlain by yellow tinted recessive and resistant alternations in offshore lime mudstone stratigraphically beneath the green claystone layers.

I: Resistant beds occasionally have mudcracks or syneresis cracks (?) on bedding planes. Pocketknife is 6 cm.

Plate 5

APPENDIX A

SUPPLEMENT TO CHAPTER TWO: TIDAL RHYTHMITES IN THE SOUTHERN BOUSE FORMATION AS EVIDENCE FOR POST-MIOCENE UPLIFT OF THE LOWER COLORADO RIVER CORRIDOR

Rationale and Methods

Tides are effective agents of sediment transport, sorting and deposition. Their effectiveness and resulting sedimentary deposits are directly related to the tidal range and resulting tidal velocity (FitzGerald and Nummedal, 1983; Boothroyd, 1985; Williams, 2000). Tidal successions can be deposited and preserved as either horizontally laminated rhythmites (e.g., Williams, 1989, 2000; Chan et al., 1994; Mueller et al., 2002), laterally accreted foresets (e.g., Visser, 1980; de Boer et al., 1989; Deynoux et al., 1993; Bose et al., 1997; Eriksson and Simpson, 2000, 2004; Mueller et al., 2002; Tape et al., 2003; Mazumder, 2004; Longhitano, 2011), or laterally accreted sigmoidal bundles (e.g., Kreisa and Moila, 1986). With this understanding, the basic data set acquired for tidal rhythmite analysis includes grains size, lithology, and thickness measurements of foreset bedding and laminae, limited to intervals with well-preserved and uninterrupted stratification. The thickness variations of two layers – one thin and one thick – typically alternate between siliciclastic-rich and bioclastic lithologies in the Bouse Formation, similar to other silic-bioclastic tidal rhythmites (e.g., Longhitano, 2011). Two layers comprise one couplet. Layer thicknesses were measured from two horizontal rhythmite successions *(n=164, and n=87)*, one dune foresest succession *(n=78)*, and one sigmoidal bundle succession *(n=36)*. The thicknesses of successive rhythmites of alternating lithologies are plotted as a thickness series (in contrast to a true time series), where layer thickness is plotted

against rhythmite layer number. Fourier analysis detects the presence of cyclicity in the dataset (Archer, 1994; Archer et al., 1995; Adkins & Eriksson, 1998). Raw data were demeaned and detrended prior to power spectral analysis. Demeaning prepares the data for detrending and removes the infinite-period component of the signal, and detrending minimizes trends of period longer than the data duration (Granger and Joyeux, 1980; Beran, 1994).

Modelling

FFTs

The tidal record shown in Fig. 3A is made using the amplitudes and phases of all major tidal components at San Felipe, in the northern Gulf of California. These are calculated using the amplitudes and frequencies of the 7 dominant tidal components (four semidiurnal and 3 diurnal).

Local basin effects control the amplitude of each of the 7 dominant and many minor solar and lunar tidal components. The major components have frequencies near 1 and 2 cycles per day, with the principal semidiurnal solar component (S2) occurring exactly twice a day. The principal semidiurnal lunar component (M2) occurs with a frequency of 1.932 cycles per day. This is driven by the P=29.53-day cycle of the Moon's phase changes, which gives a frequency of 2*[(P-1)/P] = 2*[28.53/29.53] = 1.932 cycles per day.

In modeling northern Gulf of California tides, Marinone (1997) finds these can be modeled well using only the S2 and M2 components, and that the amplitude ratio M2/S2 is about 1.65.

Table 1: (from Kvale, 2006)
for San Felipe:

Component	Period	Freq.	Amp*	Cause of component
M2	12.42	1.932	164.5	Principal lunar (semidiurnal)
S2	12.00	2.000	99.2	Principal solar (semidiurnal)
N2	12.66	1.896	42.0	Larger elliptical lunar (semidiurnal)
K2	11.97	2.005	26.4	Combined declinational lunar & declinational solar (semidiurnal)
K1	23.93	1.003	41.6	Combined declinational lunar & declinational solar (diurnal)
O1	25.82	0.930	26.3	Principal lunar (diurnal)
P1	24.07	0.997	13.0	Principal solar (diurnal)

*from Marinone (1997)

Our data are not long enough to resolve the small differences between the individual diurnal peaks. Instead, we use to the average of the three diurnal frequencies, weighted by their amplitudes given in Table 1. This gives Wa1=0.98 cycles per day. A similar calculation for the four semidiurnal frequencies gives Wa2=1.95 cycles per day.
See FFT Matlab Code, below.

Least Squares

An FFT calculates the amplitudes of constituent sine and cosine waves that have an integer number of cycles in the analyzed time window. These amplitudes are identical to the amplitudes calculated by least squares fitting of sine and cosine waves. If the energy at frequencies intermediate to integer number of cycles is of interest, sine and cosine waves of these intermediate frequencies can be found with least squares fitting. Our results of this analysis are shown in Fig. 1 Supplement. In the right-hand column of this

figure we show an enlargement of these results at the low-frequency end of the spectrum, where there are relatively few amplitude estimates obtained from the FFT.

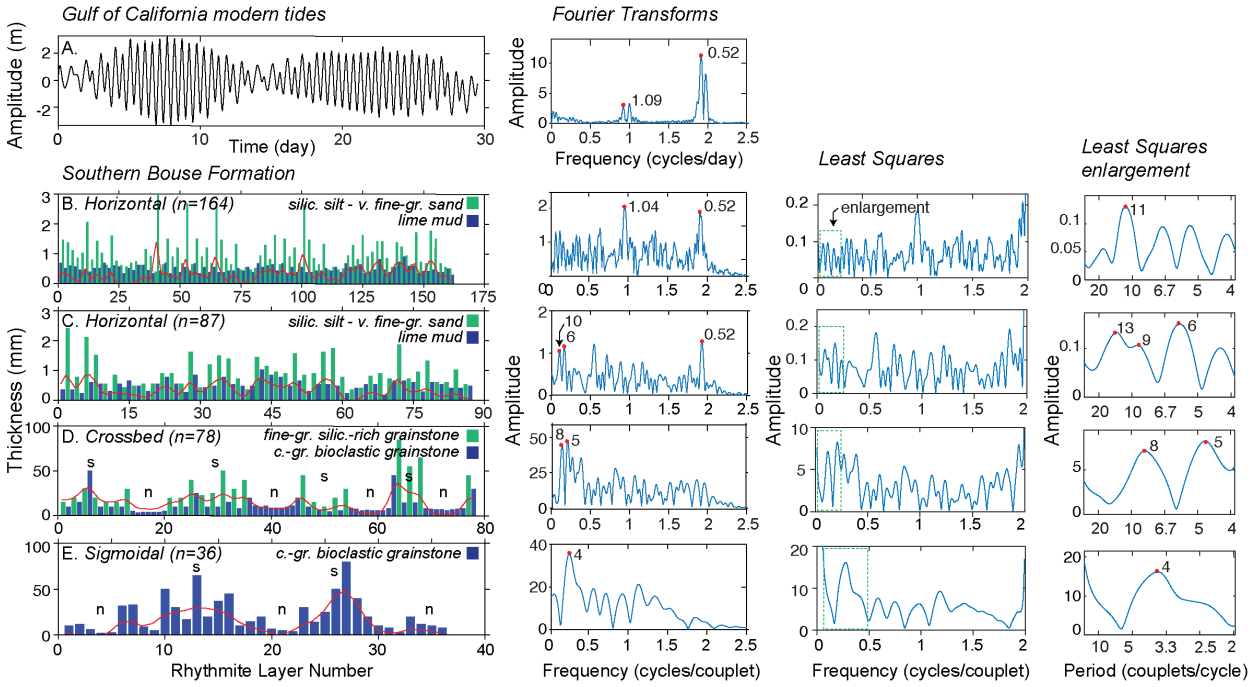

Figure A.1. FFT & Least Squares comparison. Green boxes around Least Squares column indicate enlargement under Lease Squares Enlargement column. Red dots with numbers indicate the period (1/frequency).

See Least Squares Matlab code, below

Figure 1.2 Photo Locations

Photo	**Latitude**	**Longitude**
2B	33.2893	-114.6323
2C	33.2515	-114.7792
2D	33.3562	-114.7248
2E	33.2698	-114.6421
Thalassinoides	33.2574	-114.6416
wavy, flaser, lenticular bedding	33.2696	-114.6411
horizontal thin-thick couplets	33.2633	-114.6360

MATLAB CODE – FFT

```
% Matlab Code Supplement – FFT
% for 'Tidal rhythmites in the Southern Bouse Formation as evidence for
Post-Miocene uplift of the lower Colorado River corridor'
% Brennan O'Connell, Rebecca J. Dorsey, and Eugene D. Humphreys
% Department of Earth Sciences, University of Oregon, Eugene, Oregon
97403, USA

%-----------------------------------------------------------------------
------
%-----------------------------------------------------------------------
------
%-----------------------------------------------------------------------
------

% load tide data from actual north-Gulf of California site (Tides.in)
% Figure 3A
% Tides.in  = one month of modern tide record at San Felipe, Gulf of
% California (http://sanfelipe.com.mx/weather/tide-calendars)

clear all
figure(1), clf

load Tides.in     % N. GoC tide for 31 days, picked at peaks & troughs
n= size(Tides,1);
T= Tides(:,1);    %  Time
H= Tides(:,2);    %  Hight
tlim= 31;         %  in days (truncated to 29.5 days below)

%%%%%%%  truncate to 29.5 days %%%%%
n= round(n*(29.5/31));   tlim= tlim*(29.5/31);
T= T(1:n);   H= H(1:n);

% make one continuous series
  T(107:n)= T(107:n)+(733-36);   H(107:n)= H(107:n)-(702-579);
  T( 79:n)= T( 79:n)+(726-27);   H( 79:n)= H( 79:n)-(559-429);
  T( 52:n)= T( 52:n)+(720-22);   H( 52:n)= H( 52:n)-(463-330);
  T( 25:n)= T( 25:n)+(727-29);   H( 25:n)= H( 25:n)-(283-157);

% Scale input data, using info from digitized plot
  T =  T-T(1);       % first time = 0
  T =  T*(tlim/T(n));% last  time = tlim  [scaling from plot:
T=T*(7/698)]
  H = -H*(7/97);     % scale Height to meters
  H =  H-mean(H);    % demean H   [actual low tide = -1.6 m]

% make dense and regularly sampled in time
  factor = 8;  % use integer
  H = interp(H,factor);
    H = H(1:n*factor-(factor-1));  % truncate overshoot
  T = interp(T,factor);
    T = T(1:n*factor-(factor-1));  % truncate overshoot
  [H,T] = resample(H,T);           % make regular time steps
  nt = length(T);
  dT = T(2);               % time step, in days. T = dT*[0 1 2 3 ...]
```

```
  n4 = 4*2^ceil(log2(nt));  % over 4 x nt, for Rhy & zero padding
  tlim4 = tlim*(n4/nt);     % time at end of extended (zero-padded)
array
  H =  H-mean(H);           % demeaned again

  %plot Fig.3A time series
  subplot(5,2,1), hold on
     plot(T,H), axis tight
     xlim([0 30])
     set(gca,'TickDir','out')
     title('Gulf of California modern tides')
     xlabel('Time (day)'), ylabel('Amplitude (m)')
      box on
      axis tight
      hold on

% Fourier Transform tidal record
FH = fft(H,n4)/n4;   % Fourier transform zero-padded time series,
scaled
FH = FH*(n4/n);      % scale to compensate for zero padding
                     %        Output of fft is as follows:
                     %  DC is at 0-th point, Nyquest at (nt/2+1)-th
point
                     %   D . . . N . . .     (for nt=8)
                     %   0 + + + - - - -     (sign of frequency)
FH = fftshift(FH);   % put negative frequencies on lhs where they
belong
                     %  DC is at (nt/2+1)-th point, Nyquest at 0-th
point
                     %   N . . . D . . .     (for nt=8)
                     %   - - - - 0 + + +     (sign of frequency)
nf = n4/2;           % number of non-negative frequencies
kf = 1:n4;           % kf is freq kounter:    1  2  3  4  5  6  7  8
freq=(kf-nf-1)/tlim4;% freq is actual freq: (-4 -3 -2 -1  0  1  2
3)/tlim4
                     % freq(DC)=0. Next freq is for 1 cycle. this is
dw.
FH2 = 2*FH(nf+1:n4); % from DC to highest non-Nyq. doubled for rhs
freq4=freq(nf+1:n4)';% nf+1 is DC.
  fprintf('%8.5f\n',n4*dT*freq4(2));% if 1, 1st freq is fundamental
period

  %Plot FFT
  subplot(5,2,2)
  Pa = 0.01;         % scale the phase plot
  phase = Pa*(180/pi)*atan2(imag(FH2),real(FH2));
  plot([0 29.5], 180*Pa*[1 1],'r--')
  semilogx(freq4,phase,'r')  % phase spectrum
  plot(freq4,abs(FH2))  % amplitude spectrum
  hold off
  axis tight
  hold on
  xlim([0.00 2.5])   % 33 days to 3 cycles/day
  ylim([0.00 14])
  set(gca,'YTick',[0 5 10])
  set(gca,'TickDir','out')
  title('FFT of northern GoC tides')
  xlabel('Frequency (cycles/day)'), ylabel('Amplitude')
```

```
[pks, locs]=findpeaks(abs(FH2),freq4,'SortStr','descend','NPeaks', 5)
%-------------------------------------------------------------------------
-
%-------------------------------------------------------------------------
-

% load rhythmite data from the southern Bouse Formation
% Figure 3B
% Rhy.mmHoriz  = horizontal rhythmite succession of lime mudstone and
% silt-v.f.g sand

load Rhy.mmHoriz

K = Rhy(:,1);      % layer
R = Rhy(:,2);      % layer thickness
L = Rhy(:,3);      % lithology
nr = length(K);

%logic test to plot lithology in different colors
ind_green_horiz = L==1;    %green silic. silt ? v.f.g. sand
ind_blue_horiz  = L==0;    %lime mudstone

R_blue = R;
R_blue(ind_green_horiz) = 0;
R_green = R;
R_green(ind_blue_horiz) = 0;

%plot Fig.3B rhythmites
subplot(5,2,3)
 hold on
 bar(K,R_green,'g')
 bar(K,R_blue,'b')
 xlim([0 175])
 set(gca,'TickDir','out')
 title('Horizontal Rhythmites (n=164)')
 xlabel('Rhythmite Layer Number'), ylabel('Thickness (mm)')
 box on

% trend line removed from R "detrending the data"
Line = R(1) + K*(R(nr)-R(1))/(K(nr)-K(1)); % line through 1st & last
points
R = R-Line;              % remove trend from R

% Moving average removed from R
wid = 20;
avg = 1+2*wid;          % Assures avg is odd
Z = zeros(wid,1);
Rt = [Z;R;Z];            % temp array with zero padding
Ra = zeros(size(Rt));
for k=wid+(1:nr)
  Ra(k) = mean(Rt(k-wid:k+wid));
end
R = R-Ra(wid+1:wid+nr);

Rfactor=8;
```

```
R = interp(R,Rfactor);
Ko= interp(K,Rfactor);

%FFT
FR = fft(R,n4)/n4;    % Fourier transform zero-padded time series
FR = FR*(n4/n);
FR = fftshift(FR);
FR2= 2*FR(nf+1:n4);   % DC to highest non-Nyq. doubled for use of rhs
only

%plot Fig.3B FFT
  subplot(5,2,4)
  plot(freq4,abs(FR2))  % amplitude spectrum
  xlim([0.00 2.5])
  ylim([0.00 2.5])
  set(gca,'YTick',[0 1 2])
  set(gca,'TickDir','out')
  title('FFT of Horizontal Rhythmites')
  xlabel('Frequency (cycles/couplet)'), ylabel('Amplitude')
  box on

%[pks, locs]=findpeaks(abs(FR2),freq4,'SortStr','descend','NPeaks', 5)
%find peaks

%-------------------------------------------------------------------
-
%-------------------------------------------------------------------
-

% load rhythmite data from the southern Bouse Formation
% Figure 3C
% Rhy.horizmm4  = horizontal rhythmite succession of lime mudstone and
% silt-v.f.g sand


load Rhy.horizmm4

K = Rhy(:,1);      % days (assuming 2 layers/day)
R = Rhy(:,2);      % layer thickness
L = Rhy(:,3);      % lithology
nr = length(K);

%logic test to plot lithologies in different colors
ind_green= L==0;   % green silic. silt - v.f.g. sand
ind_blue= L==1;    % lime mud

R_blue = R;
R_blue(ind_green) = 0;
R_green = R;
R_green(ind_blue) = 0;

%plot Fig.3C rhythmites
subplot(5,2,5)
 hold on
 bar(K,R_green,'g')
 bar(K,R_blue,'b')
```

```
 set(gca,'XTick',[0 15 30 45 60 75 90])
  ylim([0 3.5])
  xlim([0 90])
  set(gca,'TickDir','out')
  title('Horizontal Rhythmites (n=87)')
  xlabel('Rhythmite Layer Number'), ylabel('Thickness (mm)')
  box on

% trend line removed from R "detrending the data"
Line = R(1) + K*(R(nr)-R(1))/(K(nr)-K(1)); % line through 1st & last
points
R = R-Line;              % remove trend from R

% Moving average removed from R
wid = 20;
avg = 1+2*wid;          % Assures avg is odd
Z = zeros(wid,1);
Rt = [Z;R;Z];            % temp array with zero padding
Ra = zeros(size(Rt));
for k=wid+(1:nr)
  Ra(k) = mean(Rt(k-wid:k+wid));
end
R = R-Ra(wid+1:wid+nr);

Rfactor=8;
R = interp(R,Rfactor);
Ko= interp(K,Rfactor);

%FFT
FR = fft(R,n4)/n4;    % Fourier transform zero-padded time series
FR = FR*(n4/n);
FR = fftshift(FR);
FR2= 2*FR(nf+1:n4);   % DC to highest non-Nyq. doubled for use of rhs
only

%plot Fig.3C FFT
  subplot(5,2,6)
  plot(freq4,abs(FR2))  % amplitude spectrum
  set(gca,'TickDir','out')
  xlim([0.00 2.5])      % 30 days to 3 cycles/day
  ylim([0.0 2])
  title('FFT of Horizontal Rhythmites')
  xlabel('Frequency (cycles/couplet)'), ylabel('Amplitude')
  box on

%[pks, locs]=findpeaks(abs(FR2),freq4,'SortStr','descend','NPeaks', 5)
%find peaks

%-------------------------------------------------------------------------
-
%-------------------------------------------------------------------------
-

% load rhythmite data from the southern Bouse Formation
% Figure 3D
% Rhy.mega  = crossbed foresets
```

```
load Rhy.mega

K = Rhy(:,1);       % days (assuming 2 layers/day)
R = Rhy(:,2);       % layer thickness
L = Rhy(:,3);       % lithology
nr = length(K);

%logic test to plot lithology in different colors
ind_blue= L==1;     % c.-grained bioclastic grainstone
ind_green= L==0;    % fine-gr. silic rich grainstone

R_blue = R;
R_blue(ind_green) = 0;
R_green = R;
R_green(ind_blue) = 0;

%plot Fig.3D rhythmite
 subplot(5,2,7)
 hold on
 bar(K,R_green,'g')
 bar(K,R_blue,'b')
  xlim([0 80])   % x axis
  set(gca,'TickDir','out')
  title('Crossbed (n=78)')
   xlabel('Rhythmite Layer Number'), ylabel('Thickness (mm)')
  box on

% trend line removed from R
Line = R(1) + K*(R(nr)-R(1))/(K(nr)-K(1)); % line through 1st & last
points
R = R-Line;              % remove trend from R

% Moving average removed from R
wid = 20;
avg = 1+2*wid;          % Assures avg is odd
Z = zeros(wid,1);
Rt = [Z;R;Z];            % temp array with zero padding
Ra = zeros(size(Rt));
for k=wid+(1:nr)
  Ra(k) = mean(Rt(k-wid:k+wid));
end
R = R-Ra(wid+1:wid+nr);

Rfactor=8;
R = interp(R,Rfactor);
Ko= interp(K,Rfactor);

% FFT
FR = fft(R,n4)/n4;    % Fourier transform zero-padded time series
FR = FR*(n4/n);
FR = fftshift(FR);
FR2= 2*FR(nf+1:n4);   % DC to highest non-Nyq. doubled for use of rhs
only

% plot Fig.3C FFT
```

```
subplot(5,2,8)
  plot(freq4,abs(FR2))  % amplitude spectrum
  xlim([0.00 2.5])   % 30 days to 3 cycles/day
  ylim([0.0 60])
  set(gca,'YTick',[0 25 50])
  set(gca,'TickDir','out')
  title('FFT of Crossbed Rhythmites')
  xlabel('Frequency (cycles/couplet)'), ylabel('Amplitude')
  box on

  %[pks, locs]=findpeaks(abs(FR2),freq4,'SortStr','descend','NPeaks',
5) %find peaks

%-------------------------------------------------------------------
-
%-------------------------------------------------------------------
-

% load rhythmite data from the southern Bouse Formation
% Figure 3E
% Rhy.sig = sigmoidal bundle sequence

load Rhy.sig

K = Rhy(:,1);      % layers
R = Rhy(:,2);      % layer thickness
nr = length(K);

%plot Fig.3E Rhythmites
  subplot(5,2,9)
  bar(K,R,'b'), hold on
  set(gca,'TickDir','out')
  xlim([0 36])   % x axis
  title('Sigmoidal Bundles (n=36)')
  xlabel('Rhythmite Layer Number'), ylabel('Thickness (mm)')

% trend line removed from R
Line = R(1) + K*(R(nr)-R(1))/(K(nr)-K(1)); % line through 1st & last
points
R = R-Line;              % remove trend from R

% Moving average removed from R
wid = 20;
avg = 1+2*wid;          % Assures avg is odd
Z = zeros(wid,1);
Rt = [Z;R;Z];           % temp array with zero padding
Ra = zeros(size(Rt));
for k=wid+(1:nr)
  Ra(k) = mean(Rt(k-wid:k+wid));
end
R = R-Ra(wid+1:wid+nr);

Rfactor=8;
R = interp(R,Rfactor);
Ko= interp(K,Rfactor);
```

```
% FFT
FR = fft(R,n4)/n4;     % Fourier transform zero-padded time series
FR = FR*(n4/n);
FR = fftshift(FR);
FR2= 2*FR(nf+1:n4);    % DC to highest non-Nyq. doubled for use of rhs
only

%plot Fig.3E FFT
  subplot(5,2,10)
  plot(freq4,abs(FR2))  % amplitude spectrum
  xlim([0.03 2.5])      % 30 days to 3 cycles/day
  set(gca,'TickDir','out')
  title('FFT of Sigmoidal Rhythmites')
  xlabel('Frequency (cycles/couplet)'), ylabel('Amplitude')

 %[pks, locs]=findpeaks(abs(FR2),freq4,'SortStr','descend','NPeaks', 5)
%find peaks
%____________________the
end_____________________________________________________
```

MATLAB CODE – LEAST SQUARES

```
% Matlab Code Supplement Least Squares
% useful for resolving long-wavelength signal
% for 'Tidal rhythmites in the Southern Bouse Formation as evidence for
Post-Miocene uplift of the lower Colorado River corridor'
% Brennan O'Connell, Rebecca J. Dorsey, and Eugene D. Humphreys
% Department of Earth Sciences, University of Oregon, Eugene, Oregon
97403, USA

%-------------------------------------------------------------------------
------
%-------------------------------------------------------------------------
------
%-------------------------------------------------------------------------
------

clear all


%% Read from specified file
ch= char('horizmm4','mmHoriz','mega','sig');
fprintf('Which one:\n')
for k=1:size(ch,1)
  fprintf('   %d  Rhy.%s\n',k,ch(k,:))
end
test=1;
while test==1
  aaa = input('enter number, then return: ','s');
  aaa = str2double(aaa);
  for k=1:size(ch,1)
    if aaa==k, test=0; break, end
```

```
  end
end
pnt = find(ch(aaa,:)~=' ');
Rhy = load(['Rhy.' ch(aaa,pnt)]);

%% Rhythmite input
R  = Rhy(:,2);       % layer thickness
avg= mean(R);
R  = R-avg;

nr = length(R);
t  = (0:nr-1);        % layer, divide by 2

%% Plot Rhythmites
figure(1), clf
subplot(5,2,1)
  plot(t+1,R ,'k')  % "+1" so first point is 1
    axis tight
    yl = get(gca,'YLim');   dy=yl(2)-yl(1);
    set(gca,'YLim',[yl(1)-0.1*dy yl(2)+0.1*dy])
  title(['Rhy.' ch(aaa,pnt)])
  xlabel('layer number')

%% Least squares for [DC,As,Ac] in  R = D + As*sin(wt) + Ac*cos(wt)
inc = 0.0005;
buffer = 0.004;
lim = floor((1-2*buffer)/inc);
f  = NaN(1,lim);
DC = NaN(1,lim);
amp= NaN(1,lim);
for k=10:lim               % lower limit above 1 to avoid longest-
period part
  f(k) = buffer+k*inc;     % at Nyq when freq=0.5 (ie, 1 cycle per 2
layers)
  s = sin(2*pi*f(k)*t/2);  % /2 to put into days (at 2 layers per day)
  c = cos(2*pi*f(k)*t/2);
  ss= s.*s;
  sc= s.*c;
  cc= c.*c;
  A = [sum(s) sum(ss) sum(sc); ...    % A*CC = P
       sum(c) sum(sc) sum(cc); ...
        nr    sum(s)  sum(c)];
  P = [s*R c*R sum(R)]';
  CC = A\P;                           % invert for CC
  D  = CC(1);
  As = CC(2);
  Ac = CC(3);
  Rp = D + As*s + Ac.*c;
  DC(k) = D;
  amp(k)= sqrt(As^2+Ac^2);
end

%% plot Amplitude spectrum
subplot(5,2,1)
  plot(f*2,amp)
  title('Spectrum')
  ylim([0 .2]) %this y-axis must change depending on the rhythmite
```

```
analyzed
  xlabel('Frequency (cycles/couplet)')
subplot(5,2,2)
    nn = 20:ceil(lim/8);
    plot(f(nn)*2,amp(nn)), axis tight, hold on
    plot(f(nn)*2,DC(nn))   % plots the DC offset
  plot(get(gca,'XLim'),[0 0],'k'), hold off
  xlabel('Period (couplets/cycle)')
  title('Low Frequency Enlargement')
    xx = get(gca,'XTick');
    xx = round(10./xx)/10;
    set(gca,'XTickLabel',xx)
    yl = get(gca,'YLim');
    set(gca,'YLim',[0 yl(2)*1.15])

   [pks, locs]=findpeaks(amp(nn),f(nn)*2,'SortStr','descend','NPeaks',
5)

%____________________the end_____________________________________________
%_____________________________________________________________________
```

Modern Tidal Data (used in Figure 1.3A)

Names in parentheses (Tides.in) refer to target data in Matlab code (supplemental file)

Figure 1.3A. (Tides.in)

% Modern tidal data one month of modern tide record at San Felipe, Gulf of California, March, 1993

125 196
141 185
171 207
210 185
232 193
264 195
286 210
318 178
344 200
364 189
392 218
421 171
446 211
470 180
495 226
522 163
548 219
573 171
598 230
625 154
650 225
676 160
700 236
727 157 % 29 283
%repeat of peak
54 364 % line 25
80 285
106 372
131 281 %
156 371
183 279 % full moon
208 372
233 279
259 369
285 280
311 366
335 285
361 370
387 284
412 360
437 290
463 364
490 291
515 348
539 298
565 357
593 298
618 338
641 307
668 349
698 305
720 330 % 22 463
%repeat of trough
46 447 % line 52
74 471
108 442
139 459
159 454
185 468
217 440
245 468
268 449
292 472
320 434
348 473

371 443
394 477
422 430
449 476
471 438
497 482
523 428
549 479
574 427
597 484
625 426
650 485
675 429
700 487
726 429 % 27 559
%repeat of peak
52 620 % line 79
78 559
103 621
129 557
154 623
180 558
205 622
230 557
256 626
281 552 % new moon
306 619
331 557
357 625
383 555
408 619
432 560
458 626
484 556
509 614
533 562
558 624
585 559
609 608
634 565
659 619
687 563
711 605
733 579 % 36 702
%repeat of peak
63 747 % line 107
92 701
116 732 % 121 726
%ends 28 days
138 710
167 744
196 707
221 725
241 714
270 737
304 709
333 723
353 717
381 736
410 704
% END
% dX=698 is 7 days
% dy=97 is 7 meters

Rhythmite Thickness Data (used in Figure 3B-E)

Names in parentheses (Rhy.xxx) refer to target data in Matlab code (supplemental file)

Figure 1.3B. Horizontal *(n=162)* (Rhy.mmHoriz)
Location
33.26326°, -114.63597°

Layer#: Thickness(mm): Lithology (0=lime mud 1=silic. silt-v. fine gr. sand)

1	0.689	0
2	1.465	1
3	0.517	0
4	1.381	1
5	0.603	0
6	1.121	1
7	0.577	0
8	0.864	1
9	0.46	0
10	1.034	1
11	0.46	0
12	2.068	1
13	0.402	0
14	0.804	1
15	0.517	0
16	1.437	1
17	0.517	0
18	1.035	1
19	0.691	0
20	0.632	1
21	0.517	0
22	1.608	1
23	0.603	0
24	0.775	1
25	0.577	0
26	0.632	1
27	0.345	0
28	0.574	1
29	0.517	0
30	0.689	1
31	0.46	0
32	0.747	1
33	0.632	0
34	0.634	1
35	0.634	0
36	1.149	1
37	0.46	0
38	0.919	1
39	0.349	0
40	0.402	1
41	4.423	1
42	0.431	0
43	0.646	1
44	0.689	0
45	1.508	1
46	0.345	0
47	0.906	1
48	0.56	0
49	1.206	1
50	0.388	0

51	0.689	1
52	0.56	0
53	2.671	1
54	0.431	0
55	0.646	1
56	0.689	0
57	1.508	1
58	0.345	0
59	0.906	1
60	0.56	0
61	1.206	1
62	0.388	0
63	0.689	1
64	0.56	0
65	2.671	1
66	0.388	0
67	1.465	1
68	0.388	0
69	0.862	1
70	0.431	0
71	0.648	1
72	0.431	0
73	1.336	1
74	0.519	0
75	0.474	1
76	0.433	0
77	0.562	1
78	0.56	0
79	0.474	1
80	0.39	0
81	0.517	1
82	0.691	0
83	0.948	1
84	0.56	0
85	1.293	1
86	0.605	0
87	0.82	1
88	0.646	0
89	1.637	1
90	0.431	0
91	0.646	1
92	0.689	0
93	1.508	1
94	0.345	0
95	0.906	1
96	0.56	0
97	1.206	1
98	0.388	0
99	0.689	1
100	0.56	0
101	2.671	1
102	0.388	0
103	1.465	1
104	0.388	0
105	0.862	1
106	0.431	0
107	0.648	1
108	0.431	0
109	1.336	1
110	0.519	0
111	0.474	1
112	0.433	0
113	0.562	1
114	0.56	0
115	0.474	1
116	0.39	0
117	0.517	1
118	0.691	0
119	0.948	1
120	0.56	0
121	1.293	1
122	0.605	0
123	0.82	1
124	0.646	0
125	1.637	1
126	0.345	0
127	0.905	1
128	0.39	0
129	1.077	1
130	0.474	0
131	1.422	1
132	0.819	0
133	1.422	1
134	0.474	0
135	0.862	1
136	0.388	0
137	0.562	1
138	0.56	0
139	1.379	1
140	0.732	0
141	1.25	1
142	0.906	0
143	0.948	1
144	0.603	0
145	0.648	1
146	0.605	0
147	1.724	1
148	0.345	0
149	0.734	1
150	0.431	0
151	0.691	1
152	0.431	0
153	1.767	1
154	0.476	0
155	1.508	1
156	0.388	0
157	0.691	1
158	0.388	0
159	0.56	1
160	0.517	0
161	0.517	1
162	0.302	0

Figure 1.3C. Horizontal (*n=87)* (Rhy.horizmm4)
Location
33.26326°, -114.63597°

Layer#: Thickness(mm): Lithology (0=lime mud 1=silic. silt-v. fine gr. sand)

1	0.362	1
2	2.412	0
3	0.362	1
4	0.784	0
5	0.241	1
6	2.11	0
7	0.603	1
8	1.507	0
9	0.543	1
10	0.543	0
11	0.301	1
12	0.844	0
13	0.543	1
14	0.422	0

15	0.663	1
16	0.482	0
17	0.482	1
18	0.543	0
19	0.301	1
20	0.543	0
21	0.543	1
22	0.904	0
23	0.784	1
24	0.904	0
25	0.543	1
26	0.543	0
27	0.271	1
28	1.628	0
29	0.844	1
30	0.422	0
31	0.422	1
32	1.206	0
33	0.482	1
34	1.507	0
35	0.784	1
36	1.387	0
37	0.543	1
38	0.724	0
39	0.482	1
40	0.362	0
41	0.482	1
42	1.447	0
43	1.025	1
44	1.146	0
45	0.844	1
46	0.965	0
47	0.784	1
48	0.904	0
49	0.482	1
50	1.568	0
51	0.663	1
52	0.844	0
53	0.301	1
54	0.904	0
55	0.543	1
56	1.629	0
57	0.543	1
58	1.748	0
59	0.482	1
60	0.784	0
61	0.241	1
62	0.362	0
63	0.422	1
64	0.422	0
65	0.543	1
66	0.814	0
67	0.543	1
68	0.909	0
69	0.181	1
70	0.724	0
71	0.663	1
72	1.869	0
73	0.663	1
74	0.724	0
75	0.606	1
76	0.965	0
77	0.301	1
78	1.326	0
79	0.603	1
80	0.603	0
81	0.543	1
82	0.603	0
83	0.422	1
84	1.025	0
85	0.422	1
86	0.543	0
87	0.482	1

Figure 1.3D. Crossbed (*n=78)* (Rhy.mega)
Location:
33.269795°, -114.637463°

Layer#: Thickness(mm):
Lithology (0= fine-gr. silic.-rich grainstone, 1= c.-gr. bioclastic grainstone)

1	15	0
2	10	1
3	20	0
4	15	1
5	30	0
6	50	1
7	20	0
8	10	1
9	15	0
10	10	1
11	15	0
12	10	1
13	30	0
14	5	1
15	3.5	1
16	4	1
17	4	1
18	4	1
19	4	1
20	5.5	1
21	20	0
22	10	1
23	20	0
24	10	1
25	40	0
26	25	1
27	23	0
28	10	1
29	25	0
30	10	1
31	50	0
32	15	1
33	30	0
34	8	1
35	40	0
36	20	1
37	11	1
38	10	1
39	11	1
40	9	1
41	9	1
42	9	1
43	10	1
44	11	1
45	20	1
46	45	0
47	10	1
48	15	0
49	6	1
50	10	0
51	5	1
52	20	0
53	6	1

54	30	0	16	45
55	9	1	17	10
56	7.5	1	18	15
57	6	1	19	20
58	6.25	1	20	7
59	6.25	1	21	5
60	6.25	1	22	4
61	6.25	1	23	30
62	8.5	1	24	14
63	45	1	25	25
64	85	0	26	50
65	15	1	27	80
66	55	0	28	40
67	15	1	29	20
68	65	0	30	10
69	8.5	1	31	8
70	8	1	32	3
71	7	1	33	20
72	7	1	34	12
73	6	1	35	10
74	7	1	36	8
75	8	1		
76	8.5	1		
77	45	0		
78	30	1		

Figure 1.3E. Sigmoidal Bundles (*n=36)* (Rhy.sig)

Location:
33.2896°, *-114.6324°*

Layer#: Thickness(mm)

1	10
2	12
3	6
4	2
5	3
6	32
7	33
8	9
9	5
10	50
11	30
12	17
13	65
14	20
15	37

APPENDIX B

LITHOFACIES DESCRIPTIONS

Facies Association	Facies	Name and Description	Interpretation
Baal Cobble Lag: Ravinement Surface	**A**	Well-sorted volcaniclastic cobbles distributed as a single-clast horizon (lag deposit) overlying Miocene fan conglomerate. Overlain by mixed carbonate-siliciclastic facies of the Bouse basal carbonate member. Includes bioclastic carbonate sand in poorly to well sorted whitish sandy matrix.	Transgressive ravinement surface formed during initial transgression that flooded the former alluvial basin (e.g., Numedal and Swift 1987; Catuneanu et al., 2011). Water currents winnowed and removed finer sediment, reworking and concentrating cobble clasts on the erosional surface at top of the Miocene alluvial-fan conglomerate. This records the earliest influence of marine inundation at the base of a regionally significant transgressive systems tract.
Matted calc-siltstone: Salt marsh to shallow water	**B**	Recessive, poorly-sorted, weakly laminated to massive carbonate-sandy lime mudstone. Abundant carbonate plant material is the primary constituent. Fine-grained siliciclastic component is <1%. Interfingers and is gradually overlain by Facies C of this association. Locally includes ~7- to 10-cm thick beds of poorly sorted locally-derived granular sandy conglomerate with sharp erosional bases and tops. Carbonate lime mud and sandy carbonate matrix. Clasts angular to sub-rounded, with matrix-supported pebbles concentrated at base. No imbrication.	Matted fine grained carbonate silt and clay deposited by biological trapping (reeds and grasses) in low-energy, supratidal salt marsh environment. Marshes experienced occasional inundation during extra high (spring) high tides and/or or tidal creek floods. Total sedimentation in salt marsh reflects balance between storm and tidal sedimentation. Poorly sorted pebbly beds are likely storm deposits.
	C	Poorly sorted lime-mud-rich carbonate sandstone. Matted lenticular thin beds drape over cobble clasts, displaying pinch-and-swell along bedding planes. Abundant carbonate plant material is the primary constituent. Grassy plant matter concentrated on matted bedding surfaces. Individual carbonate mats are 1 mm to 2 cm thick. Wavy discontinuous, thicker mats have fine mm-scale wavy laminations. Coarser-grained (richer in carbonate sand) and more resistant than the muddier facies of this association (Facies B).	

Basal Cobble Lag: Ravinement Surface	**D**	Golden Gravel: Golden brown to gray green, rounded to sub-rounded, typically well-sorted, coarse siliciclastic sandstone to pebble conglomerate. Tabular cross stratification with cross-bed sets 0.5 to 3 m thick. Primary dips ranging from nearly horizontal to steep foresets (~20-30º). Normally graded and ungraded sandstone beds. Systematic up-slope and down-slope variations in grain size on foresets. Clasts consist primarily of granitic and intermediate plutonic, volcanic breccia, and unwelded volcanic tuff. Matrix is mixed carbonate and siliciclastic sand. Often discontinuous laterally, exhibiting strongly lenticular geometry. Granules to pebbles found locally within grainstone rich heterolithic facies (E–G), as distinct thin beds. Pebble beds 1 to 3 granule to small pebble grains thick, extending laterally from toe of lenticular cross-bedded gravel foresets interbedded with the Heterolithic Association.	Locally sourced gravels transported, reworked, and deposited by migrating gravelly bedforms in wave- and tide-reworked beach ridges, gilbert delta-front lobes, and detached nearshore bars. Pebble beds were transported by high energy storm and rip-tide currents; tidal currents likely sorted and transported fine-grained sediment.
Heterolithic: Tidal Flats & Shallow Subtidal	**E**	Sandy calcarenite and calcarenitic sandstone: White to gray, pale green, and light tan, well-rounded to subrounded, moderately to well-sorted, fine- to-medium- grained, laminated to thick-bedded, admixed carbonate sandstone (calcarenite), calcareous siliciclastic sandstone, and sandy calcarenite. Siliciclastic component ranges from 10% to 70% in the siliciclastic-carbonate mixture. Internal sedimentary structures include asymmetrical and symmetrical ripple cross lamination, trough and tabular cross-bed sets, and parallel lamination overlain by asymmetrical ripples. Interbedded with other facies of the heterolithic association, including lime-mudstone. *Thalassinoides* burrows pass laterally into continuous bioturbated beds of lime mudstone (Facies G).	Intertidal and shallow bottomsets of Gravel Association, upper tidal mudflats, mixed tidal flats, and shallow subtidal bottomsets of tidal dunes of the Grainstone association. Muddy facies represent upper tidal flat carbonate mudflats or low-energy lagoonal. Interbedded sandier facies likely record deposition in tidal flat and shallow subtidal settings. More siliciclastic sand-rich deposits represent proximal bottomsets of gilbert deltas and gravelly bars of the Golden Gravel facies association, while more carbonate sand-rich deposits represent the bottomsets of the grainstone association dunes. Few occurrences of massive, mottled, and bioturbated beds may represent subtidal low-energy lagoonal environments (Laporte, 1971). *Thalassinoides* burrows are commonly formed by burrowing crustaceans in intertidal to shallow subtidal marine environments (Myrow, 1995).
	F	Heterolithic, interbedded silty carbonate clay and marl: White, gray, to light pink. Mm-cm scale laminations to very thin beds that alternate between lime mudstone and mm laminations of either white micrite or pale green siliciclastic clay. Weathers platey. Wavy beds that pinch and swell along bedding planes. Mudcracks common. High silica content locally, concoidal weathering pattern. Sometimes massive and bioturbated with mollusk, bivalve, and barnacle shells preserved. Some in-situ communities of barnacles found.	

Heterolithic: Tidal Flats & Shallow Subtidal	**G**	Lime mudstone with silt–f.g. laminations to thin beds with, wavy, flaser, and lenticular bedding. Starved ripples common. Distinct beds with abundant *Thalassinoides* burrows present (trace fossil I.D. by Steve Hasiotis). Includes horizontal f.g sand and carbonate mud rhythmites. Abundant stacked, wavy, lenticular and flaser bedding in a well-sorted and segregated silt and clay that display mm– to cm-scale alternations with lime mud. Close association with the grainstone facies association.	Heterolithic bedding likely represents deposition in low to middle intertidal setting and offshore subtidal resulting from declining current energy and decrease in the sand to mud ratio laterally and are common to ancient tidal deposits (Demicco and Hardie, 1994; Ghomashi, 2008; Lasemi, 1986; Lasemi et al., 2008). Sandy facies exhibit graded bedding and vertical transitions from upper-plane-bed parallel lamination to ripple-cross lamination providing strong evidence for deposition under decelerating flow, perhaps tide-controlled. Starved ripples form when a layer of sand under traction transport has an insufficient sediment supply or the current strength was too low to create a complete bedform. Sparse presence of golden gravel association thin pebble beds point to storm conditions. Storm lags are gravels transported during storms and laterally spread out into sheets over fine sediment (Brenner and Davies, 1973). The nearly complete lack of scattered course-grained sediment in the heterolithic deposits with which the pebble beds are deposited clearly indicates lateral transport of coarse-grained sediment from gravel-rich adjacent environments and not winnowing of gravel-rich sediment.
Grainstone: Tidal Dunes and Bars	H	Bioclastic barnacle and oncoid sandy grainstone to grainstone hash: Tan brown weathered, white to gray fresh. Coarse to very coarse, rounded to well-rounded, well-sorted barnacle and oncoid shell fragments. Steep forests dip ~30º at top of massive (up to ~3 m tall) crossbed sets. Bedding dips shallow laterally into flat-lying equivalent bottomsets. These grade laterally into small scale asymmetrical ripples with lime mud drapes (Facies I).Those pass laterally into heterolithic sand-to mud rhythmites with flaser, wavy, and lenticular bedding of the heterolithic association (Facies F).	Sedimentary structures of this association display many criteria for recognition of tide-dominated deposits. They include: (1) lateral bundle/bottomset thickness variation; (2) bundle thickness variation that tracks cyclic astronomical cycles; (3) common reactivation surfaces with reverse ripples; and (4) common opposing bidirectional paleocurrents (Nio and Yang, 1991).

Grainstone: Tidal Dunes and Bars	H	Locally cross-bedded foresets alternate between tan–white bioclastic grainstone hash with <5% silicliclastic sediment, and tan–gray fine grainstone with ~30% siliciclastic sediment. Grainstone hash is more resistant to weathering, and gray fine grainstone is poorly indurated and recessive. Massive cross-bed sets have abundant more gently dipping (~15-25º) erosive reactivation surfaces with up-dip migration of ripples. Locally ~10–15 cm thick, and up to 80 cm long sigmoidal tidal bundles with alternating thin and thick sigmoidal interbeds of grainstone hash and fine grainstone. Thin sigmoidal interbeds pass laterally into thick bottomsets, and thick sigmoidal interbeds may have thin or truncated, unpreserved bottomsets. Massive crossbed sets and sigmoidal tidal bundles have consistent paleocurrent directions toward the west on the east side of the basin, and to the east on the west side of the basin. Bimodal-bipolar paleocurrents are locally present, but rare, Strong unimodal small-trough crossbedding on top of bedding planes oriented at 90º toward the south-southwest. Sedimentary structures are well-exposed and include: (1) ripple cross lamination; (2) trough cross-bedding; (3) parallel lamination; (4) marl intraclasts; (7) lateral offshooting and bedform discordancy; and (8) bundled-upbuilding ripple lamination geometries. This facies is typically composed of >90% biological carbonate material, and the siliciclastic component is generally <20%, but when preset is commonly comprised of granules to small pebble siliciclastic grains. Grainstone facies are interbedded and laterally into lateral facies equivalents of packstone to wackestone. Sparse interbedded *Thalassinoides* burrows.	Massive crossbed sets of alternating thin and thick grainstone hash and fine grainstone are interpreted to record deposition by migrating dunes and tidal bars, with systematic hydraulic sorting of carbonate and siliciclastic sediment by tidal currents, under the influence of cyclic solar cycles. Reactivation surfaces are common in megaripple cross-bed sets, and are characteristic of alternating, but unequally strong tidal currents (Boersma, 1969; Klein, 1970). Bimodal-bipolar paleocurrents reflect a weak flood tidal current. Troughs oriented at 90º to primary migration of 2D large-scale bedforms may represent late-stage emergence ripples. It is curious, however, why trough paleocurrents are unimodal toward the south-southwest. Lateral bottomset thickness variations are commonly observed. The process interpretation of thickening and thinning of bottomsets is as follows: during spring tides, the strong dominant current will have erosional ¬power in the trough, producing a deep trough in front of the migrating ripple that results in poorly-developed bottomsets. Conversely, during neap tides, weaker currents decrease the erosional power of the bottom vortex, favoring the formation of well-developed bottomsets (Nio and Yang, 1991). Packstone and wackestone represent lower-energy equivalents of high energy barnacle tidal dunes and bars. Prominent current indicators toward the basin center reflect deposition by ebb-dominated tidal dunes.
	I	Pink, tan, white, v.f.g. to f.g. mixed-carbonate and siliciclastic sand (~50:50). Small scale, bimodal-bipolar, asymmetrical ripples in fine grainstone. Ripple crests are rarely preserved. Abundant small scale reactivation surfaces with lime mudstone drapes. Interbedded with 3–4 cm of continuous parallel laminated fine grainstone beds with fossil hash and laminated very thin beds of white carbonate clay and silty clay.	
	J	Wackestone and packstone barnacle oncoid hash. 5–12 cm thick beds of white, pale green, poorly sorted, unstratified to weakly stratified packstone and wackestone. Lateral equivalents of bioclastic barnacle and oncoid sandy grainstone to grainstone hash.	

Lime Mudstone: subtidal, offshore	**K**	Lime mudstone (marl 2). Clay rich, silt-sized lime component is uncommon. Interbedded carbonate paper shale thin beds (3–10cm) of very thinly laminated (1–3mm) clay and thick massive beds of white marl with no internal structure and laminations. Clams, fish fossils, snails, and ostracodes common in more massive bioturbated beds. Fauna is sparse in thinly laminated paper shale beds. More bioturbated, fauna rich-beds create more blubby resistant weathering, while more carbonate paper shale beds are easily eroded and weather recessively. Top of lime mudstone defines (in many localities) a gradual transition to green claystone of the siliciclastic unit.	Subtidal lime-mudstone with deposition by suspension settling and slow fallout of carbonate from ambient water column.

APPENDIX C

BOUSE FORMATION MEASURED SECTIONS

Measured Section Key

MEMBERS

Upper Bioclastic Member

Siliciclastic Member

Basal Carbonate Member

Mfg: Miocene Conglomerate

LITHOLOGY

Qt conglomerate

Conglomerate (locally with carb.)

Sandstone

Mudstone

Claystone

Carbonate (locally with silic.)

xxxxx Ash

FACIES

UL1-4	Upper Bioclastic Limestone*
CRS	Colorado River Sand**
CRM	Colorado River Red Mudstone**
CRC	Colorado River Green Claystone**
M2	Offshore Association
BH	Grainstone Association (Barnacle Hash)
Het	Heterolithic Association
GG	Gravel Association (Golden Gravel)
SM	Salt Marsh Association
CG	Miocene Conglomerate
TU	Tufa
CH	Charophyte

* Facies descriptions in O'Connell et al., 2016 DS

** Facies descriptions in Homan, 2014

Measured Section Key

SEDIMENTARY STRUCTURES and BIOLOGY

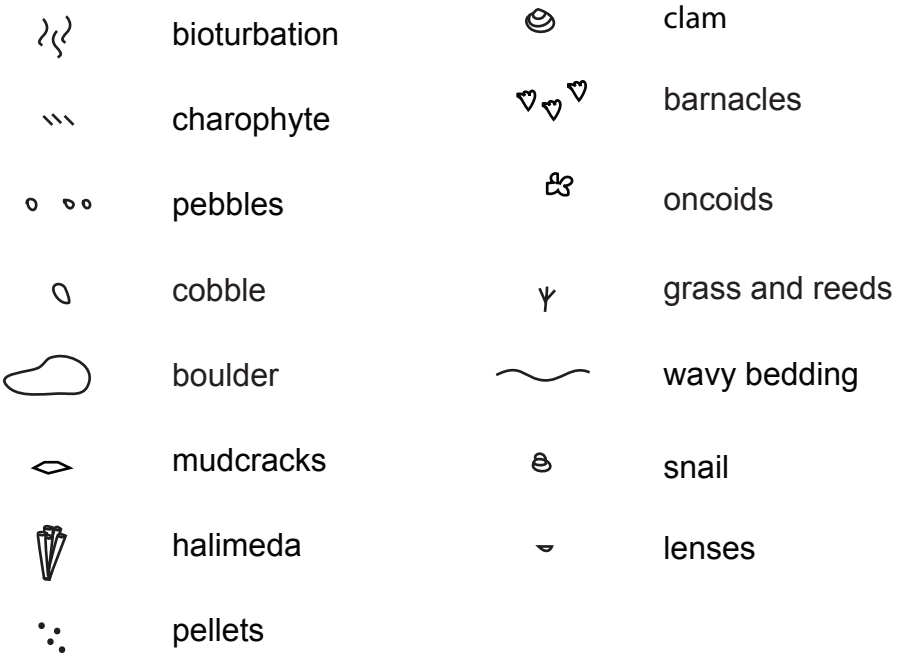

Note. Sections measured in 2015 use clay, silt, fine-grained sand to coarse-grained sand, granule, pebble, and cobble grain size indicators on the measured section scale. A rock with a primary component of carbonate (>50%) is indicated by a white background where a siliciclastic rock is designated by specific lithologic patterns, as indicated in the ‘measured section key’.

Sections measured in 2016 use the Dunham classification (lime mudstone, wackestone, packstone, grainstone) *only* for the grainstone association (BH). Other facies associations are classified using the 2015 convention.

Section 1

Start N 33.255487
W -114.640378
elev. 96 m

End N 33.25549
W -114.64043
elev. 119 m

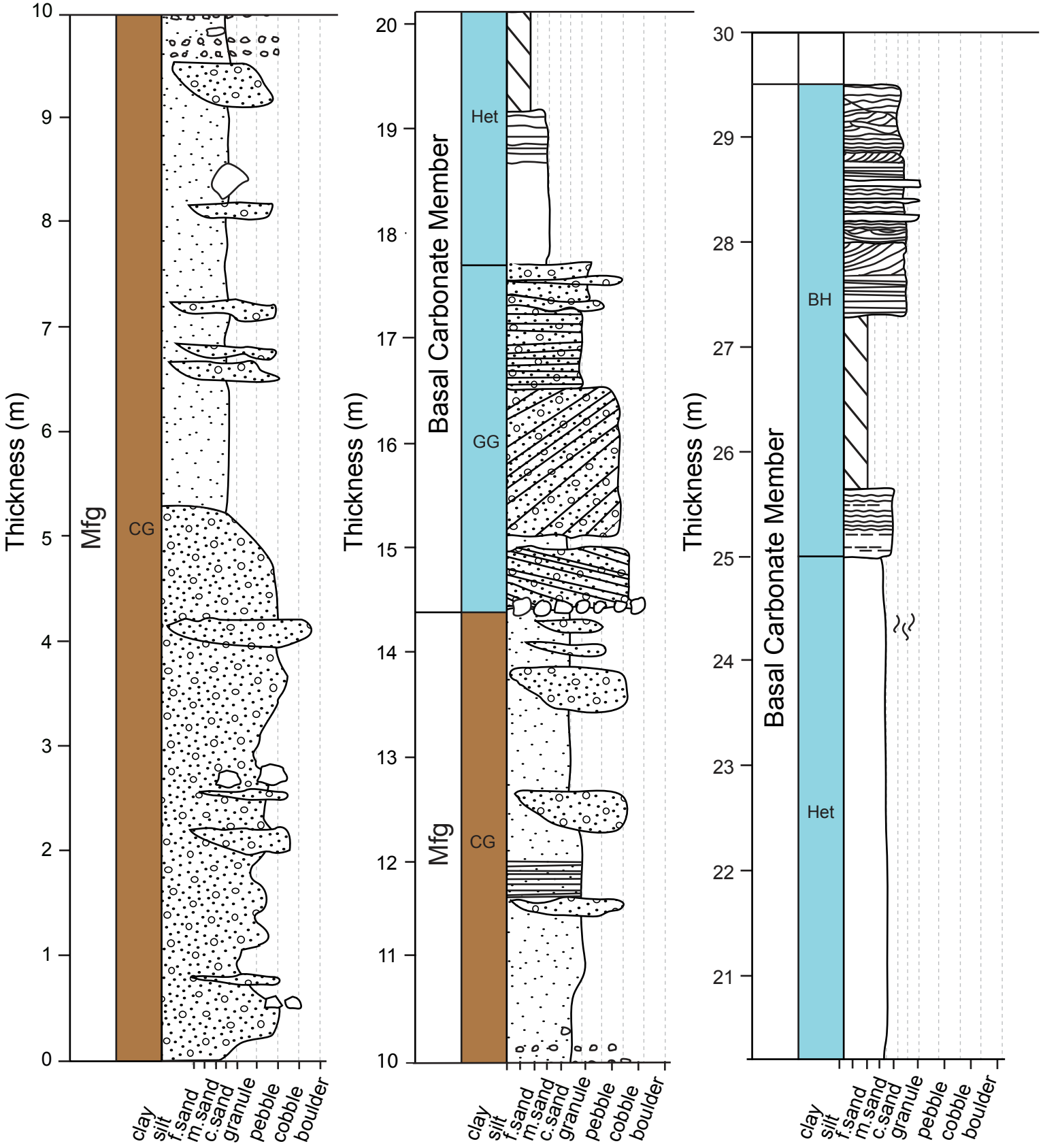

Section 2

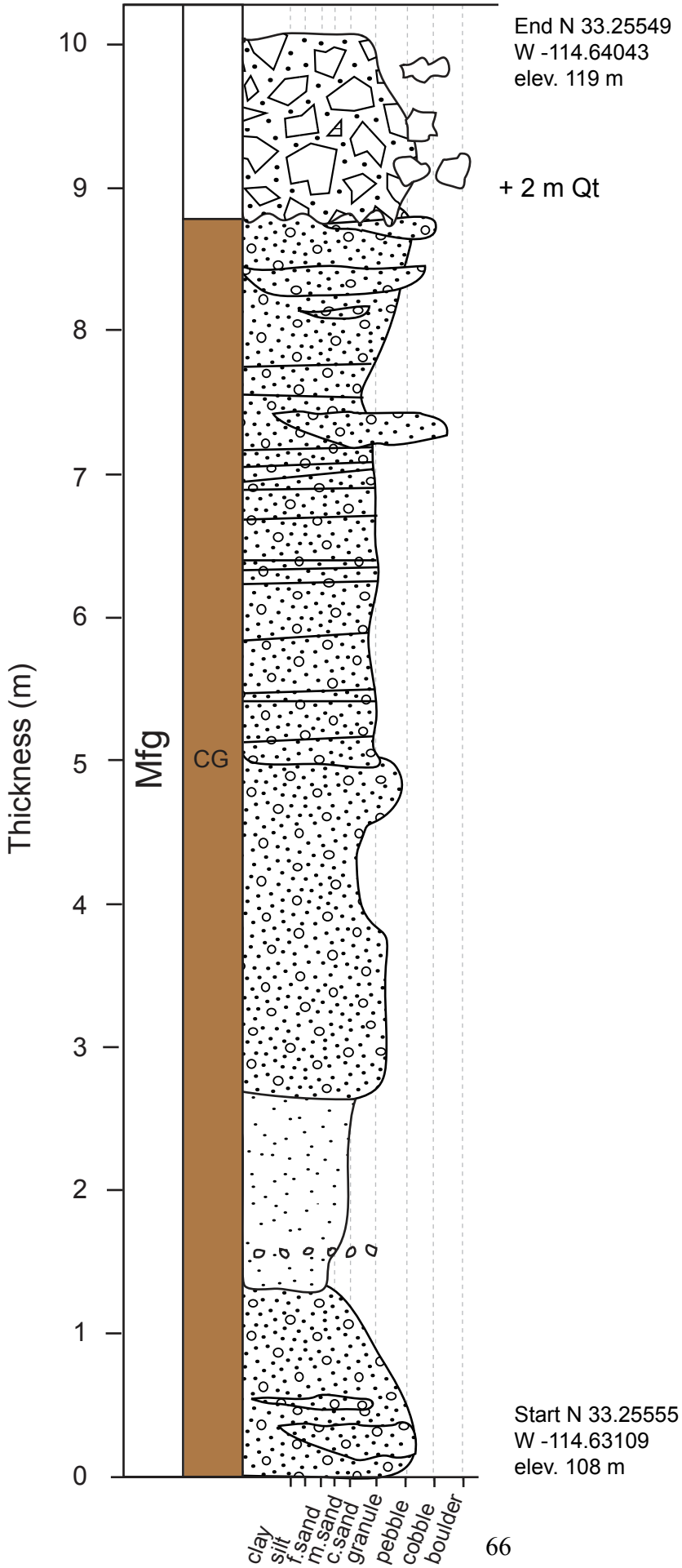
End N 33.25549
W -114.64043
elev. 119 m
+ 2 m Qt
Thickness (m)
10
9
8
7
6
5
4
3
2
1
0
Mfg
CG
Start N 33.25555
W -114.63109
elev. 108 m
clay
silt
f.sand
m.sand
c.sand
granule
pebble
cobble
boulder

Section 3

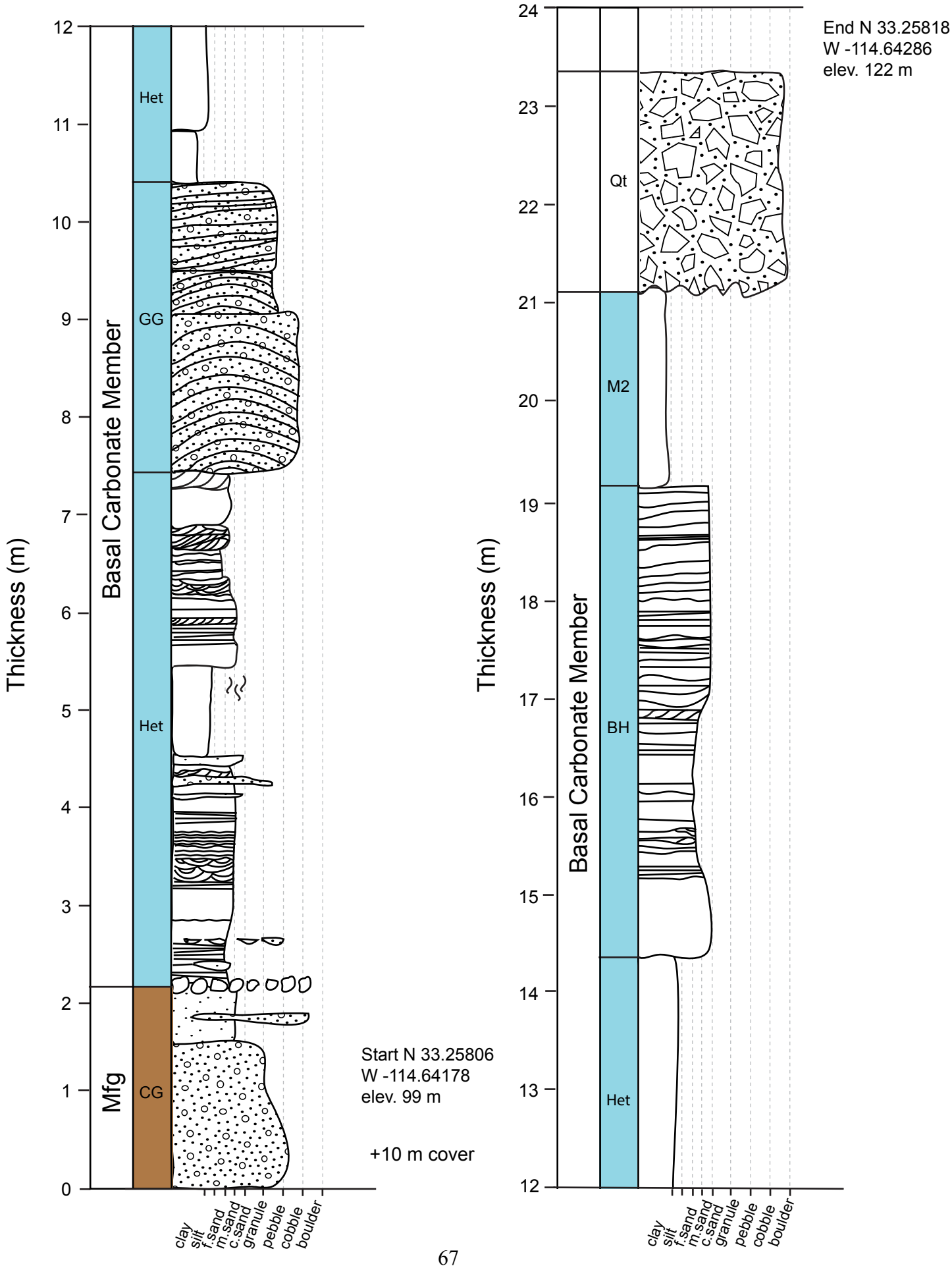
Thickness (m)
Basal Carbonate Member
Mfg
Het
GG
Het
CG
Qt
M2
BH
Het
clay
silt
f.sand
m.sand
c.sand
granule
pebble
cobble
boulder
Start N 33.25806
W -114.64178
elev. 99 m
+10 m cover
End N 33.25818
W -114.64286
elev. 122 m

Section 4

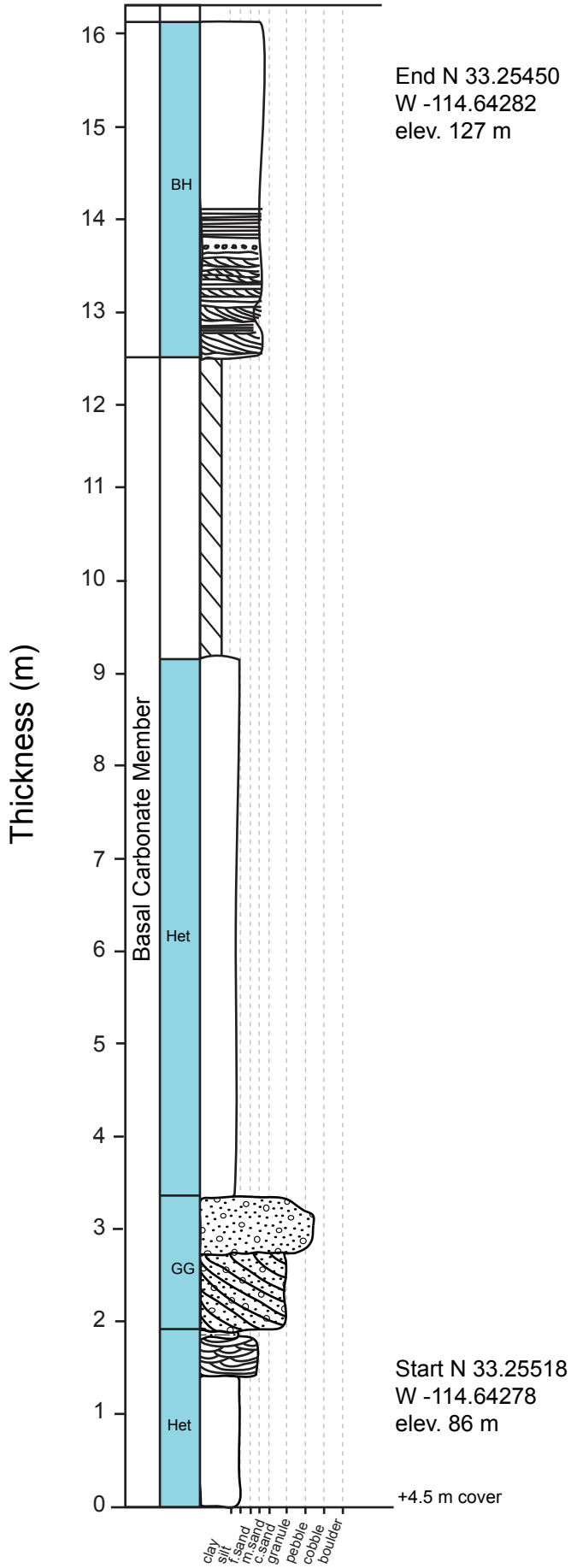
Thickness (m)
16
15
14
13
12
11
10
9
8
7
6
5
4
3
2
1
0
Basal Carbonate Member
BH
Het
GG
Het
End N 33.25450
W -114.64282
elev. 127 m
Start N 33.25518
W -114.64278
elev. 86 m
+4.5 m cover
clay
silt
f.sand
m.sand
c.sand
granule
pebble
cobble
boulder

Section 5

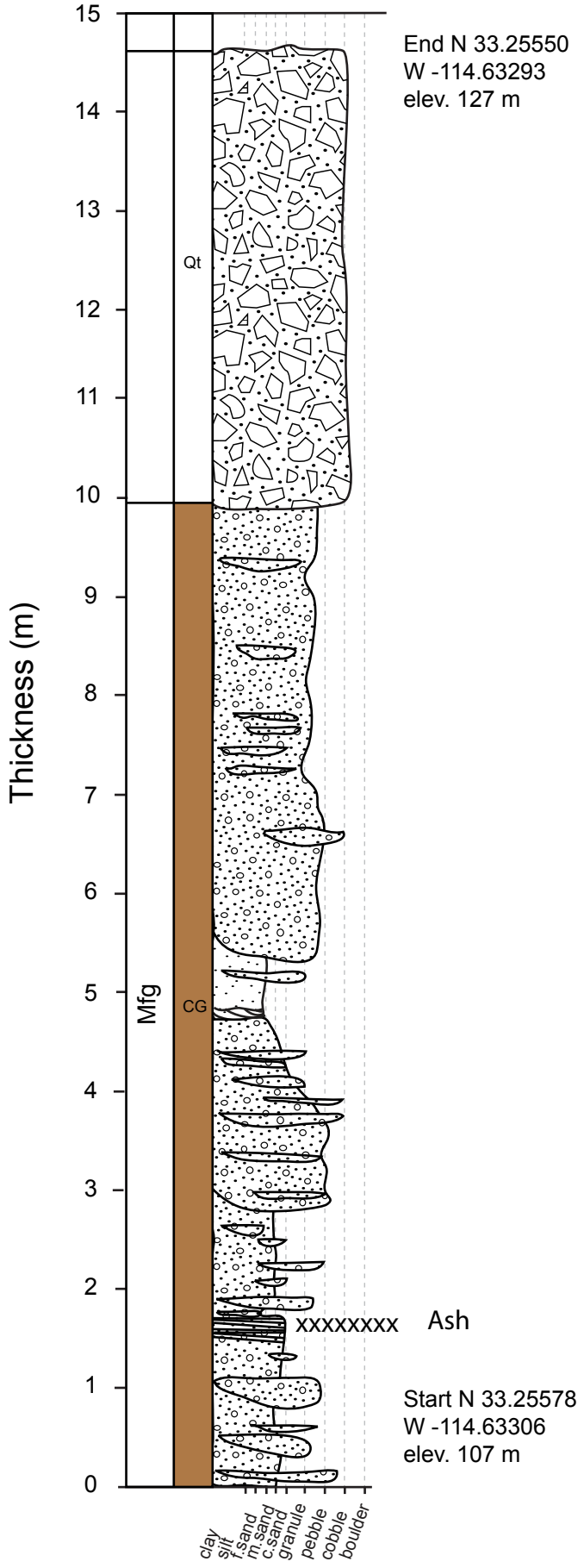
End N 33.25550
W -114.63293
elev. 127 m
Qt
Mfg
CG
xxxxxxxx
Ash
Start N 33.25578
W -114.63306
elev. 107 m
Thickness (m)
15
14
13
12
11
10
9
8
7
6
5
4
3
2
1
0
clay
silt
f.sand
m.sand
c.sand
granule
pebble
cobble
boulder

Section 6

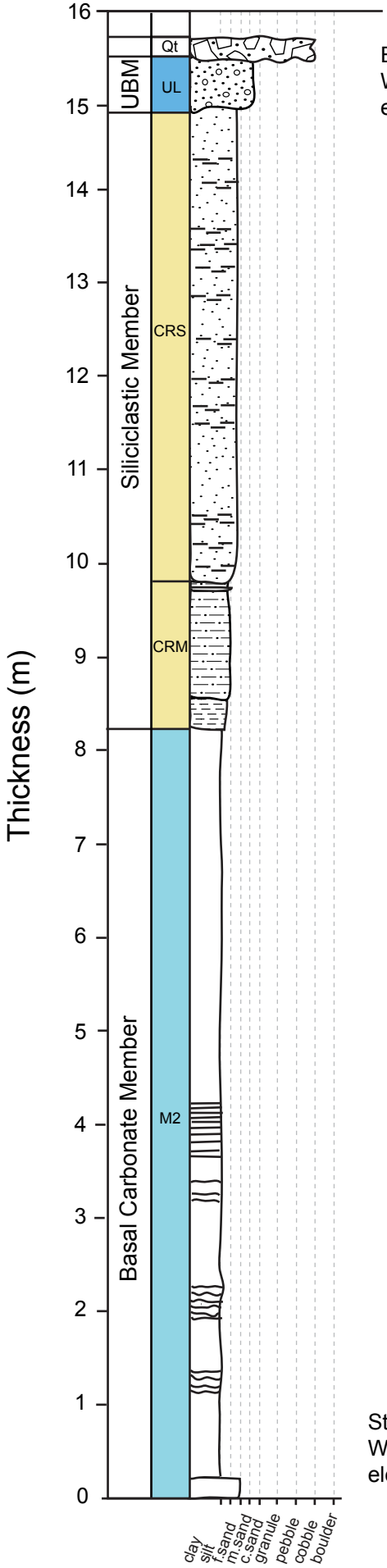

End N 33.26394
W -114.63590
elev. 120 m

Start N 33.26369
W -114.63579
elev. 108 m

Section 7

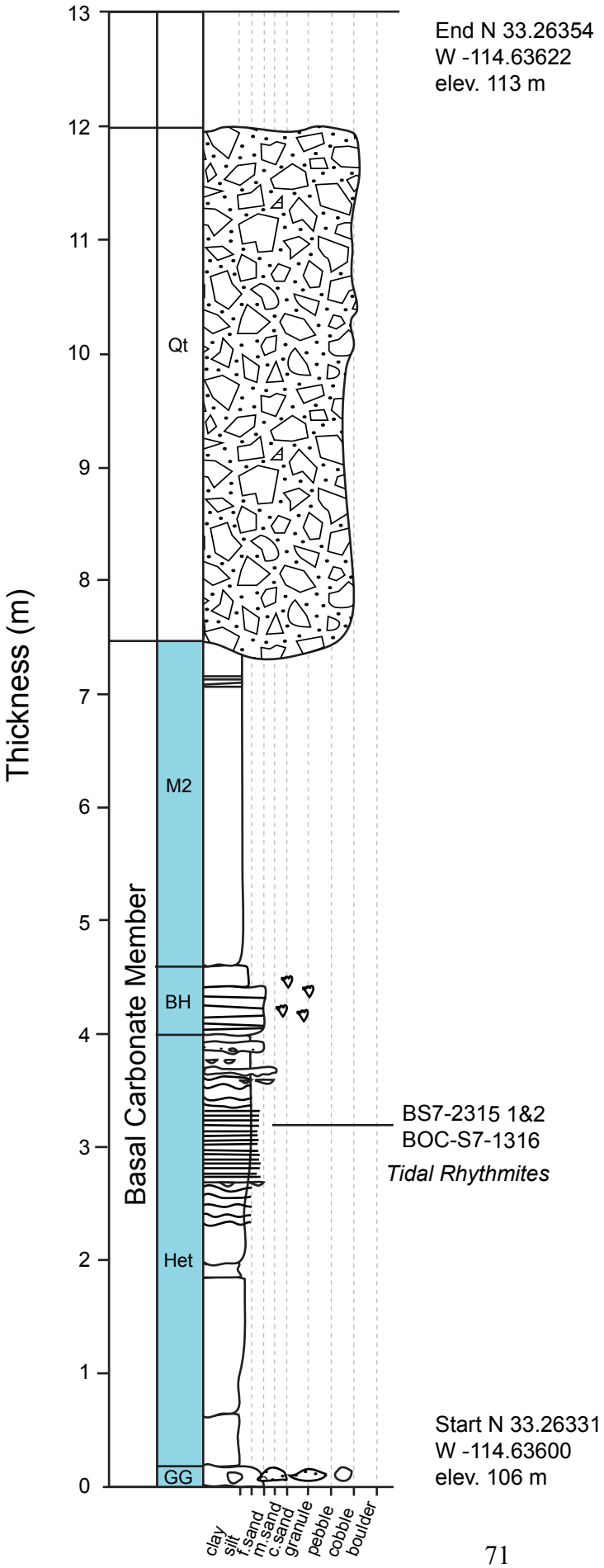
End N 33.26354
W -114.63622
elev. 113 m
Thickness (m)
13
12
11
10
9
8
7
6
5
4
3
2
1
0
Qt
M2
BH
Het
GG
Basal Carbonate Member
BS7-2315 1&2
BOC-S7-1316
Tidal Rhythmites
Start N 33.26331
W -114.63600
elev. 106 m
clay
silt
f.sand
m.sand
c.sand
granule
pebble
cobble
boulder

Section 8

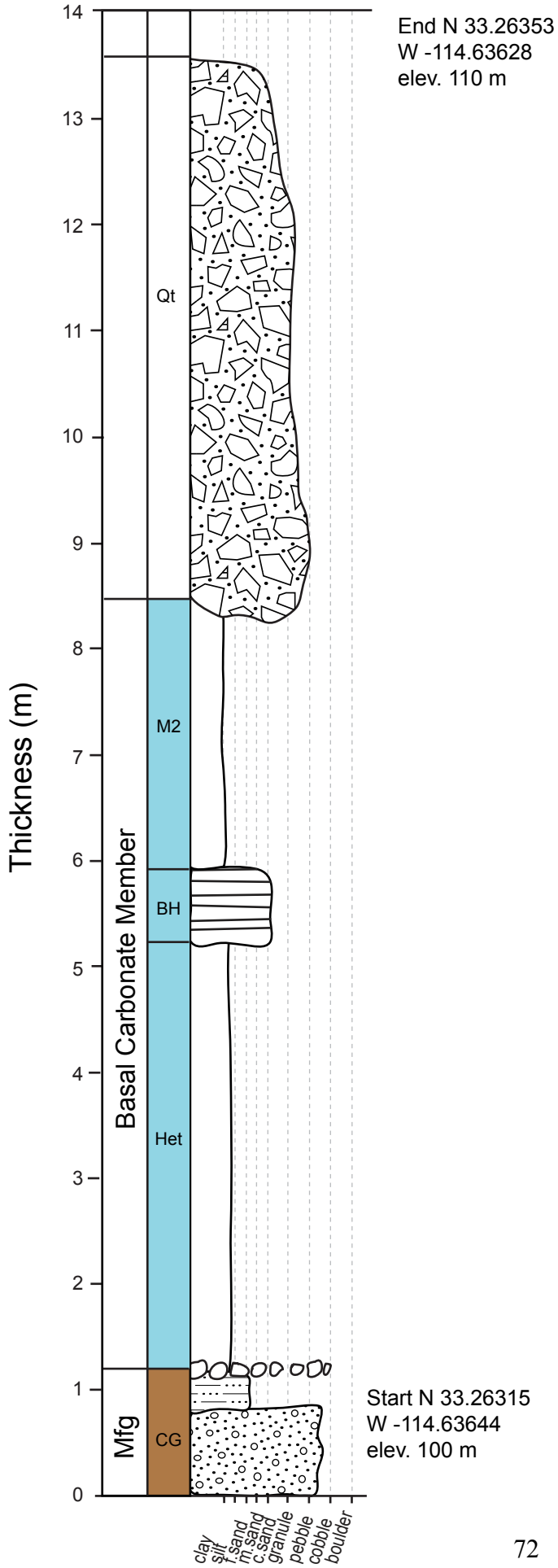
End N 33.26353
W -114.63628
elev. 110 m
Start N 33.26315
W -114.63644
elev. 100 m
Thickness (m)
Basal Carbonate Member
Mfg
Qt
M2
BH
Het
CG
clay
silt
f.sand
m.sand
c.sand
granule
pebble
cobble
boulder

Section 9

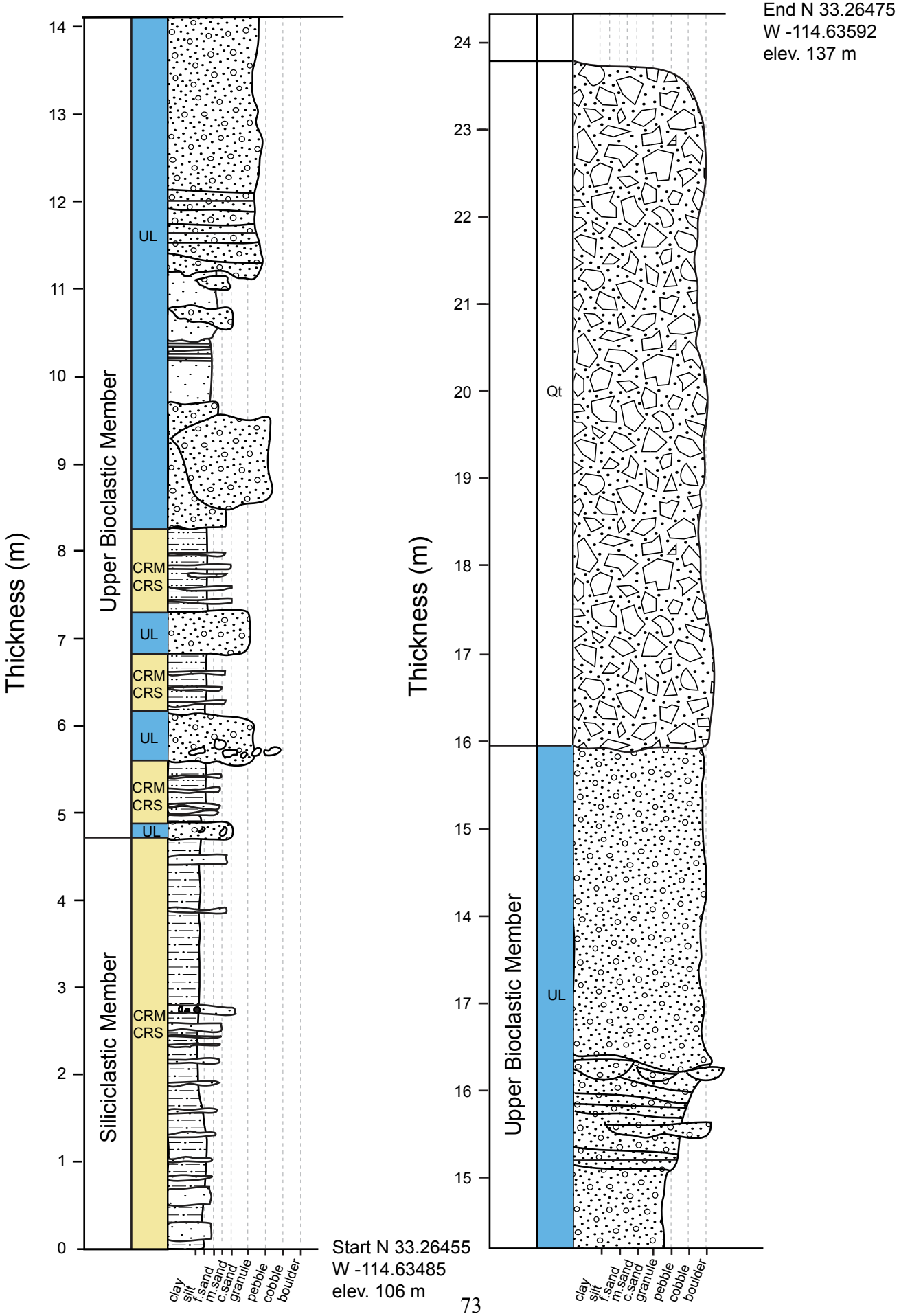

Start N 33.26455
W -114.63485
elev. 106 m

End N 33.26475
W -114.63592
elev. 137 m

Section 10

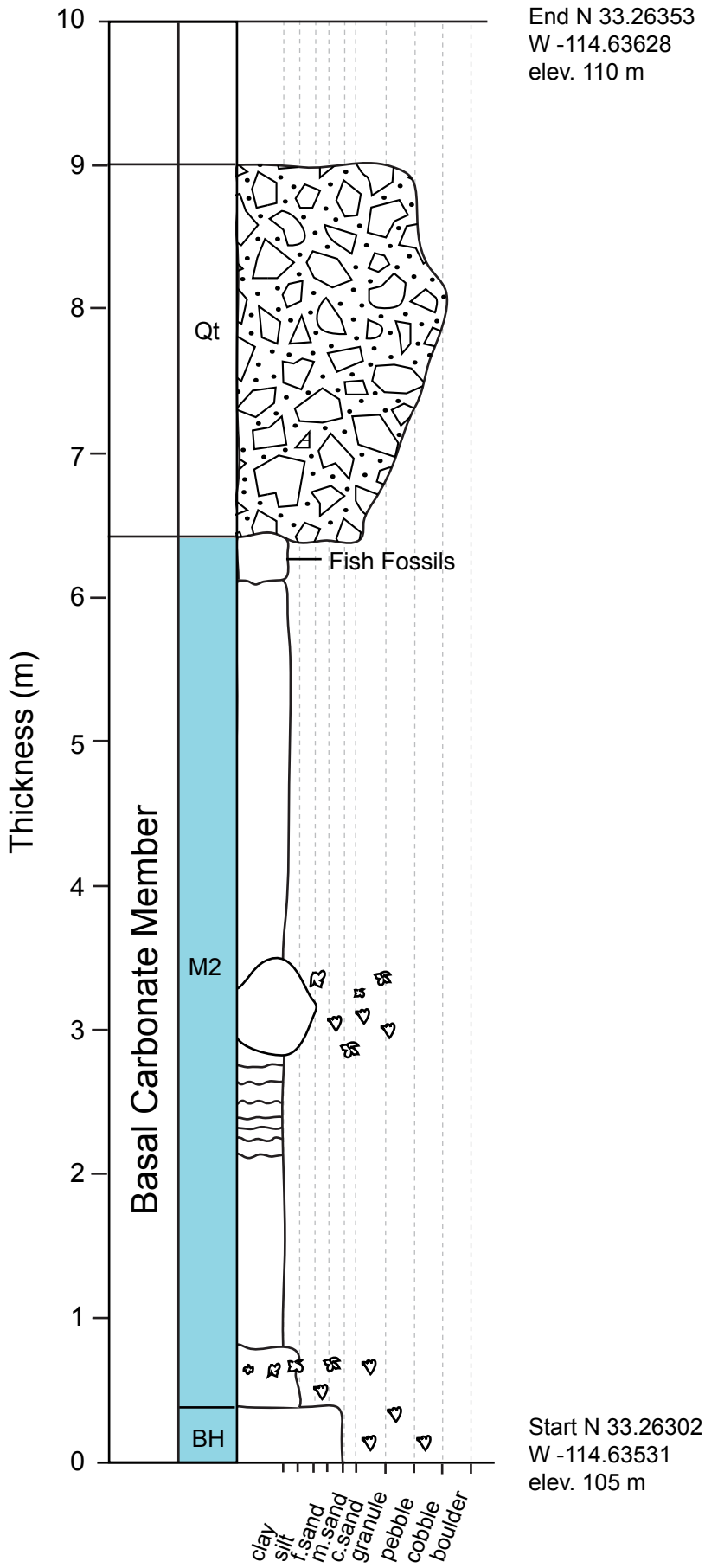
End N 33.26353
W -114.63628
elev. 110 m
Thickness (m)
10
9
8
7
6
5
4
3
2
1
0
Qt
Fish Fossils
Basal Carbonate Member
M2
BH
clay
silt
f.sand
m.sand
c.sand
granule
pebble
cobble
boulder
Start N 33.26302
W -114.63531
elev. 105 m

Section 11

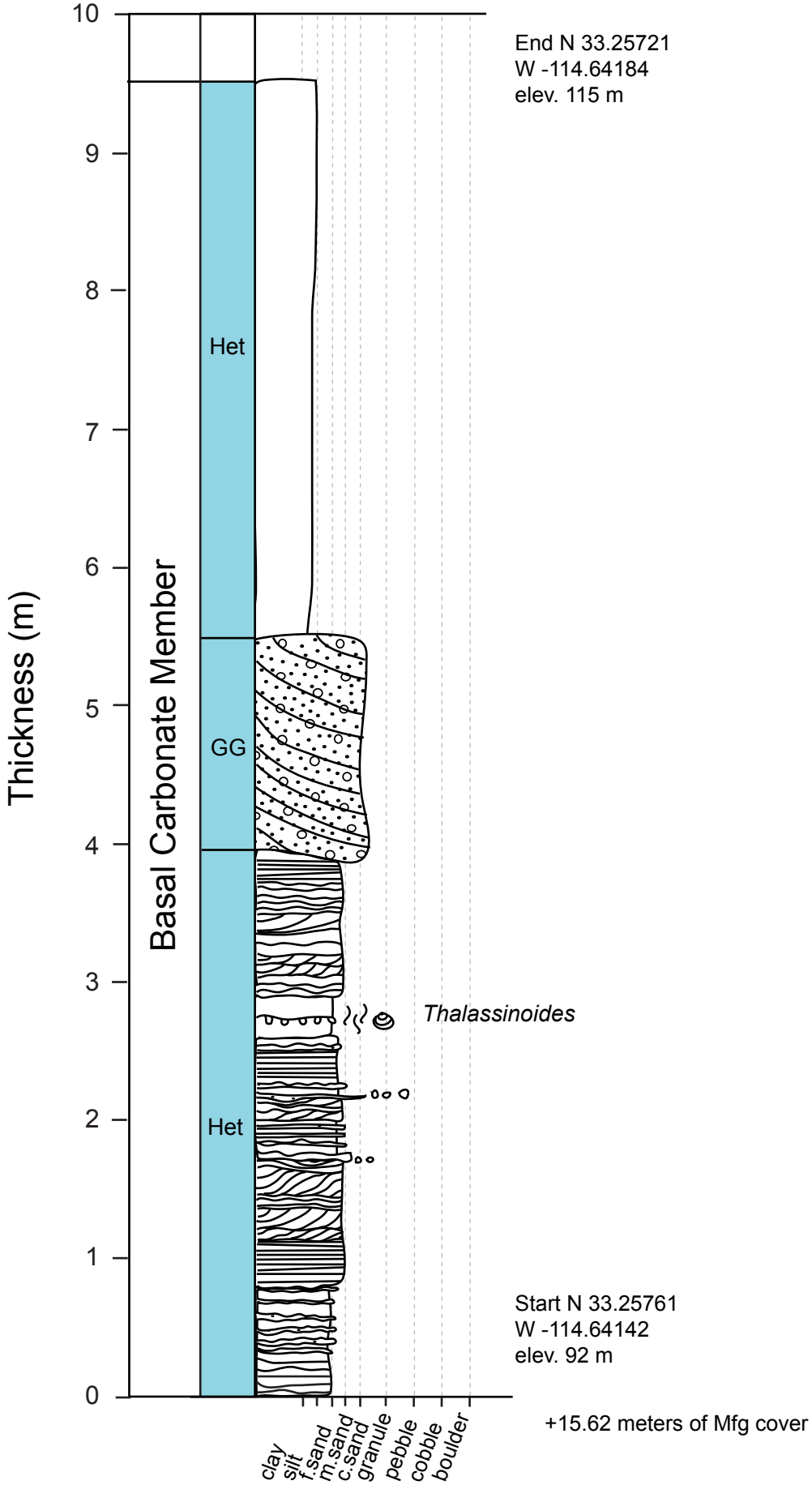

End N 33.25721
W -114.64184
elev. 115 m

Start N 33.25761
W -114.64142
elev. 92 m

+15.62 meters of Mfg cover

Section 12

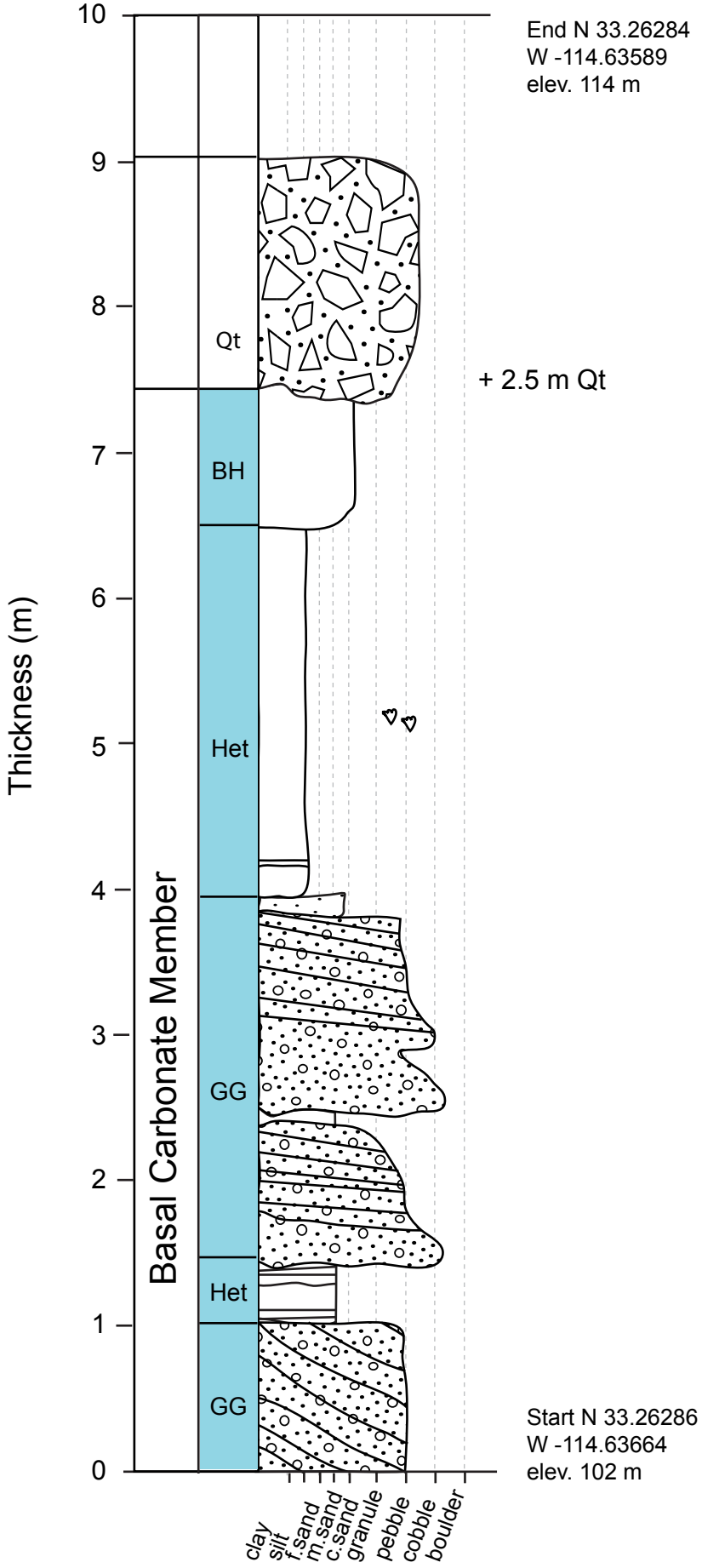
End N 33.26284
W -114.63589
elev. 114 m
+ 2.5 m Qt
Start N 33.26286
W -114.63664
elev. 102 m
Thickness (m)
Basal Carbonate Member
Qt
BH
Het
GG
Het
GG
10
9
8
7
6
5
4
3
2
1
0
clay
silt
f.sand
m.sand
c.sand
granule
pebble
cobble
boulder

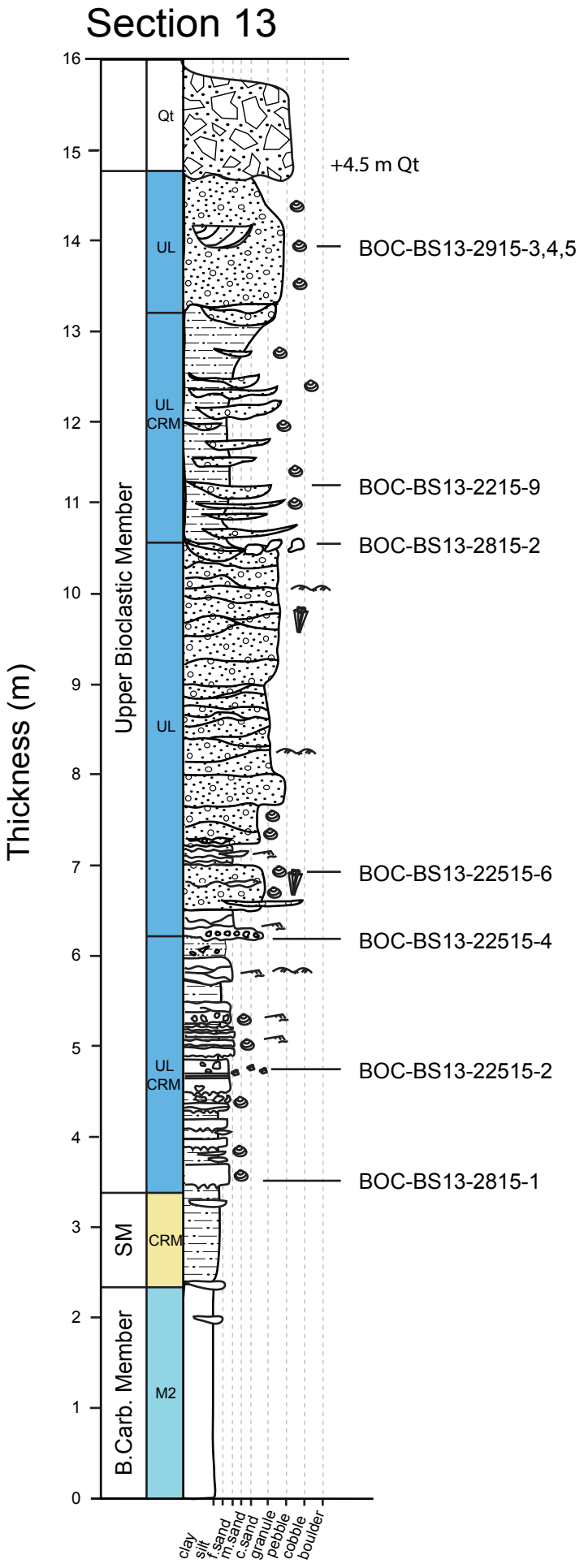
Section 13
Thickness (m)
16
15
14
13
12
11
10
9
8
7
6
5
4
3
2
1
0
Qt
UL
UL
CRM
UL
UL
CRM
CRM
M2
Upper Bioclastic Member
SM
B.Carb. Member
+4.5 m Qt
BOC-BS13-2915-3,4,5
BOC-BS13-2215-9
BOC-BS13-2815-2
BOC-BS13-22515-6
BOC-BS13-22515-4
BOC-BS13-22515-2
BOC-BS13-2815-1
clay
silt
f.sand
m.sand
c.sand
granule
pebble
cobble
boulder

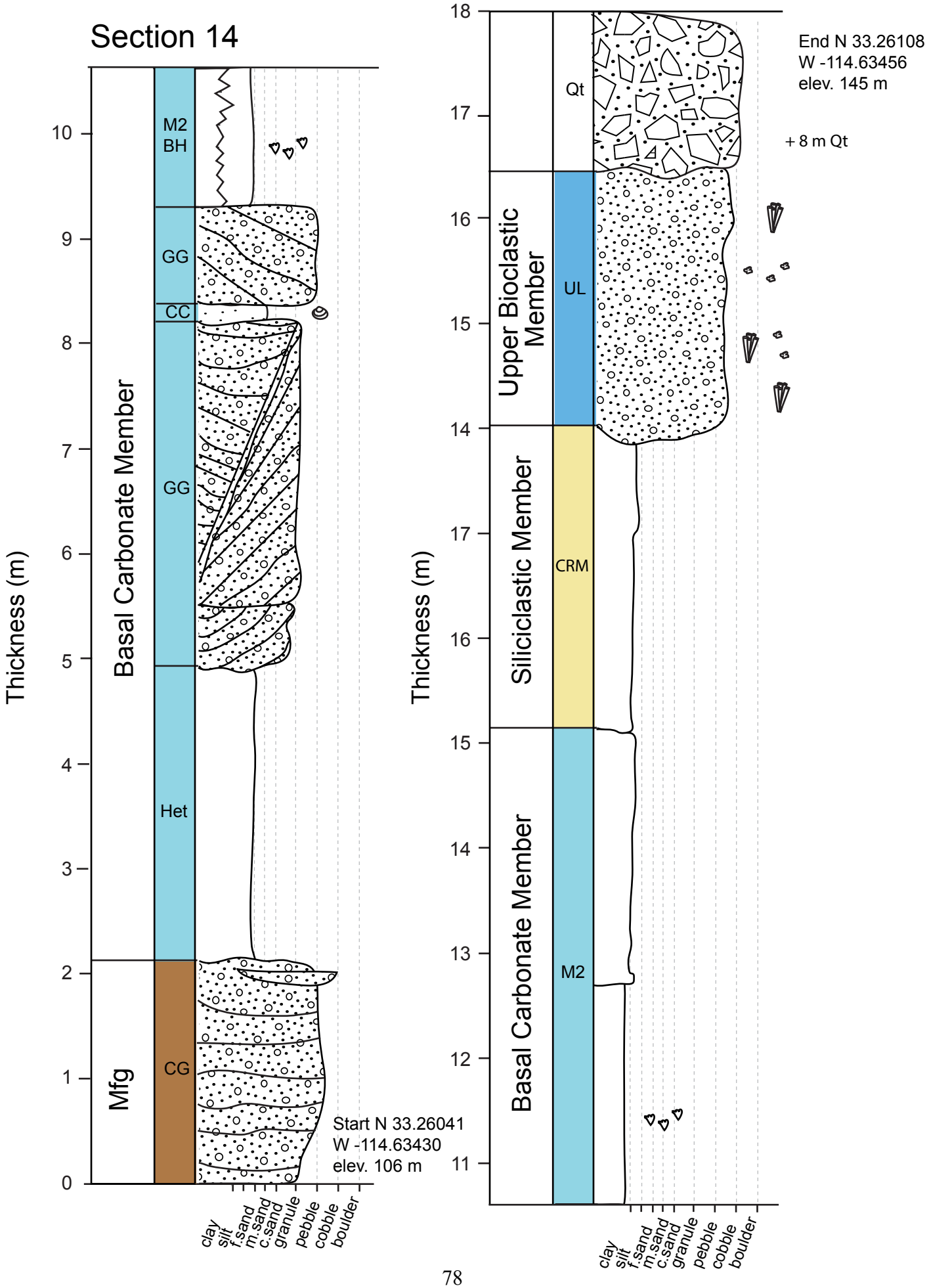
Section 14
Thickness (m)
Basal Carbonate Member
Mfg
M2
BH
GG
CC
GG
Het
CG
Start N 33.26041
W -114.63430
elev. 106 m
clay
silt
f.sand
m.sand
c.sand
granule
pebble
cobble
boulder
Thickness (m)
Qt
Upper Bioclastic Member
UL
Siliciclastic Member
CRM
Basal Carbonate Member
M2
End N 33.26108
W -114.63456
elev. 145 m
+ 8 m Qt
clay
silt
f.sand
m.sand
c.sand
granule
pebble
cobble
boulder

Section 15

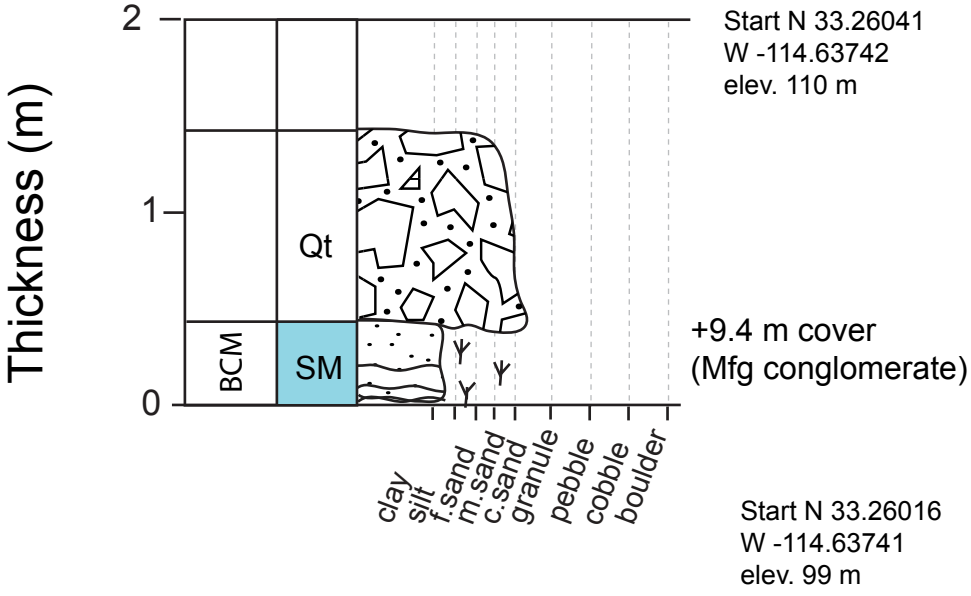
Thickness (m)
2
1
0
Qt
BCM
SM
clay
silt
f.sand
m.sand
c.sand
granule
pebble
cobble
boulder
Start N 33.26041
W -114.63742
elev. 110 m
+9.4 m cover
(Mfg conglomerate)
Start N 33.26016
W -114.63741
elev. 99 m

Section 16

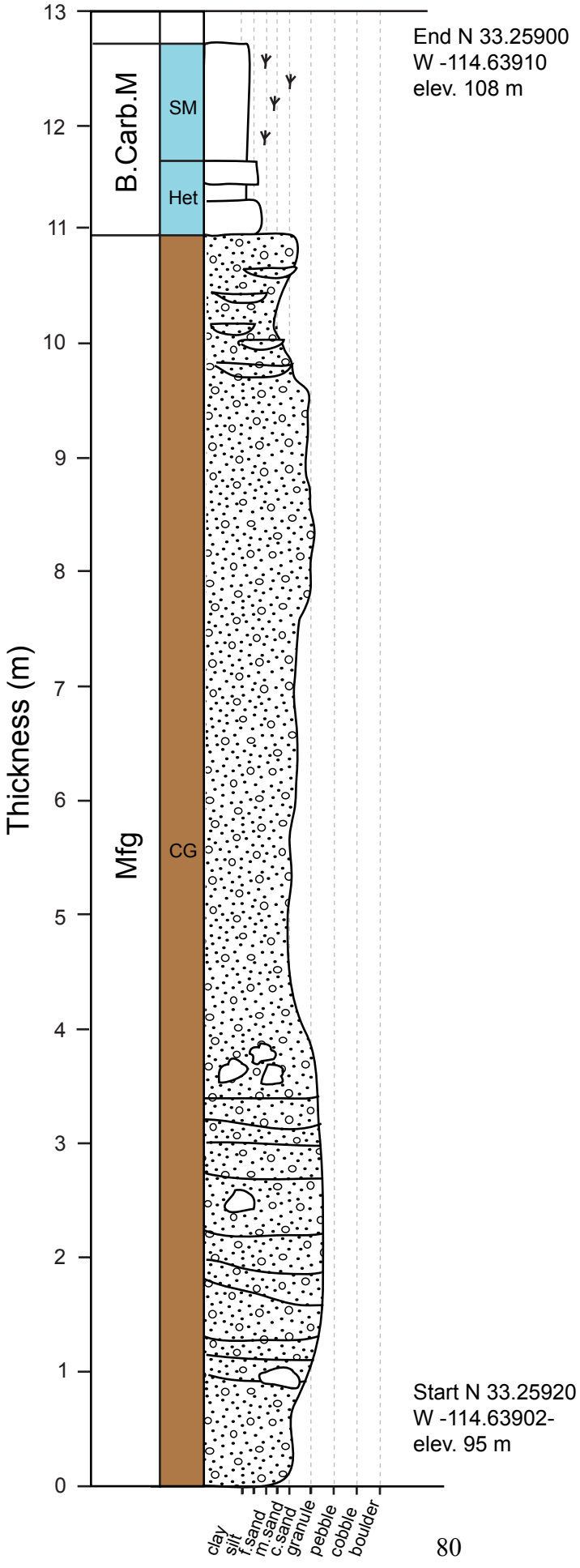
Thickness (m)
13
12
11
10
9
8
7
6
5
4
3
2
1
0
B.Carb.M
SM
Het
Mfg
CG
End N 33.25900
W -114.63910
elev. 108 m
Start N 33.25920
W -114.63902-
elev. 95 m
clay
silt
f.sand
m.sand
c.sand
granule
pebble
cobble
boulder

Section 17

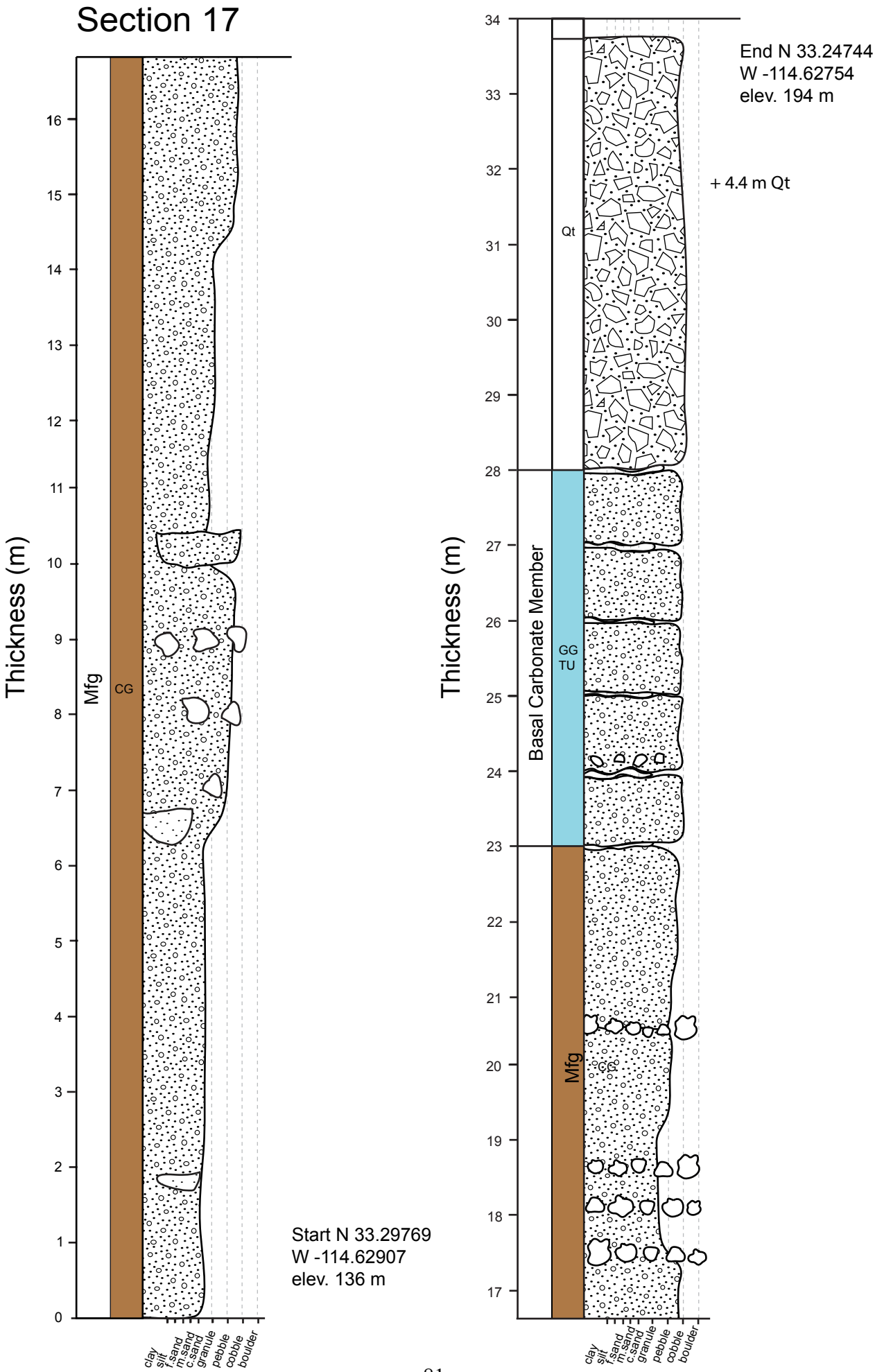

Start N 33.29769
W -114.62907
elev. 136 m

End N 33.24744
W -114.62754
elev. 194 m

+ 4.4 m Qt

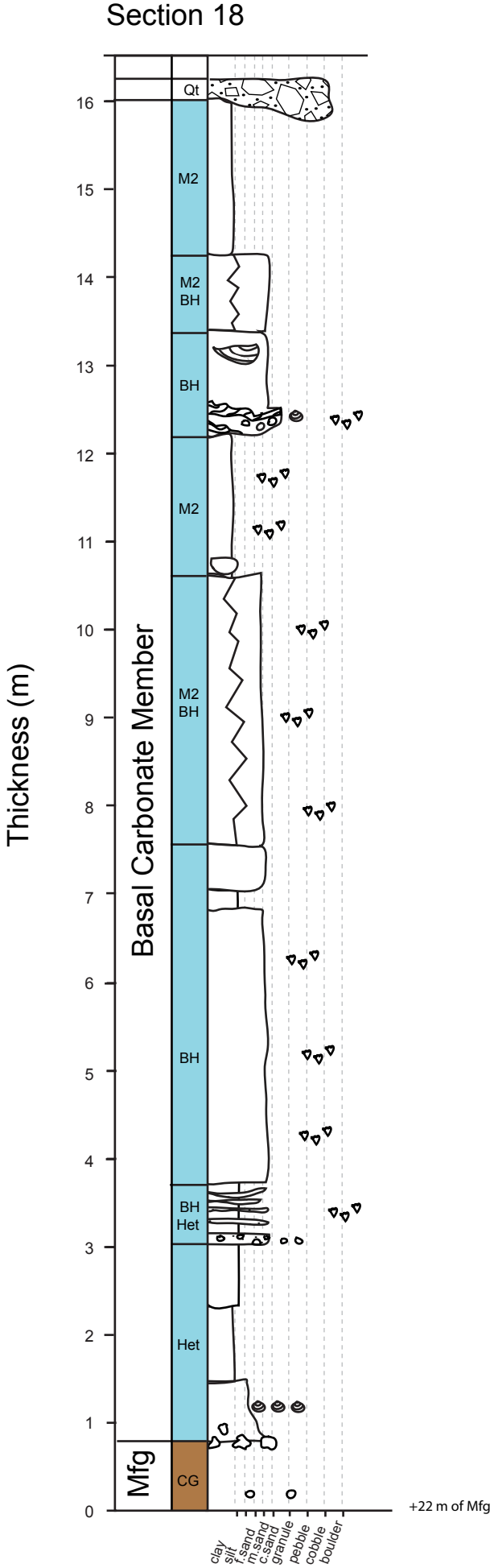
Section 18
Thickness (m)
Basal Carbonate Member
Mfg
Qt
M2
M2
BH
BH
M2
M2
BH
BH
BH
Het
Het
CG
+22 m of Mfg
clay
silt
f.sand
m.sand
c.sand
granule
pebble
cobble
boulder

Section 19

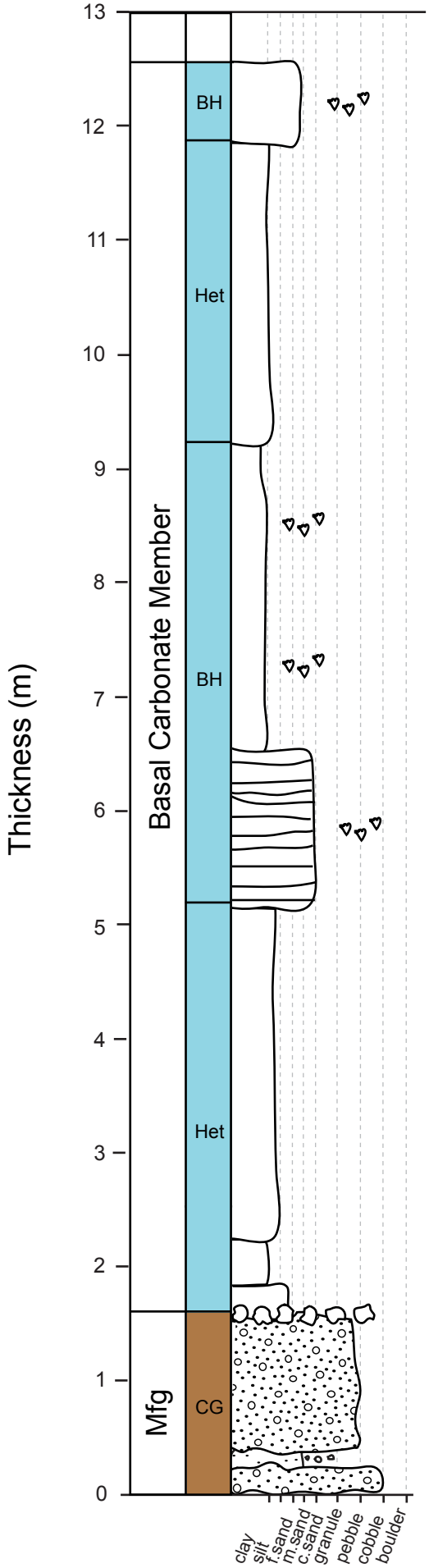

End N 33.25549
W -114.64043
elev. 119 m

Start N 33.25299
W -114.63376
elev. 129 m

+ 5 m Mfg cover

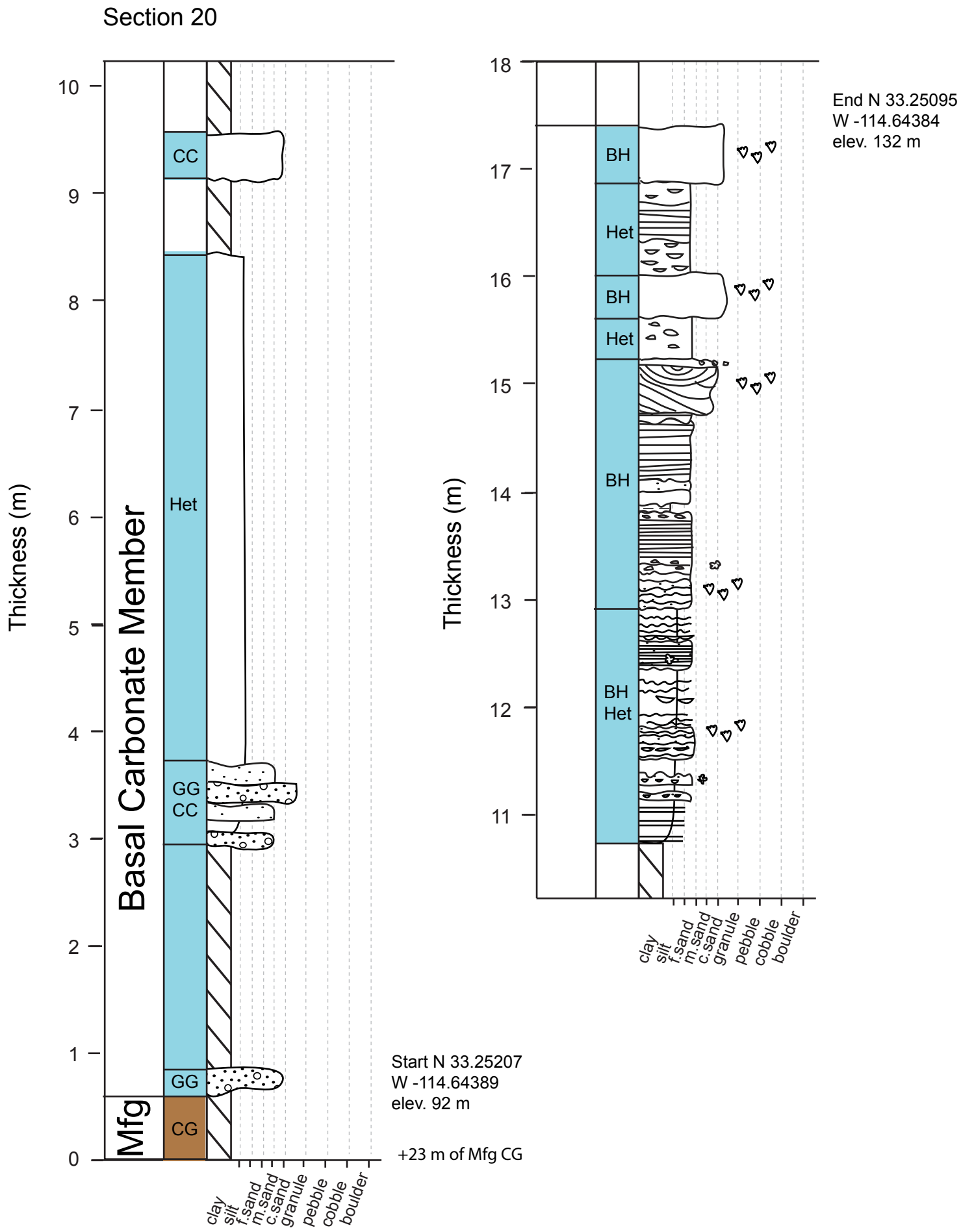
Section 20
Thickness (m)
Basal Carbonate Member
Mfg
CG
GG
Het
CC
GG
CC
BH
Het
BH
Het
BH
BH
Het
clay
silt
f.sand
m.sand
c.sand
granule
pebble
cobble
boulder
Start N 33.25207
W -114.64389
elev. 92 m
+23 m of Mfg CG
End N 33.25095
W -114.64384
elev. 132 m

Section 21

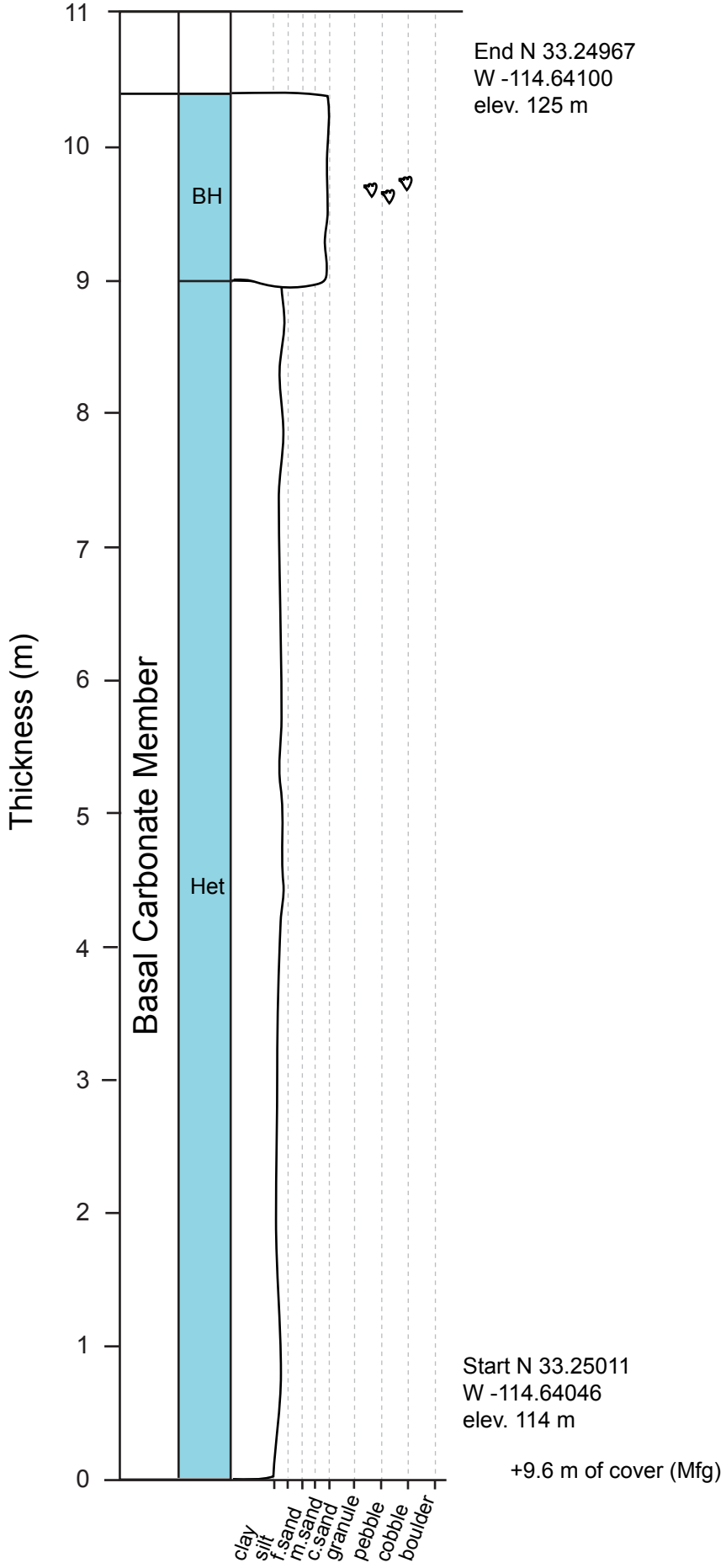

End N 33.24967
W -114.64100
elev. 125 m

Start N 33.25011
W -114.64046
elev. 114 m

+9.6 m of cover (Mfg)

Section 22

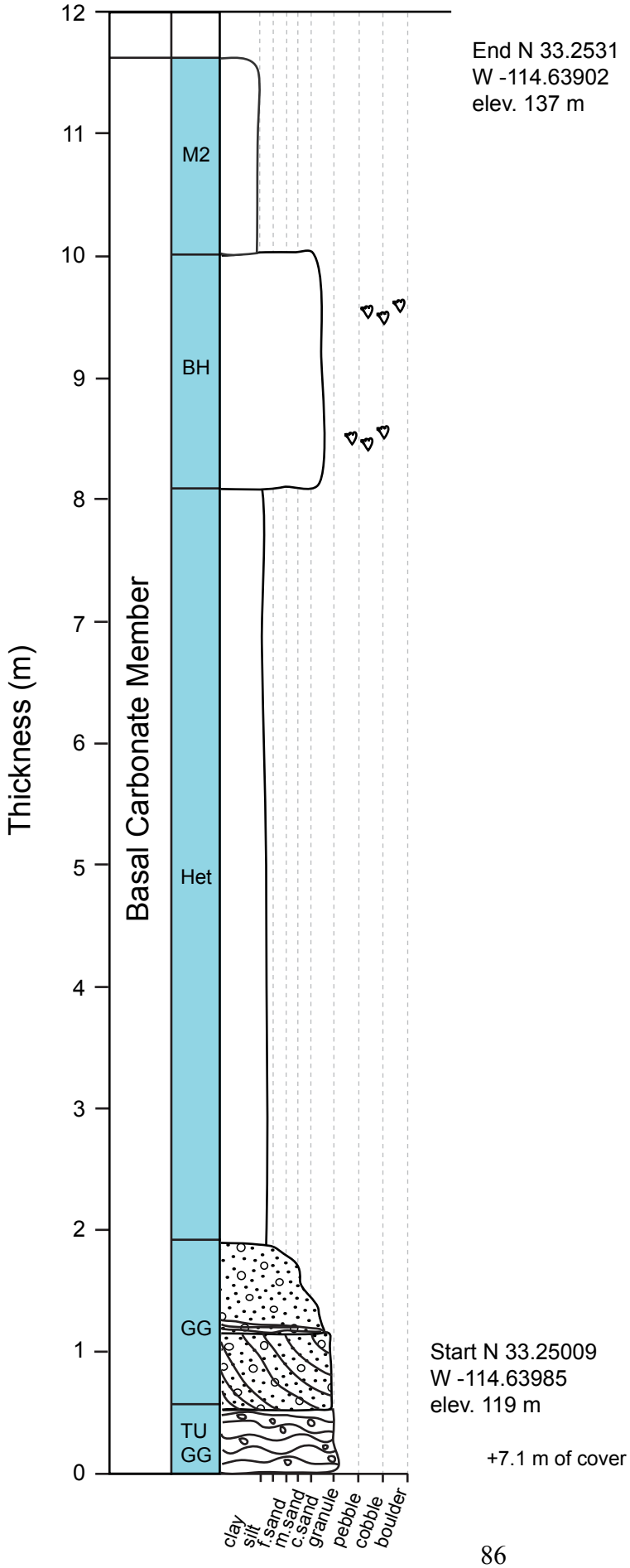

End N 33.2531
W -114.63902
elev. 137 m

Start N 33.25009
W -114.63985
elev. 119 m

+7.1 m of cover

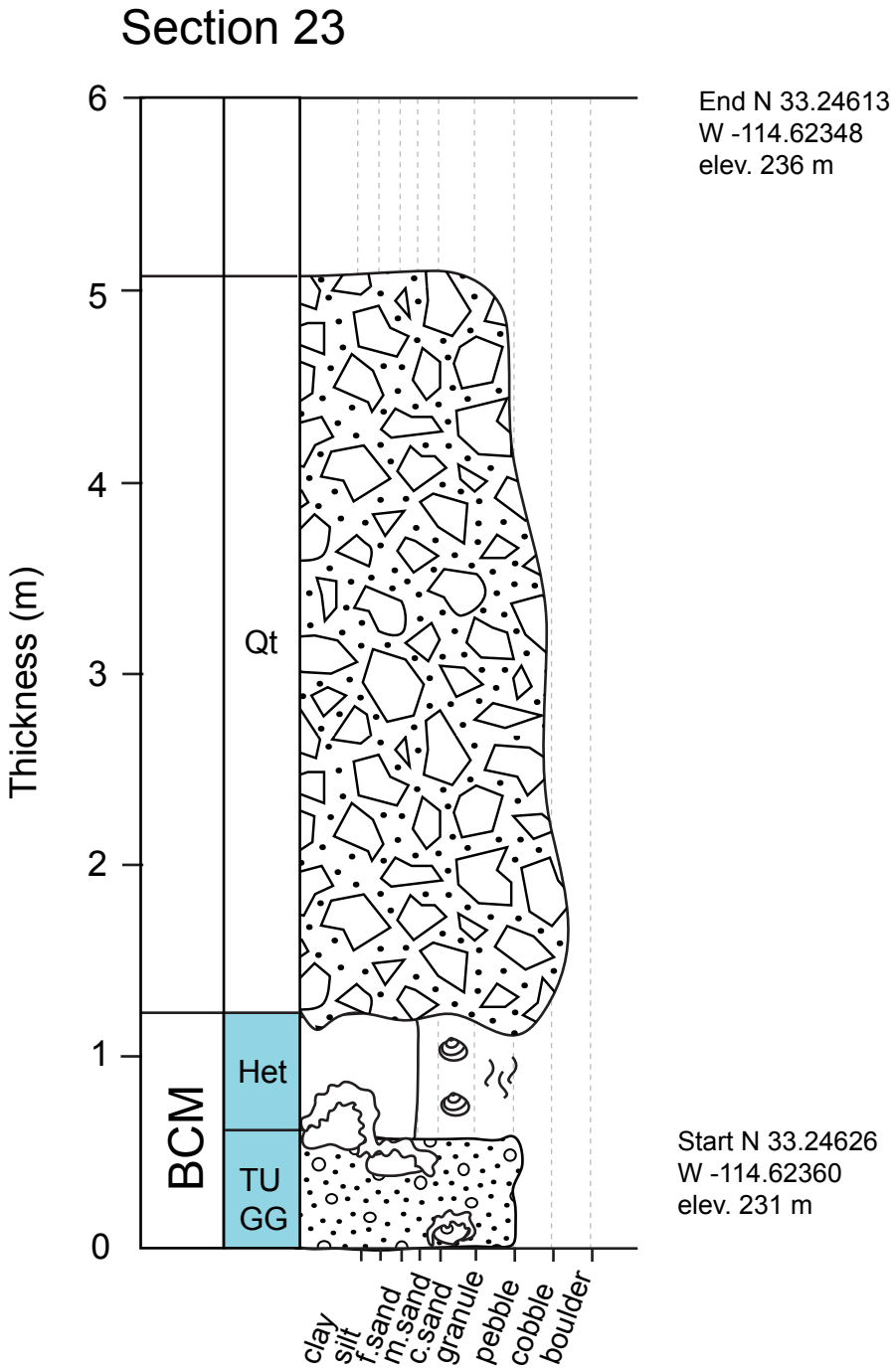
Section 23
End N 33.24613
W -114.62348
elev. 236 m
Start N 33.24626
W -114.62360
elev. 231 m
Thickness (m)
6
5
4
3
2
1
0
Qt
BCM
Het
TU
GG
clay
silt
f.sand
m.sand
c.sand
granule
pebble
cobble
boulder

Section 24

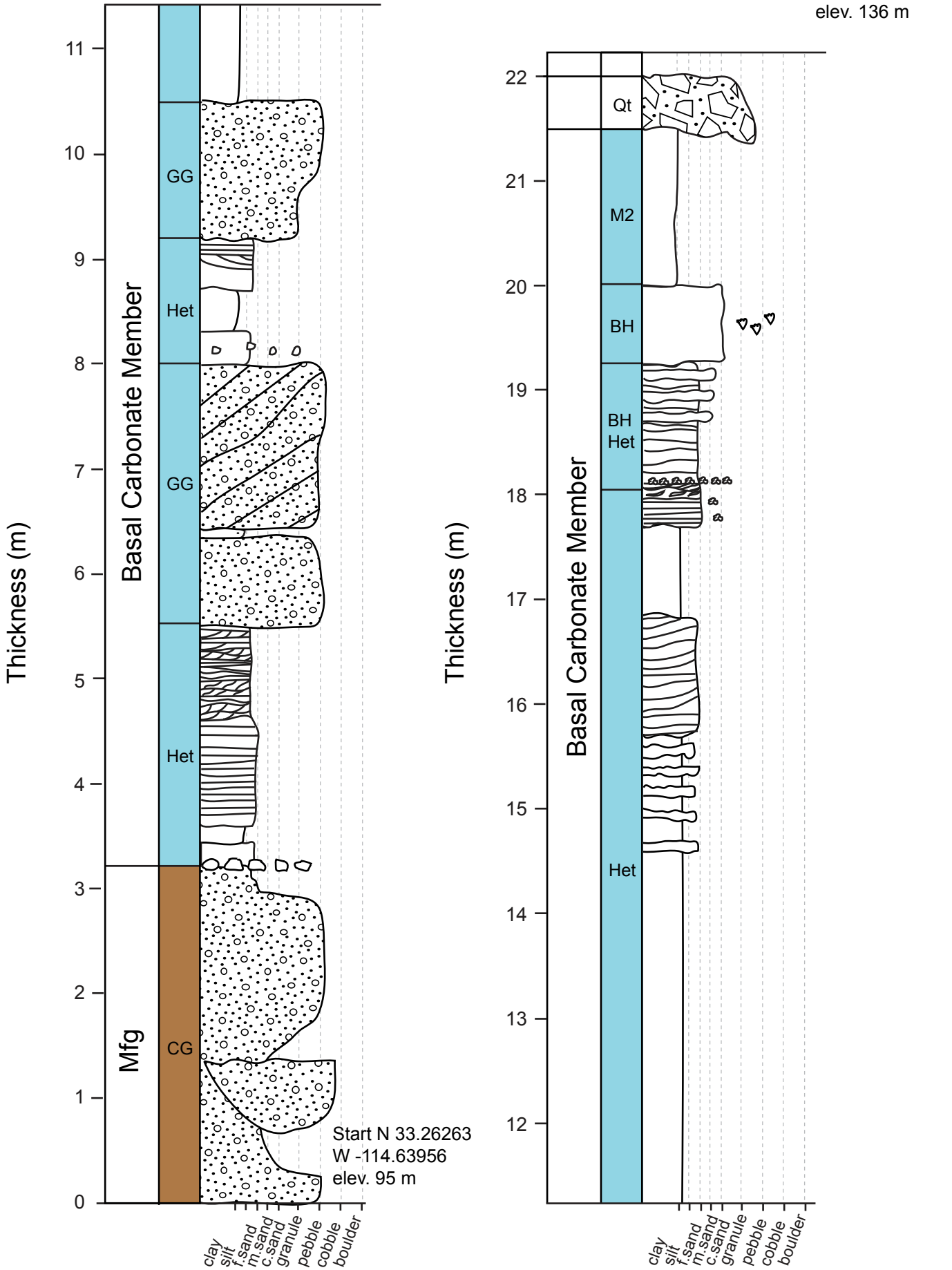
End N 33.26414
W -114.63950
elev. 136 m
Thickness (m)
Basal Carbonate Member
Mfg
GG
Het
GG
Het
CG
Qt
M2
BH
BH
Het
Het
Start N 33.26263
W -114.63956
elev. 95 m
clay
silt
f.sand
m.sand
c.sand
granule
pebble
cobble
boulder

Section 25

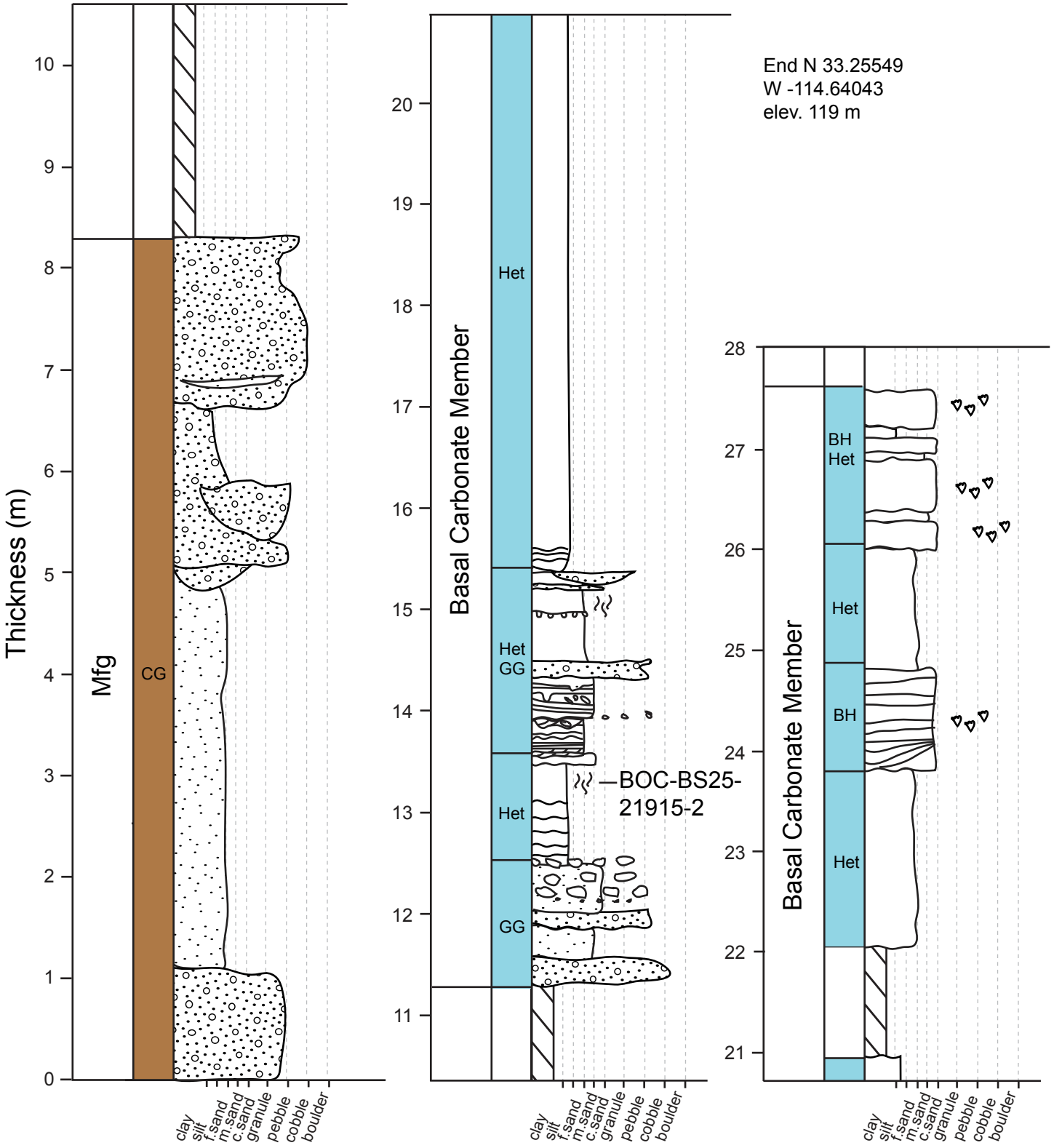

Start N 33.25694
W -114.64025
elev. 93 m

End N 33.25549
W -114.64043
elev. 119 m

Section 26

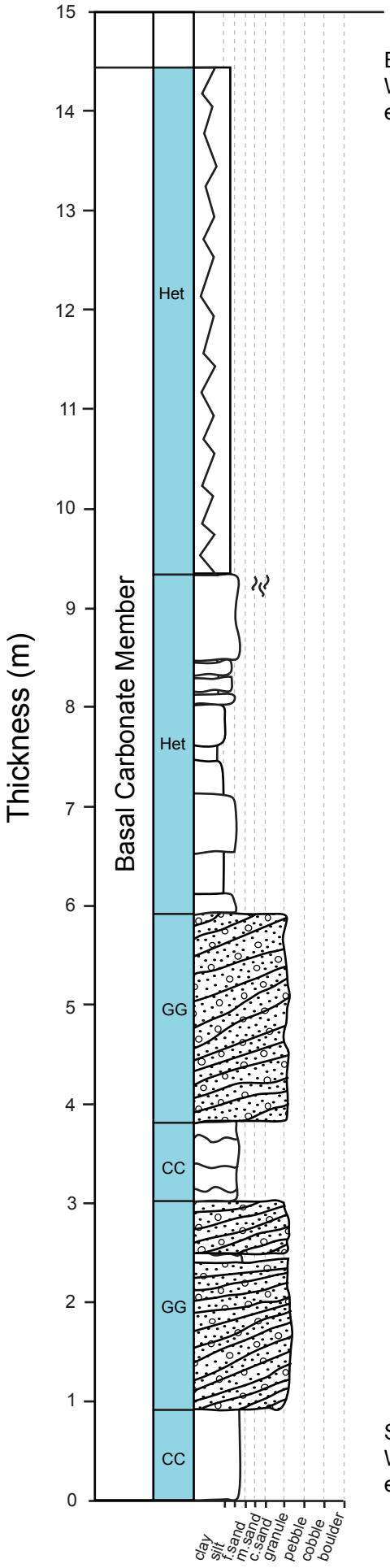

End N 33.25849
W -114.64626
elev. 111 m

Start N 33.25887
W -114.64538
elev. 92 m

Section 27

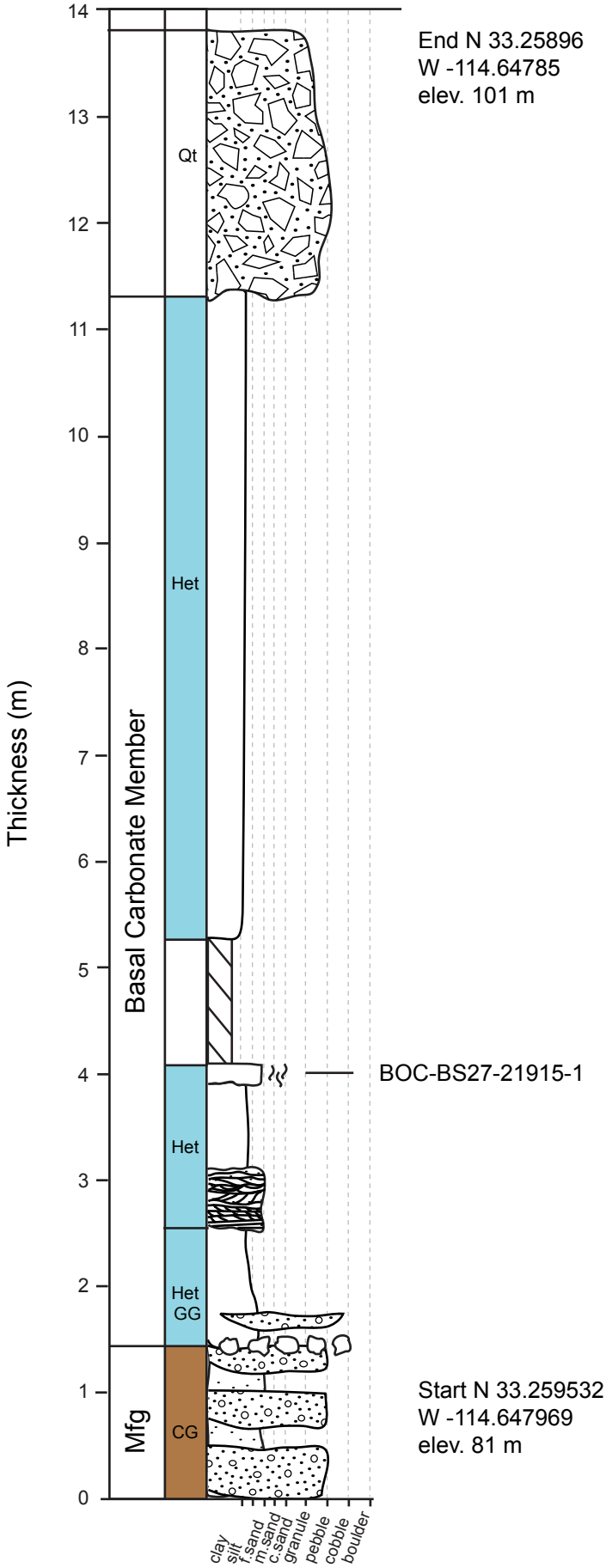
Thickness (m)
14
13
12
11
10
9
8
7
6
5
4
3
2
1
0
Basal Carbonate Member
Mfg
Qt
Het
Het
Het
GG
CG
clay
silt
f.sand
m.sand
c.sand
granule
pebble
cobble
boulder
End N 33.25896
W -114.64785
elev. 101 m
BOC-BS27-21915-1
Start N 33.259532
W -114.647969
elev. 81 m

Section 28

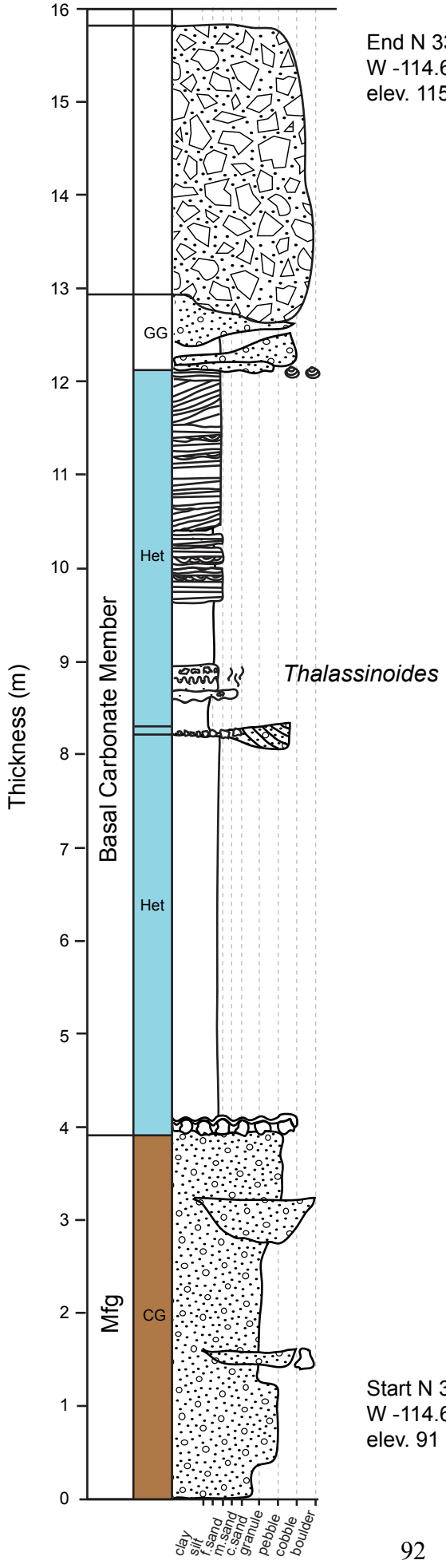

End N 33.26104
W -114.64256
elev. 115 m

Start N 33.26035
W -114.64284
elev. 91 m

Section 29

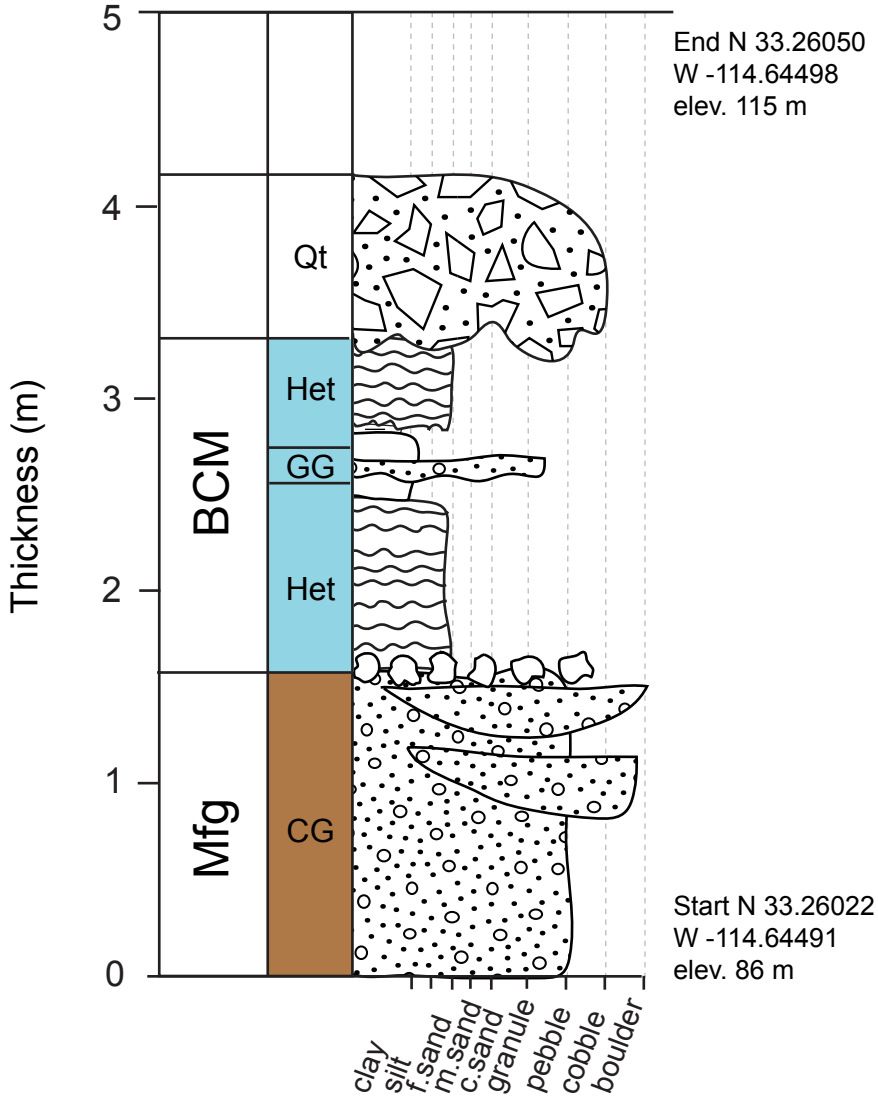
Thickness (m)
5
4
3
2
1
0
BCM
Mfg
Qt
Het
GG
Het
CG
End N 33.26050
W -114.64498
elev. 115 m
Start N 33.26022
W -114.64491
elev. 86 m
clay
silt
f.sand
m.sand
c.sand
granule
pebble
cobble
boulder

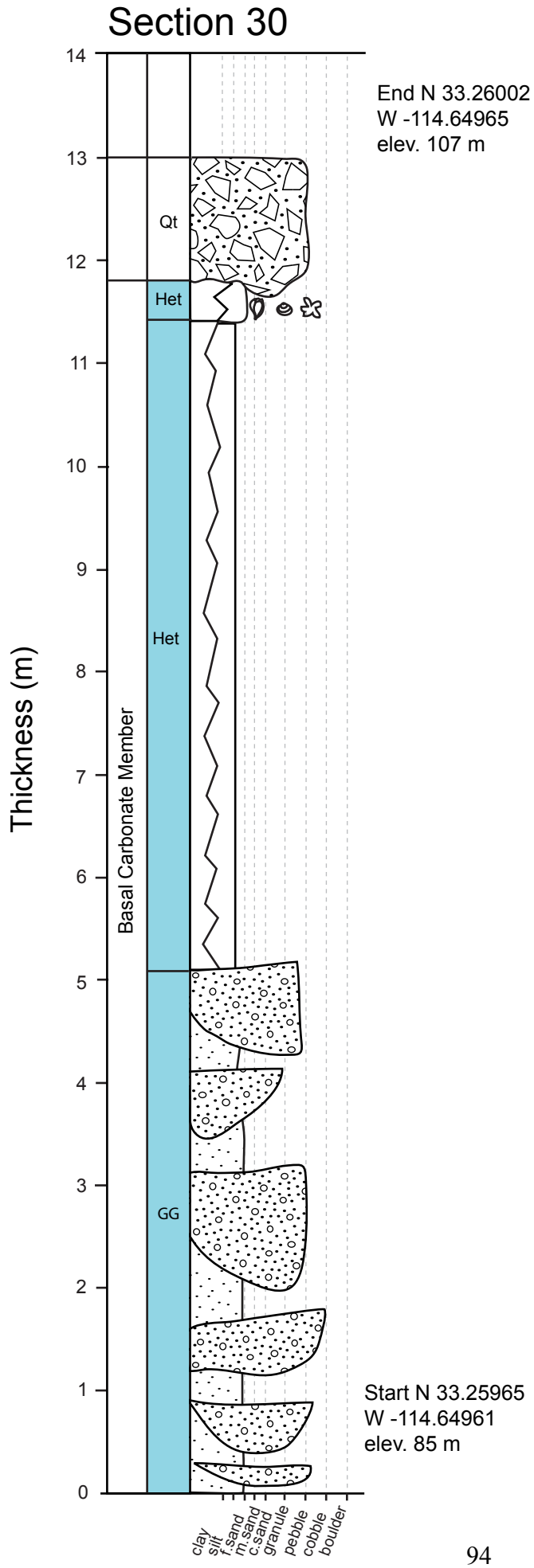
Section 30
Thickness (m)
14
13
12
11
10
9
8
7
6
5
4
3
2
1
0
Qt
Het
Het
GG
Basal Carbonate Member
clay
silt
f.sand
m.sand
c.sand
granule
pebble
cobble
boulder
End N 33.26002
W -114.64965
elev. 107 m
Start N 33.25965
W -114.64961
elev. 85 m

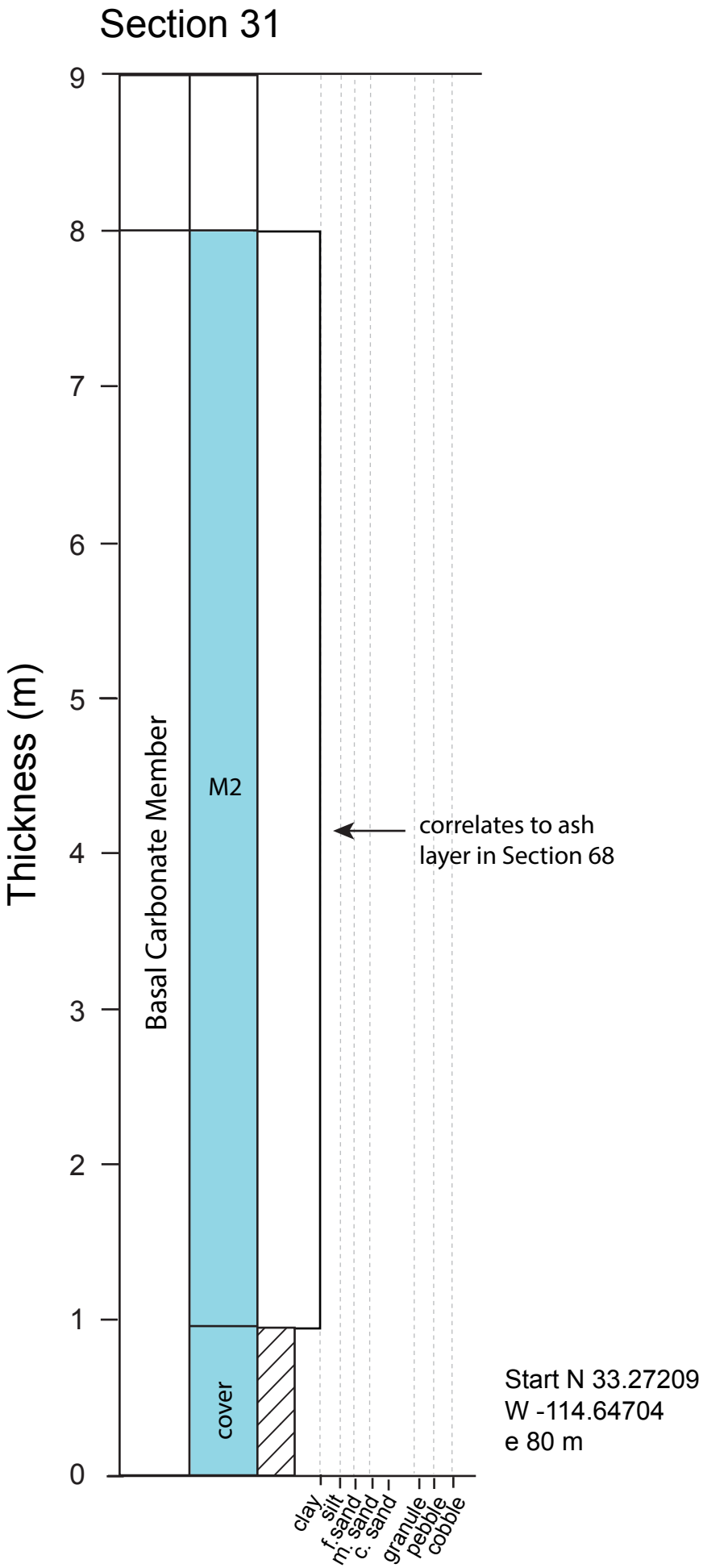
Section 31
Thickness (m)
9
8
7
6
5
4
3
2
1
0
Basal Carbonate Member
M2
cover
correlates to ash
layer in Section 68
clay
silt
f. sand
m. sand
c. sand
granule
pebble
cobble
Start N 33.27209
W -114.64704
e 80 m

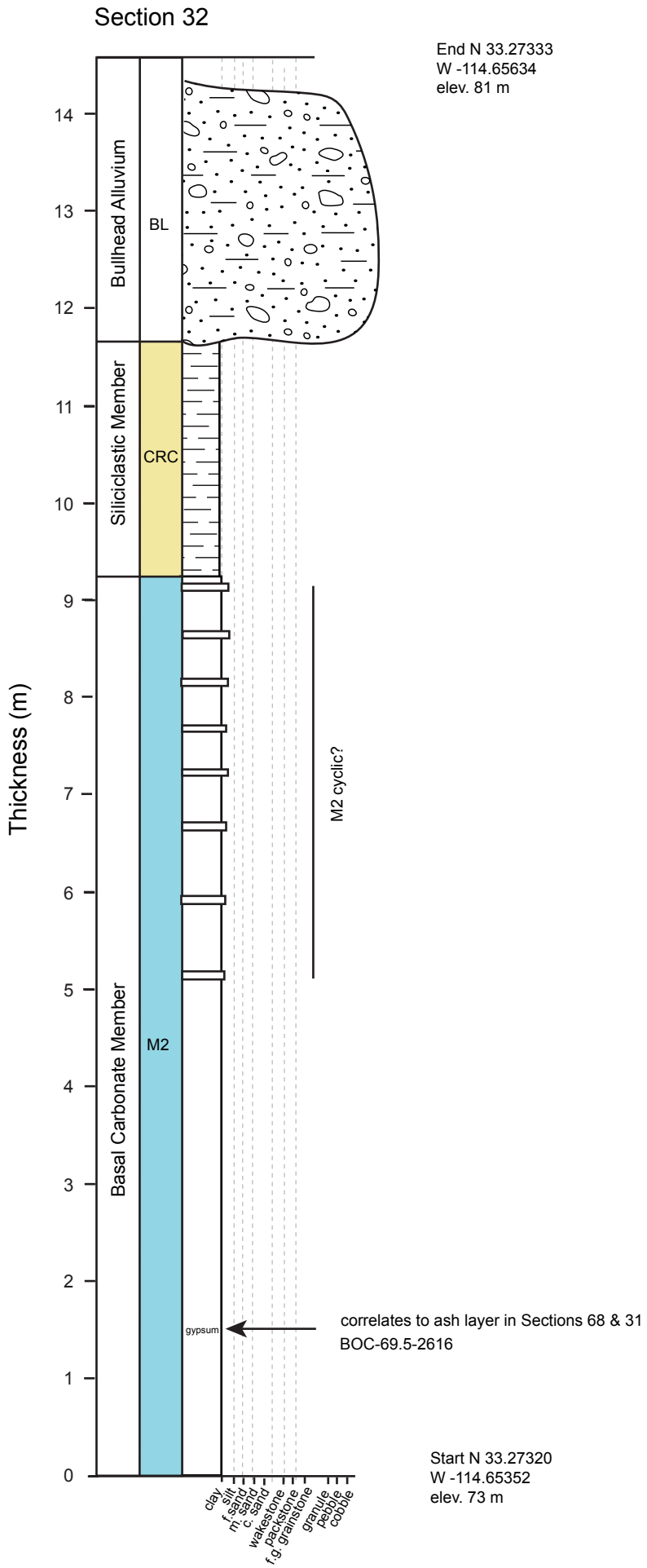
Section 32
End N 33.27333
W -114.65634
elev. 81 m
Bullhead Alluvium
BL
Siliciclastic Member
CRC
Basal Carbonate Member
M2
M2 cyclic?
gypsum
correlates to ash layer in Sections 68 & 31
BOC-69.5-2616
Start N 33.27320
W -114.65352
elev. 73 m
Thickness (m)
0
1
2
3
4
5
6
7
8
9
10
11
12
13
14
clay
silt
f. sand
m. sand
c. sand
wakestone
packstone
f.g. grainstone
granule
pebble
cobble

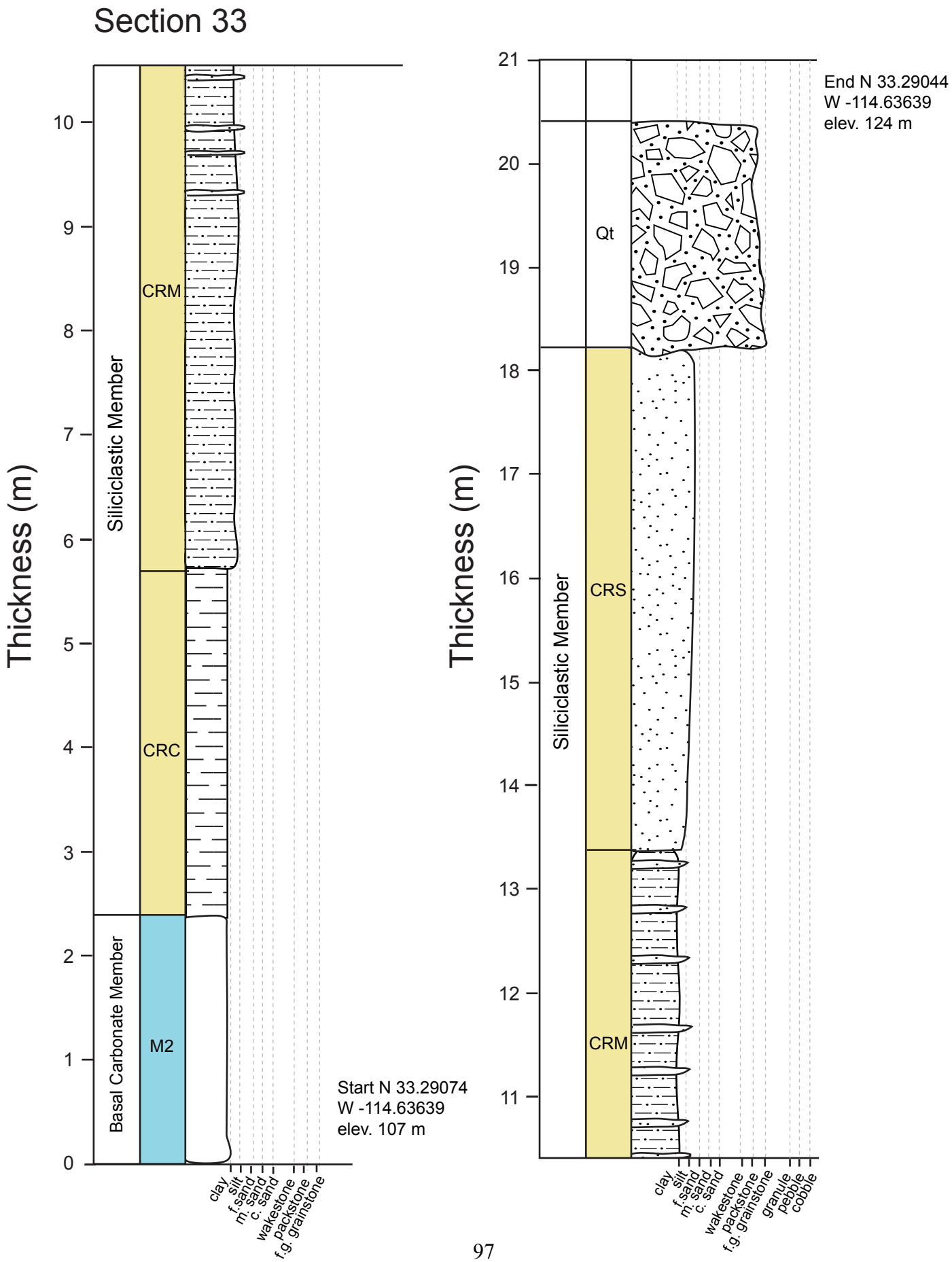
Section 33
Thickness (m)
Siliciclastic Member
Basal Carbonate Member
CRM
CRC
M2
CRS
Qt
Start N 33.29074
W -114.63639
elev. 107 m
End N 33.29044
W -114.63639
elev. 124 m
clay
silt
f.sand
m. sand
c. sand
wakestone
packstone
f.g. grainstone
granule
pebble
cobble

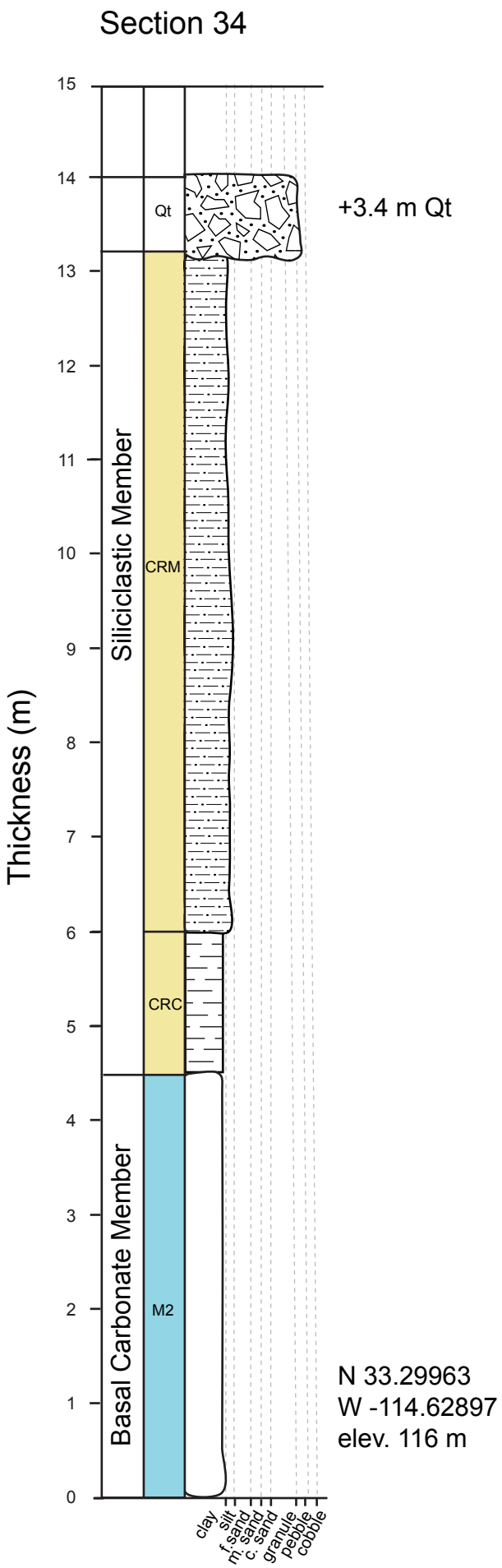
Section 34
Thickness (m)
15
14
13
12
11
10
9
8
7
6
5
4
3
2
1
0
Qt
CRM
CRC
M2
Siliciclastic Member
Basal Carbonate Member
+3.4 m Qt
N 33.29963
W -114.62897
elev. 116 m
clay
silt
f. sand
m. sand
c. sand
granule
pebble
cobble

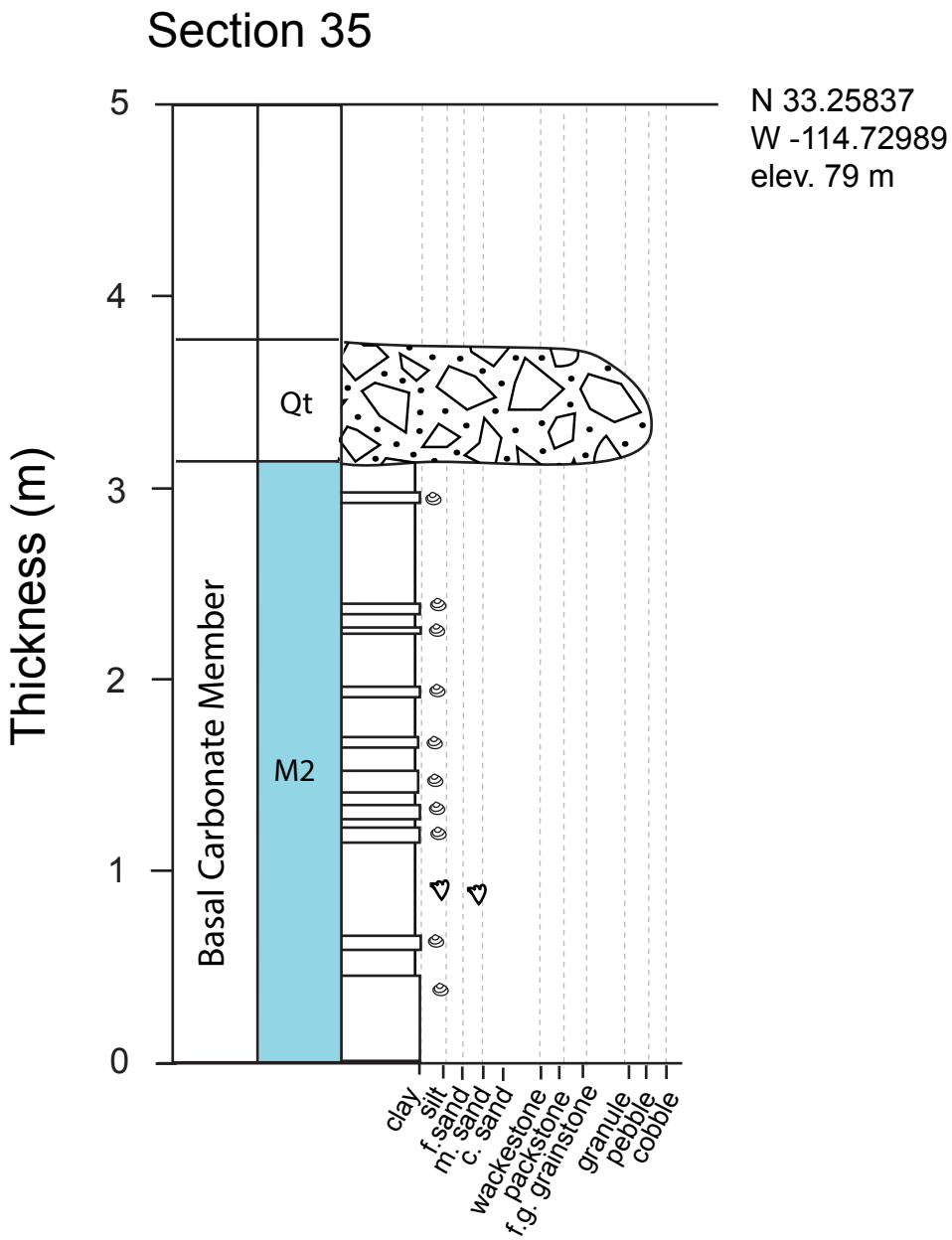
Section 35
N 33.25837
W -114.72989
elev. 79 m
Thickness (m)
5
4
3
2
1
0
Qt
Basal Carbonate Member
M2
clay
silt
f.sand
m. sand
c. sand
wackestone
packstone
f.g. grainstone
granule
pebble
cobble

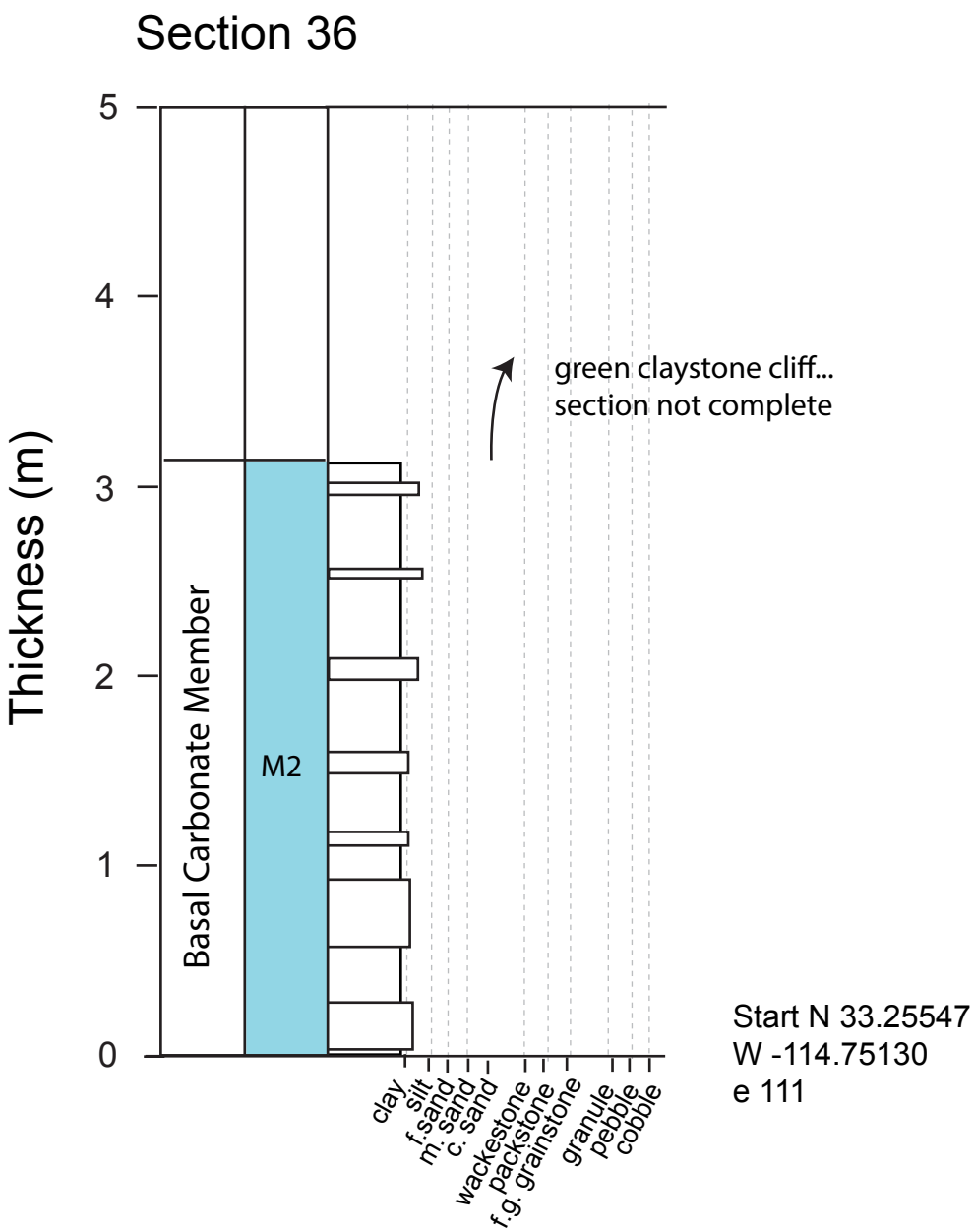
Section 36
Thickness (m)
5
4
3
2
1
0
Basal Carbonate Member
M2
green claystone cliff...
section not complete
clay
silt
f. sand
m. sand
c. sand
wackestone
packstone
f.g. grainstone
granule
pebble
cobble
Start N 33.25547
W -114.75130
e 111

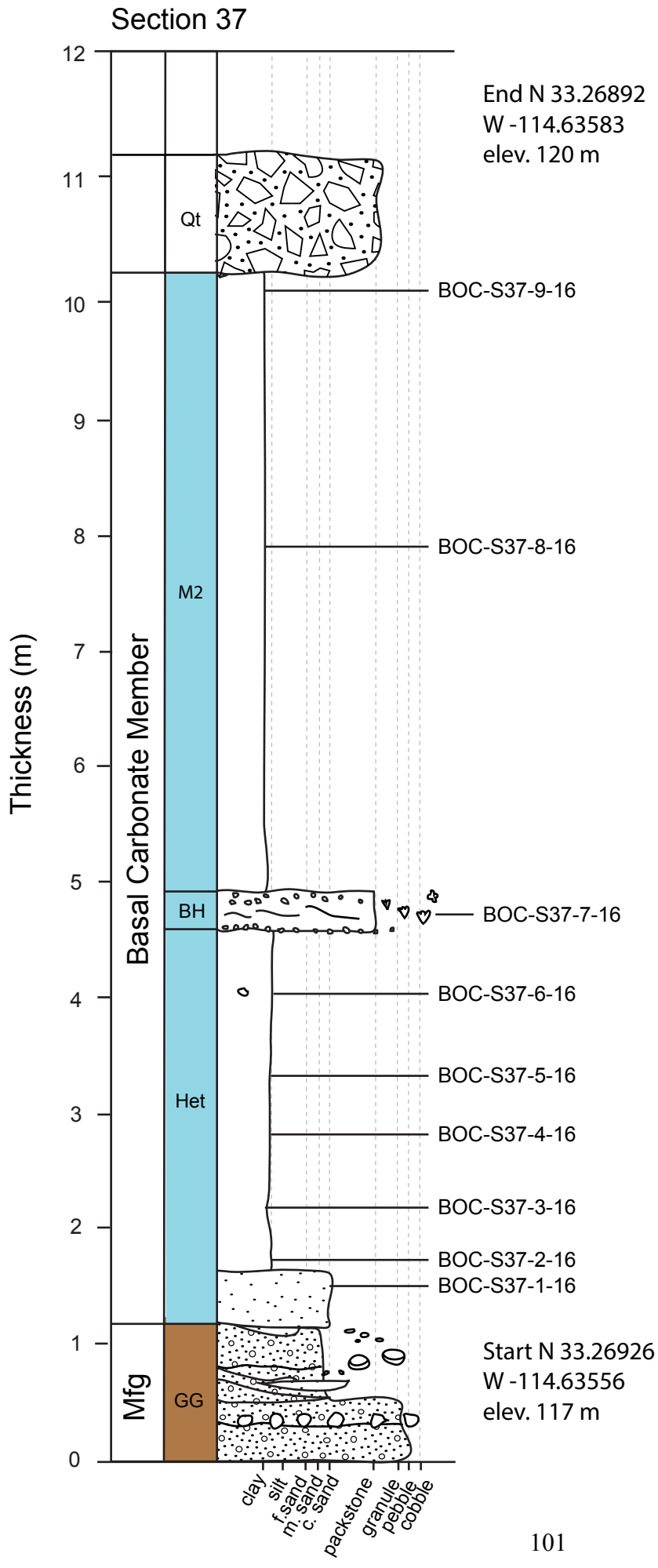
Section 37
Thickness (m)
12
11
10
9
8
7
6
5
4
3
2
1
0
Basal Carbonate Member
Mfg
Qt
M2
BH
Het
GG
End N 33.26892
W -114.63583
elev. 120 m
BOC-S37-9-16
BOC-S37-8-16
BOC-S37-7-16
BOC-S37-6-16
BOC-S37-5-16
BOC-S37-4-16
BOC-S37-3-16
BOC-S37-2-16
BOC-S37-1-16
Start N 33.26926
W -114.63556
elev. 117 m
clay
silt
f.sand
m.sand
c. sand
packstone
granule
pebble
cobble

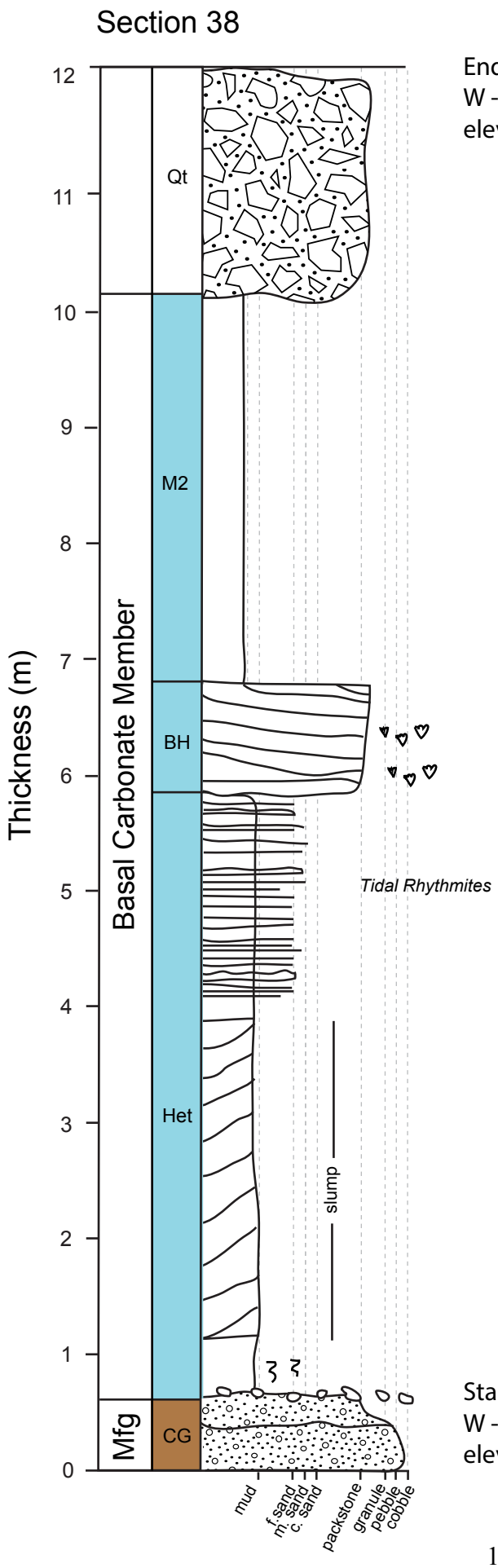
Section 38
End N 33.26947
W -114.63668
elev. 115 m
Start N 33.26965
W -114.63663
elev. 97 m
Thickness (m)
Basal Carbonate Member
Qt
M2
BH
Het
Mfg
CG
Tidal Rhythmites
slump
mud
f. sand
m. sand
c. sand
packstone
granule
pebble
cobble

Section 39

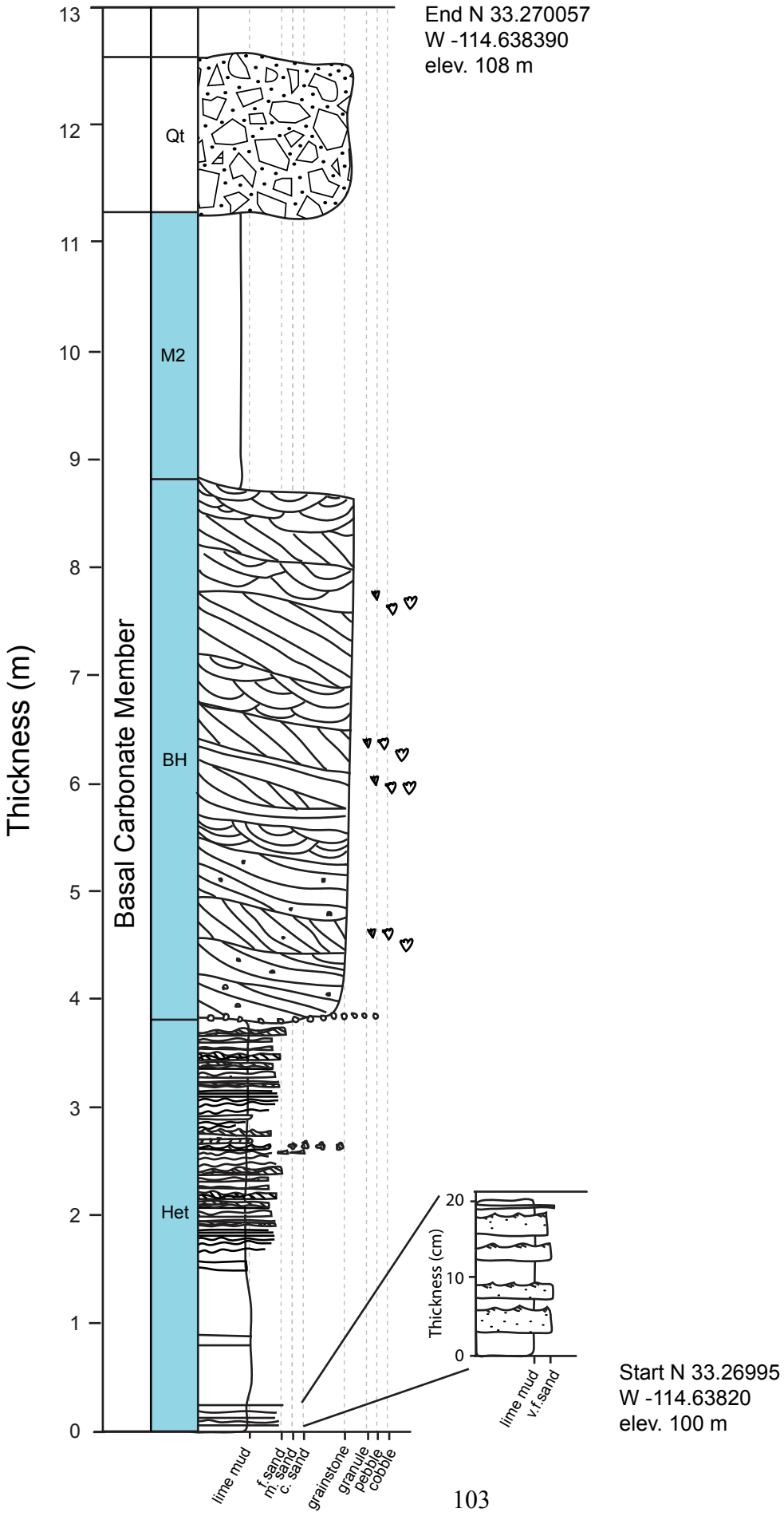
End N 33.270057
W -114.638390
elev. 108 m
Thickness (m)
Basal Carbonate Member
Qt
M2
BH
Het
13
12
11
10
9
8
7
6
5
4
3
2
1
0
lime mud
f.sand
m. sand
c. sand
grainstone
granule
pebble
cobble
Thickness (cm)
20
10
0
lime mud
v.f.sand
Start N 33.26995
W -114.63820
elev. 100 m

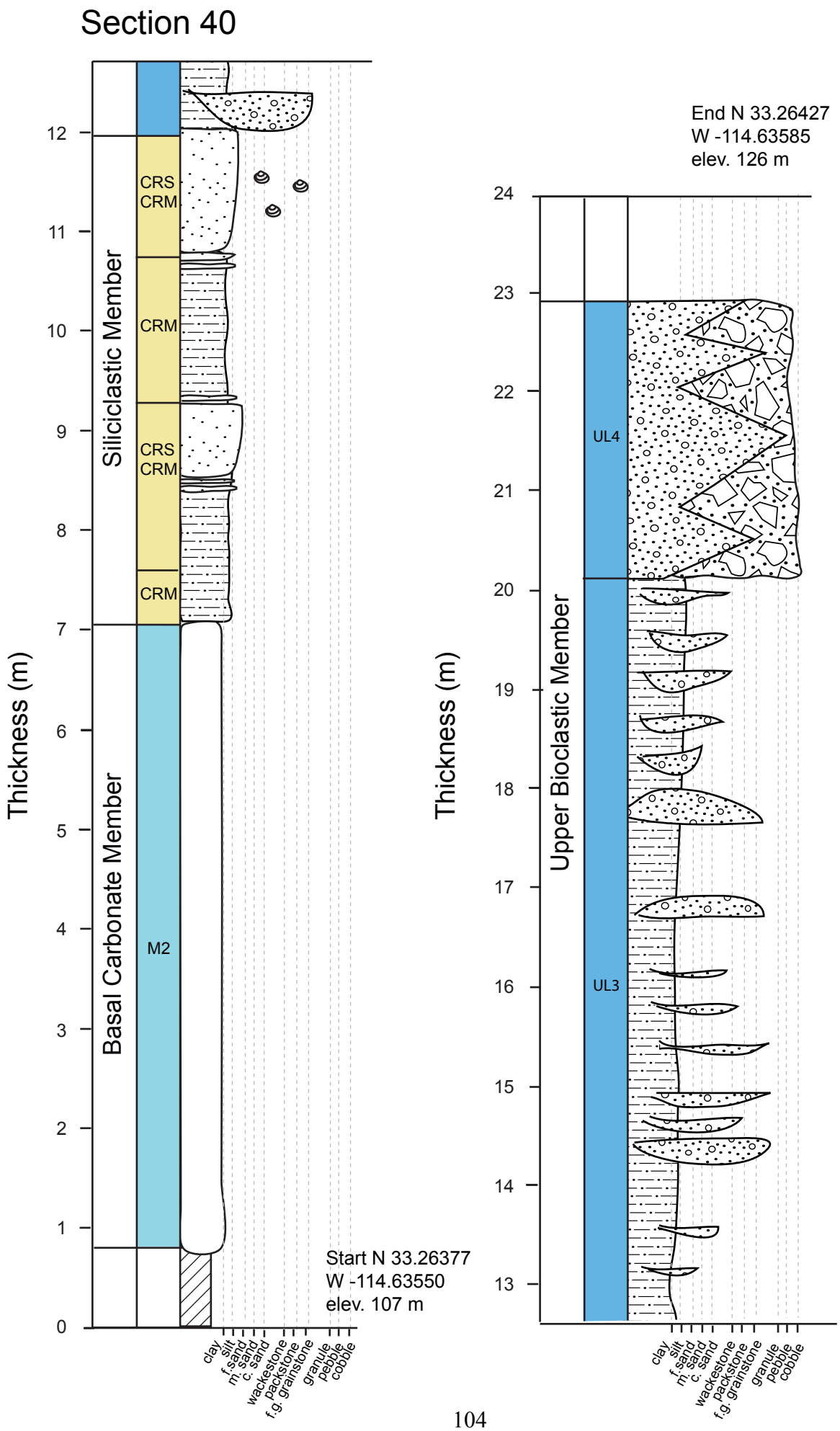
Section 40
Thickness (m)
Siliciclastic Member
Basal Carbonate Member
CRS
CRM
CRM
CRS
CRM
CRM
M2
Start N 33.26377
W -114.63550
elev. 107 m
End N 33.26427
W -114.63585
elev. 126 m
Upper Bioclastic Member
UL4
UL3
clay
silt
f. sand
m. sand
c. sand
wackestone
packstone
f.g. grainstone
granule
pebble
cobble

Section 41

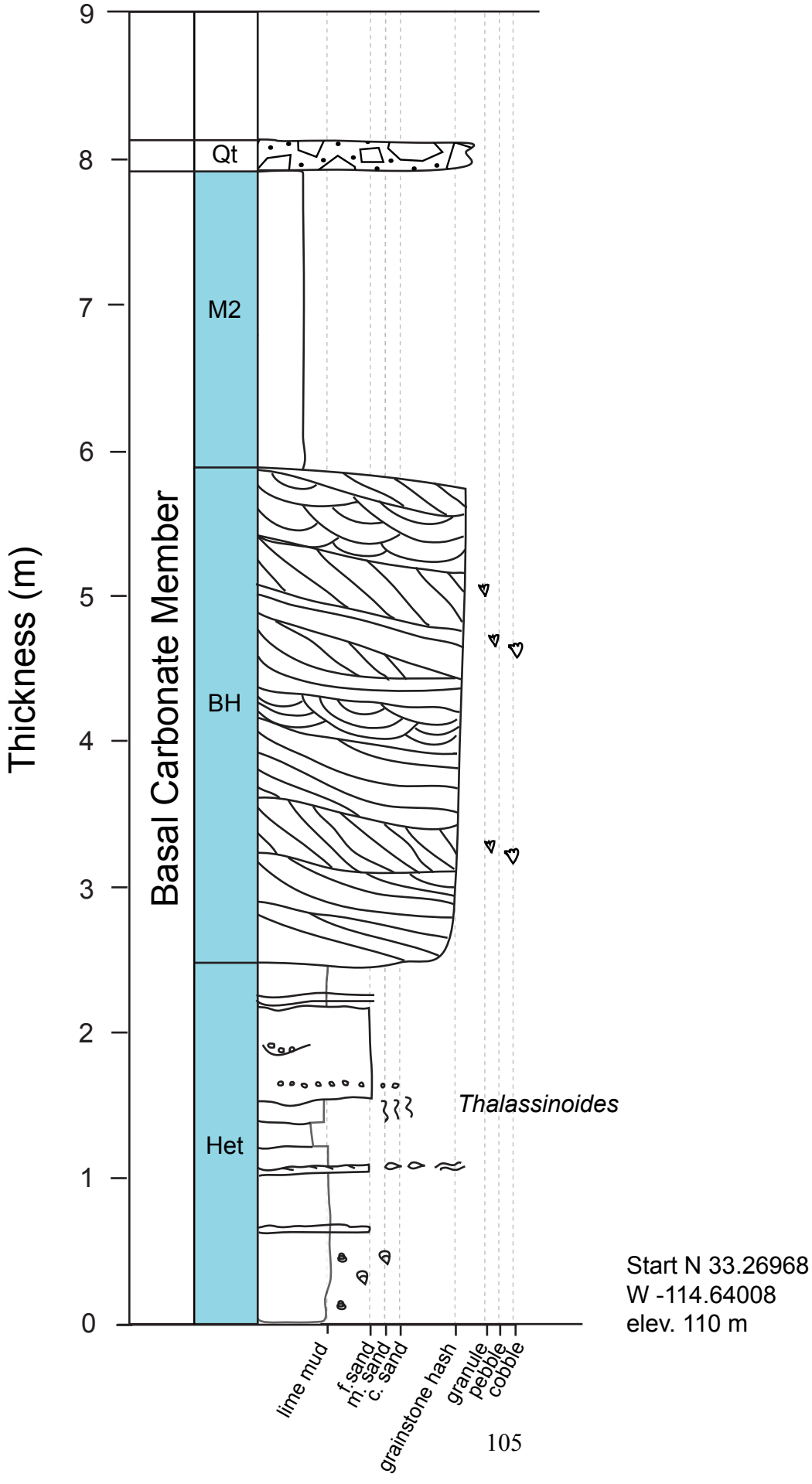

Start N 33.26968
W -114.64008
elev. 110 m

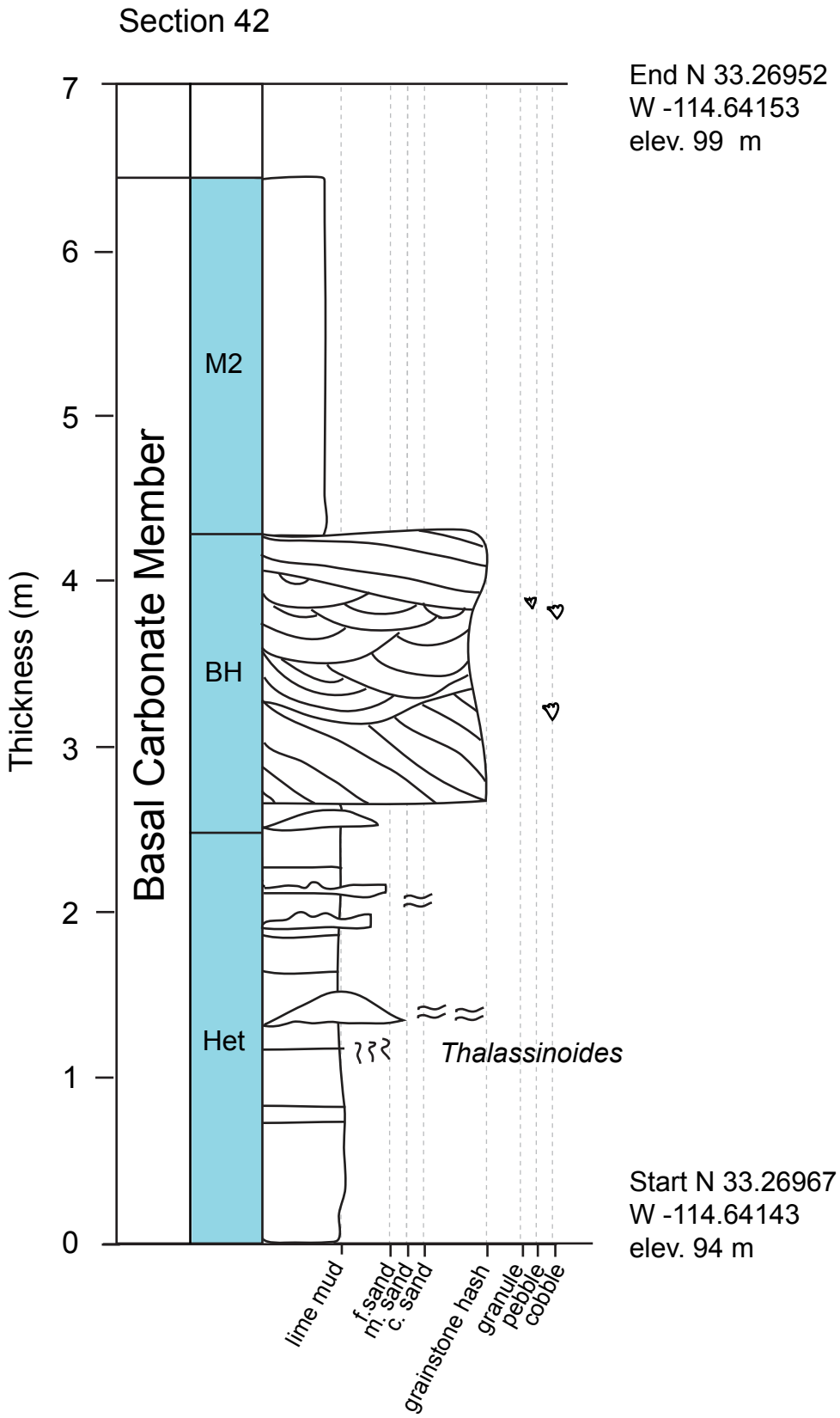
Section 42
End N 33.26952
W -114.64153
elev. 99 m
Start N 33.26967
W -114.64143
elev. 94 m
Thickness (m)
0
1
2
3
4
5
6
7
Basal Carbonate Member
M2
BH
Het
Thalassinoides
lime mud
f.sand
m. sand
c. sand
grainstone hash
granule
pebble
cobble

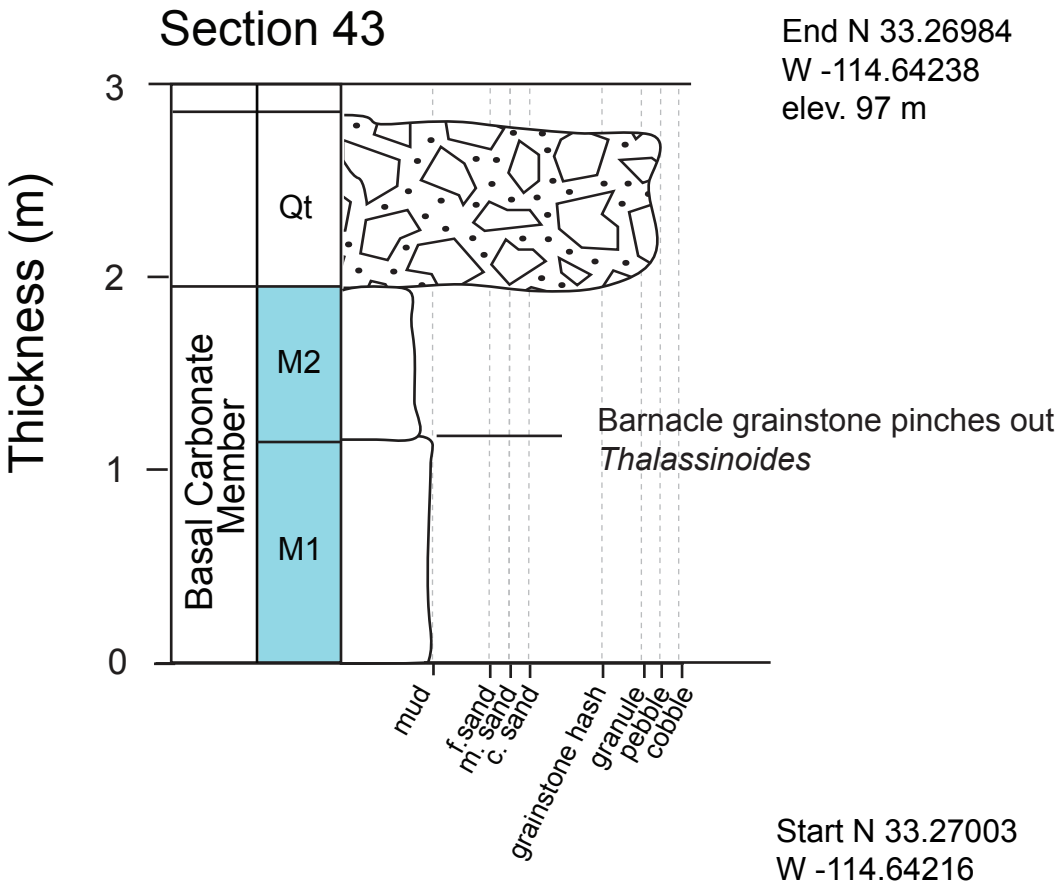
Section 43
End N 33.26984
W -114.64238
elev. 97 m
Thickness (m)
3
2
1
0
Qt
M2
M1
Basal Carbonate Member
Barnacle grainstone pinches out
Thalassinoides
mud
f. sand
m. sand
c. sand
grainstone hash
granule
pebble
cobble
Start N 33.27003
W -114.64216
elev. 96 m

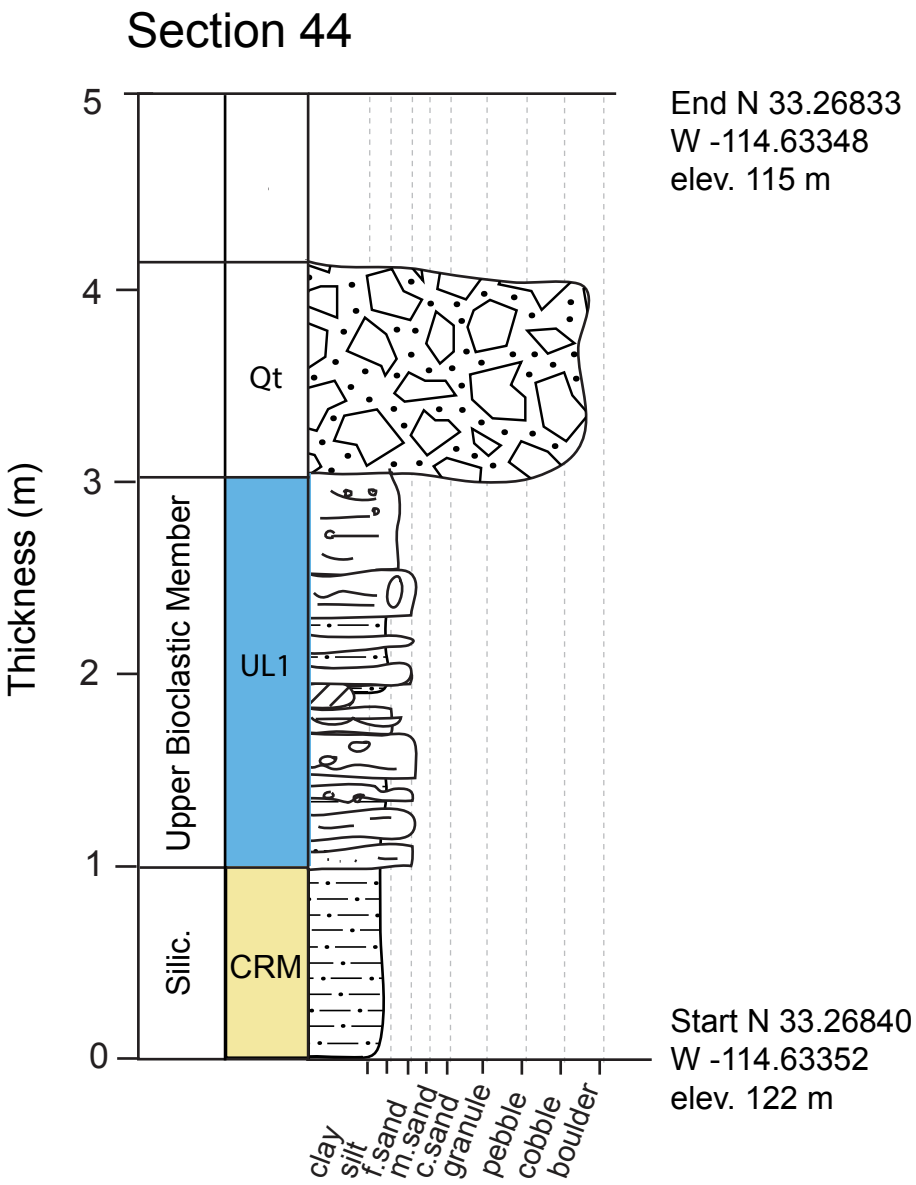
Section 44
Thickness (m)
5
4
3
2
1
0
Qt
Upper Bioclastic Member
UL1
Silic.
CRM
clay
silt
f.sand
m.sand
c.sand
granule
pebble
cobble
boulder
End N 33.26833
W -114.63348
elev. 115 m
Start N 33.26840
W -114.63352
elev. 122 m

Section 45

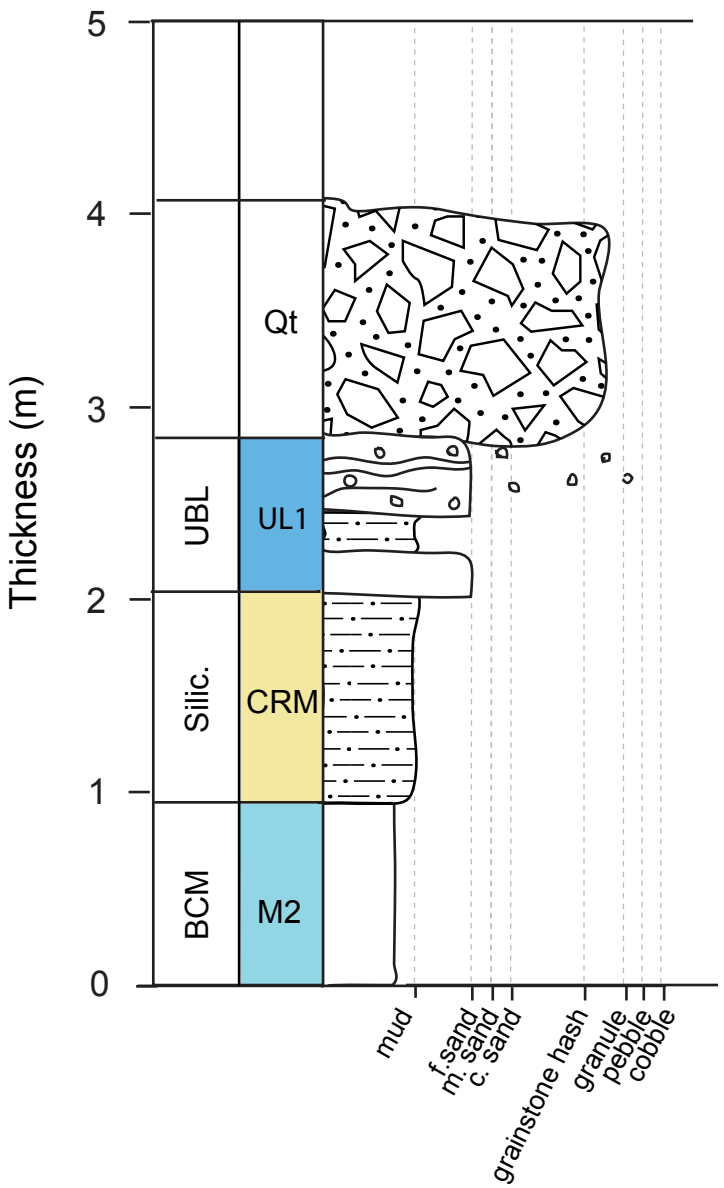

End N 33.26851
W -114.63277
elev. 123 m

Start N 33.26847
W -114.63274
elev. 119 m

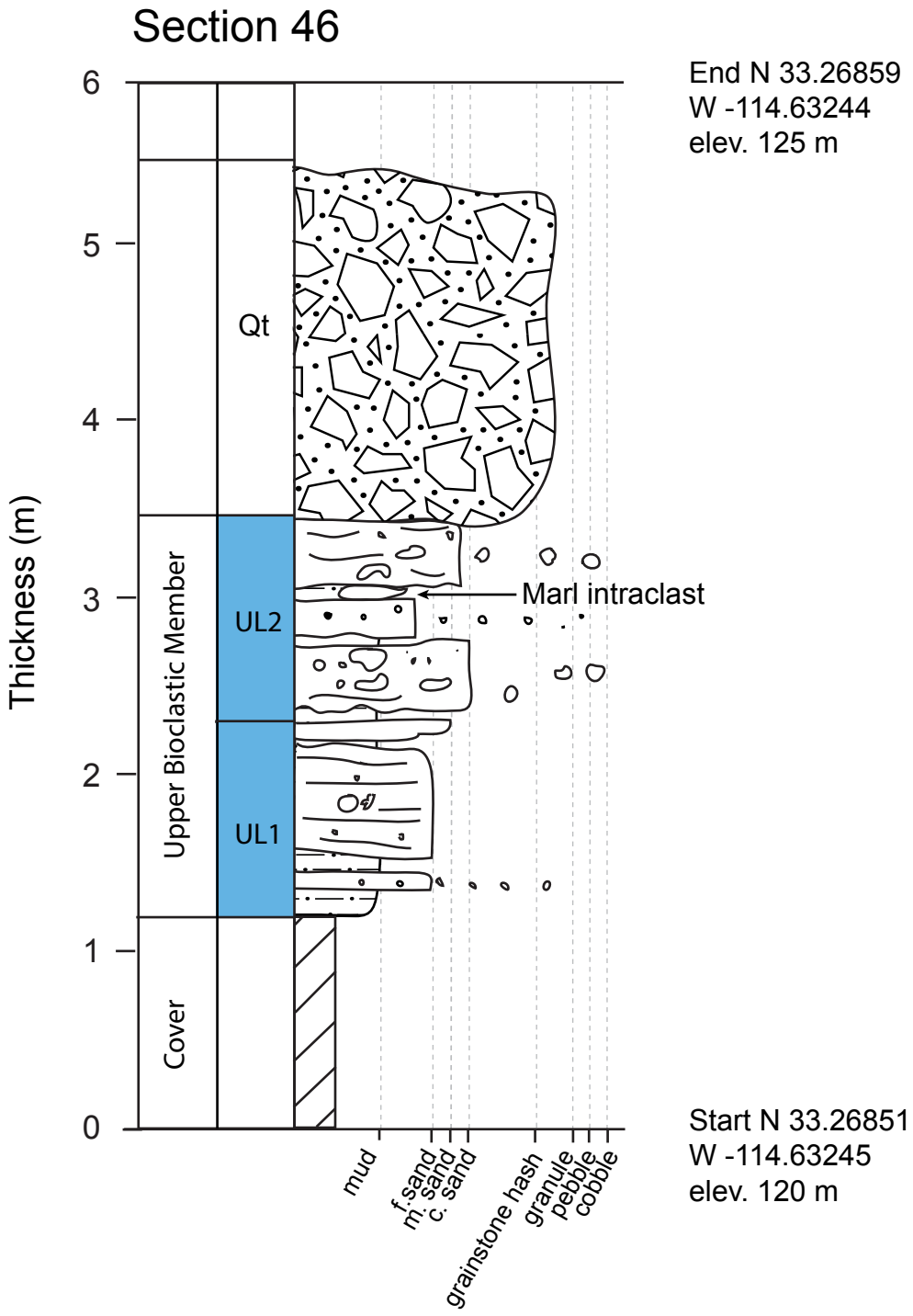
Section 46
End N 33.26859
W -114.63244
elev. 125 m
Thickness (m)
6
5
4
3
2
1
0
Qt
Upper Bioclastic Member
UL2
UL1
Cover
Marl intraclast
mud
f.sand
m.sand
c. sand
grainstone hash
granule
pebble
cobble
Start N 33.26851
W -114.63245
elev. 120 m

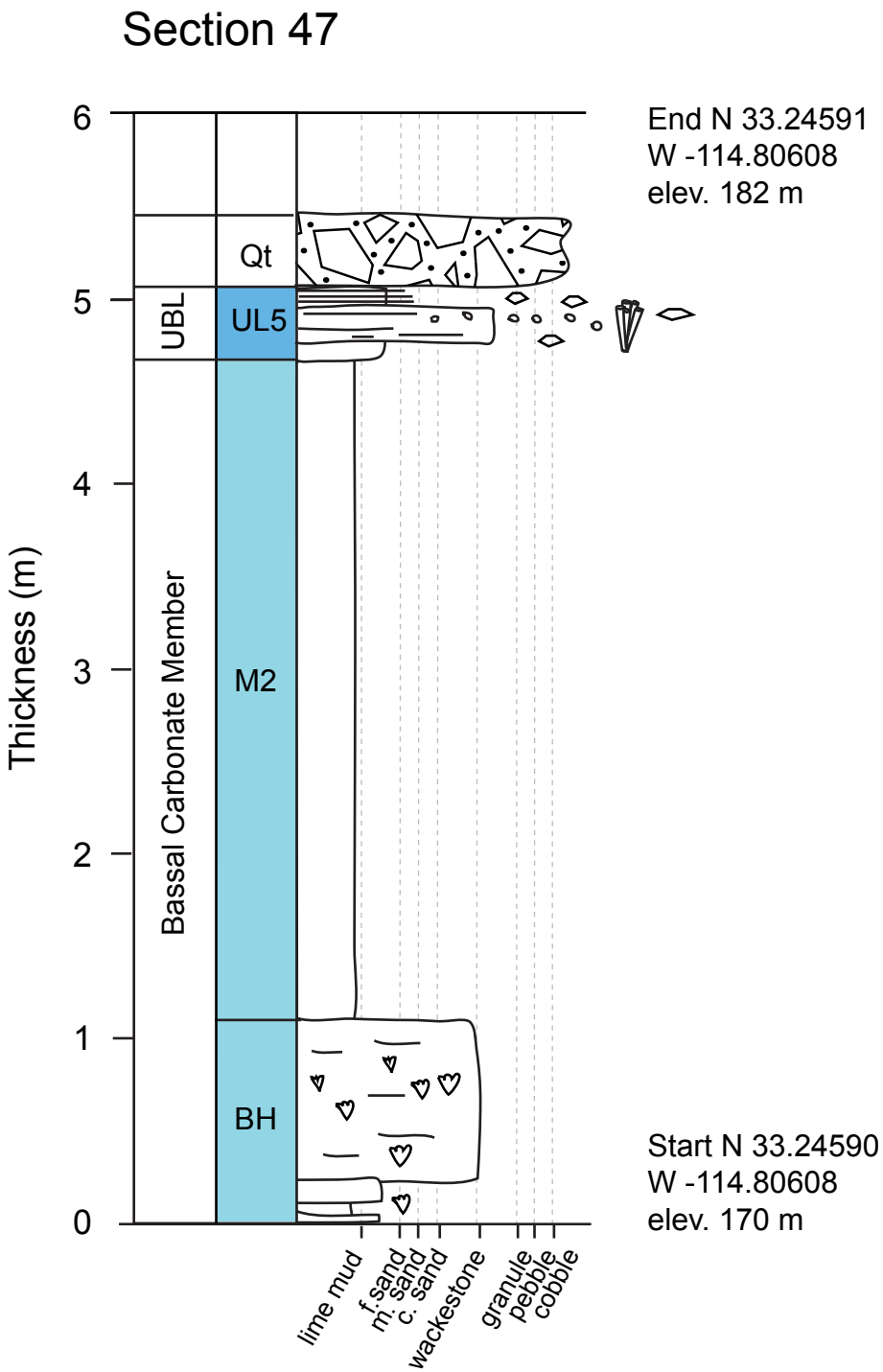
Section 47
Thickness (m)
6
5
4
3
2
1
0
Qt
UBL
UL5
M2
BH
Bassal Carbonate Member
End N 33.24591
W -114.80608
elev. 182 m
Start N 33.24590
W -114.80608
elev. 170 m
lime mud
f. sand
m. sand
c. sand
wackestone
granule
pebble
cobble

Section 48

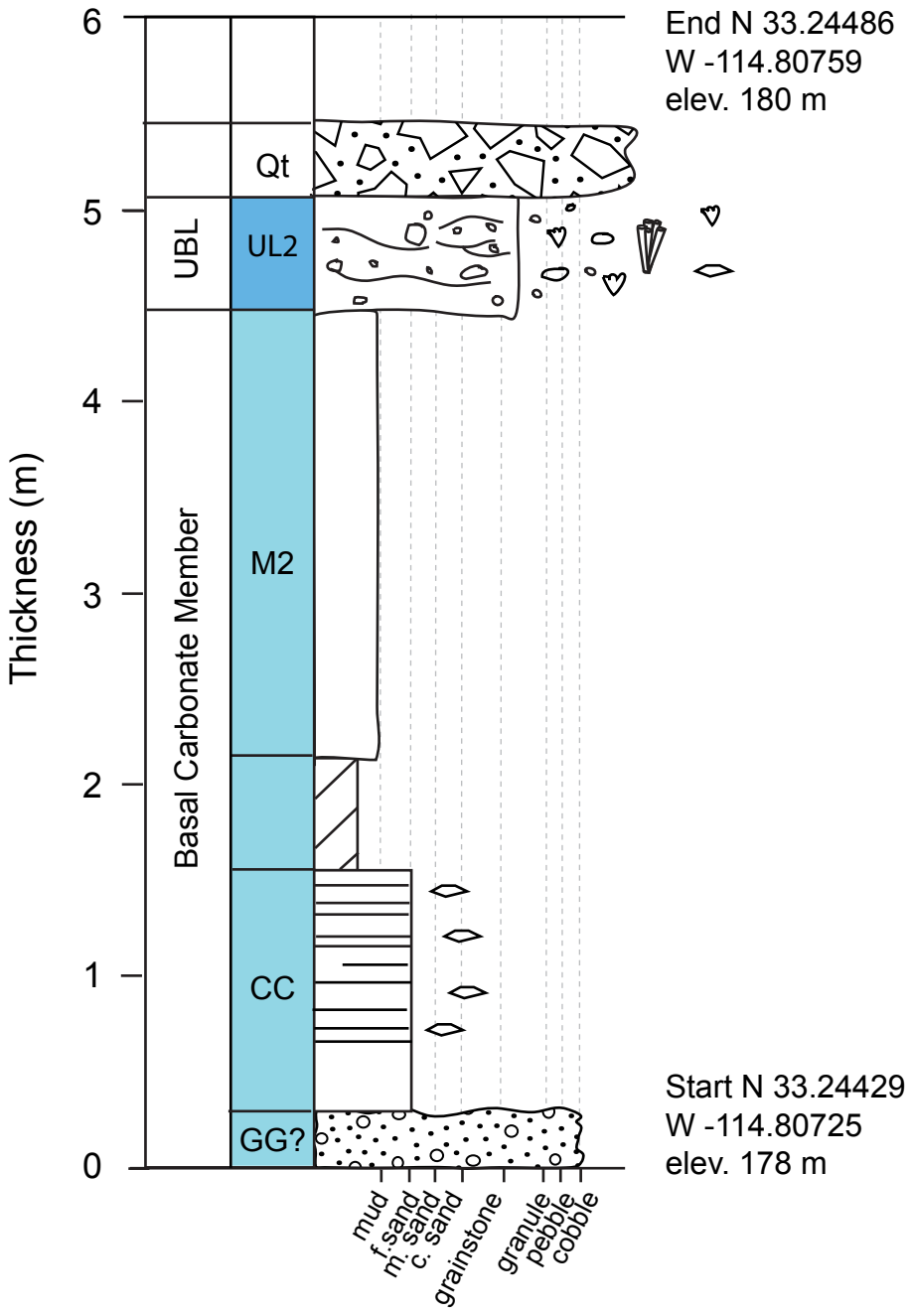
End N 33.24486
W -114.80759
elev. 180 m
Start N 33.24429
W -114.80725
elev. 178 m
Thickness (m)
6
5
4
3
2
1
0
Qt
UBL
UL2
M2
Basal Carbonate Member
CC
GG?
mud
f.sand
m.sand
c. sand
grainstone
granule
pebble
cobble

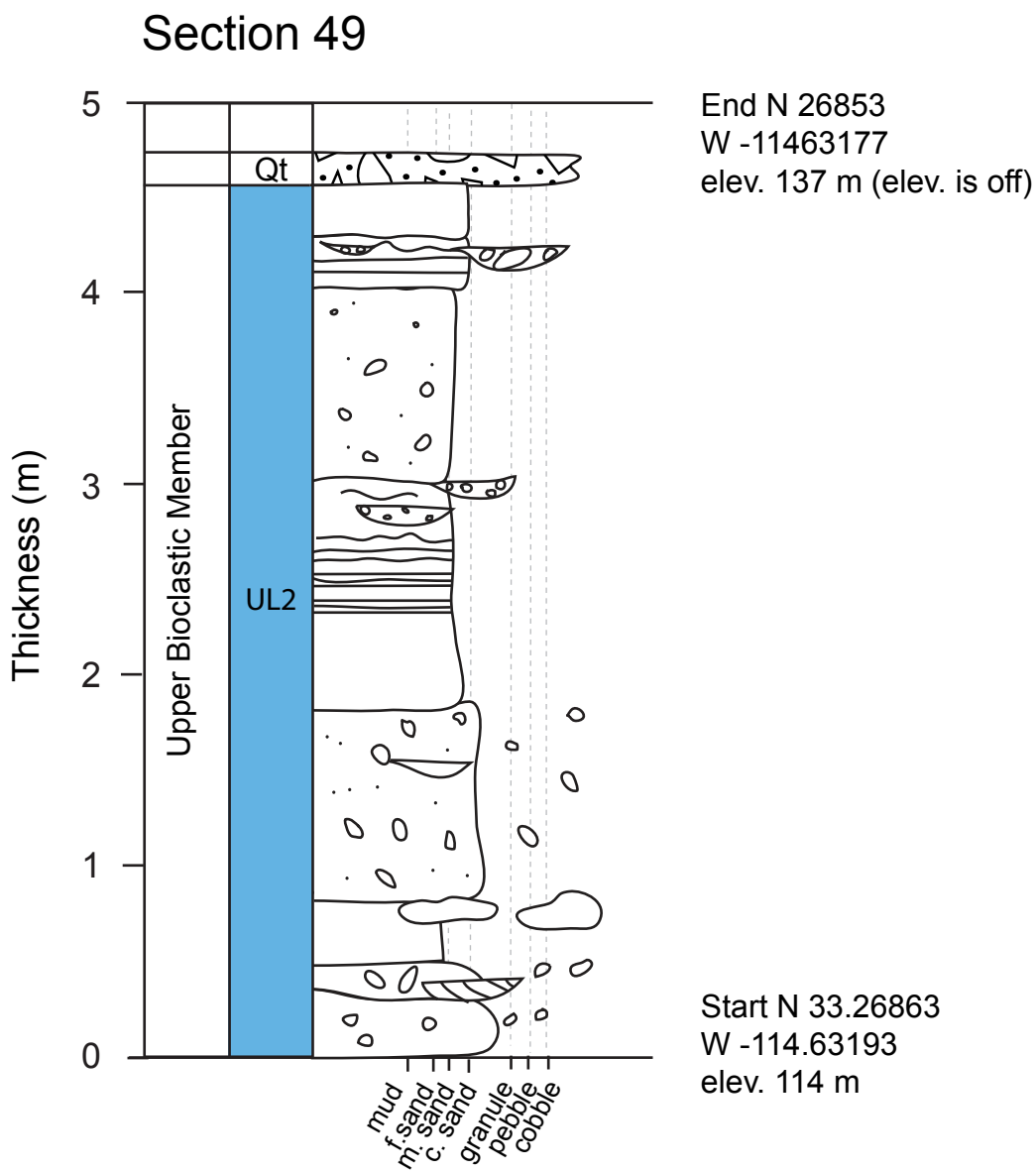
Section 49
Thickness (m)
5
4
3
2
1
0
Qt
UL2
Upper Bioclastic Member
mud
f. sand
m. sand
c. sand
granule
pebble
cobble
End N 26853
W -11463177
elev. 137 m (elev. is off)
Start N 33.26863
W -114.63193
elev. 114 m

Section 50

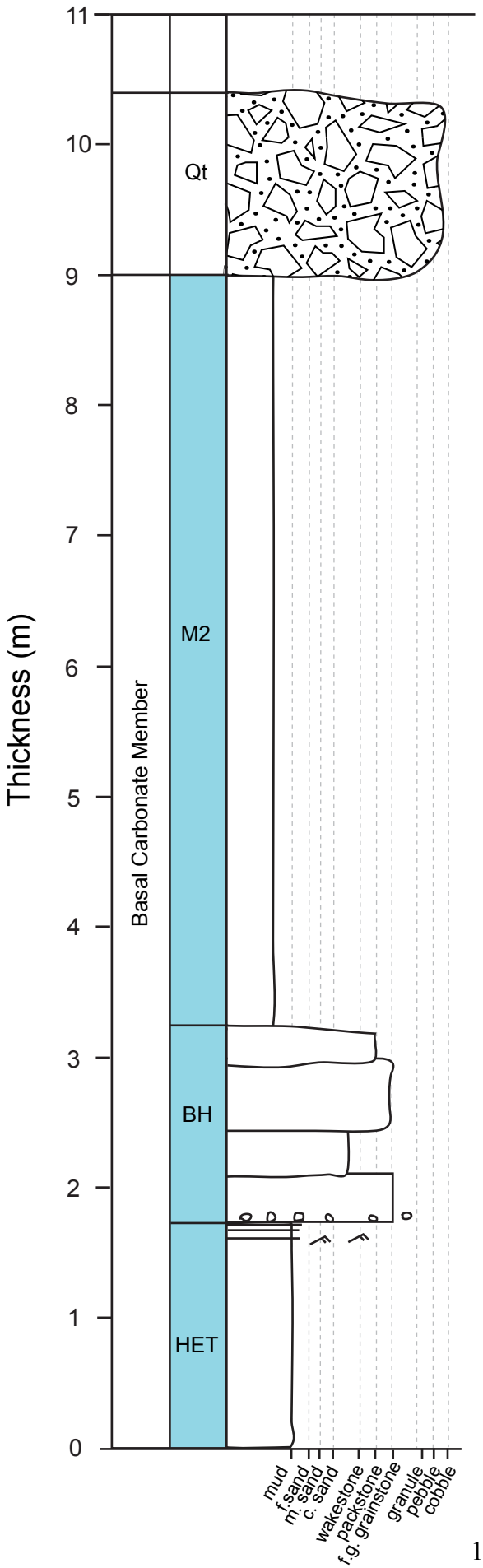

End N 33.27007
W -114.63461
elev. 130 m

Start N 33.26950
W -114.63440
elev. 108 m

Section 51

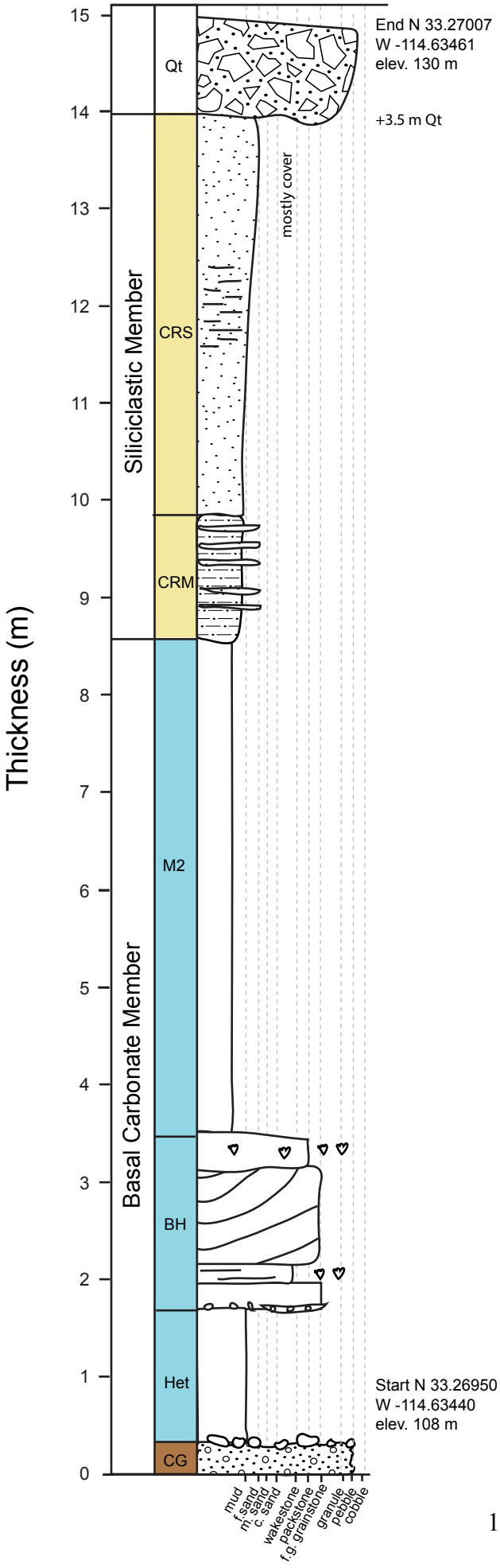
Thickness (m)
15
14
13
12
11
10
9
8
7
6
5
4
3
2
1
0
Qt
CRS
CRM
M2
BH
Het
CG
Siliciclastic Member
Basal Carbonate Member
End N 33.27007
W -114.63461
elev. 130 m
+3.5 m Qt
mostly cover
Start N 33.26950
W -114.63440
elev. 108 m
mud
f. sand
m. sand
c. sand
wakestone
packstone
f.g. grainstone
granule
pebble
cobble

Section 52

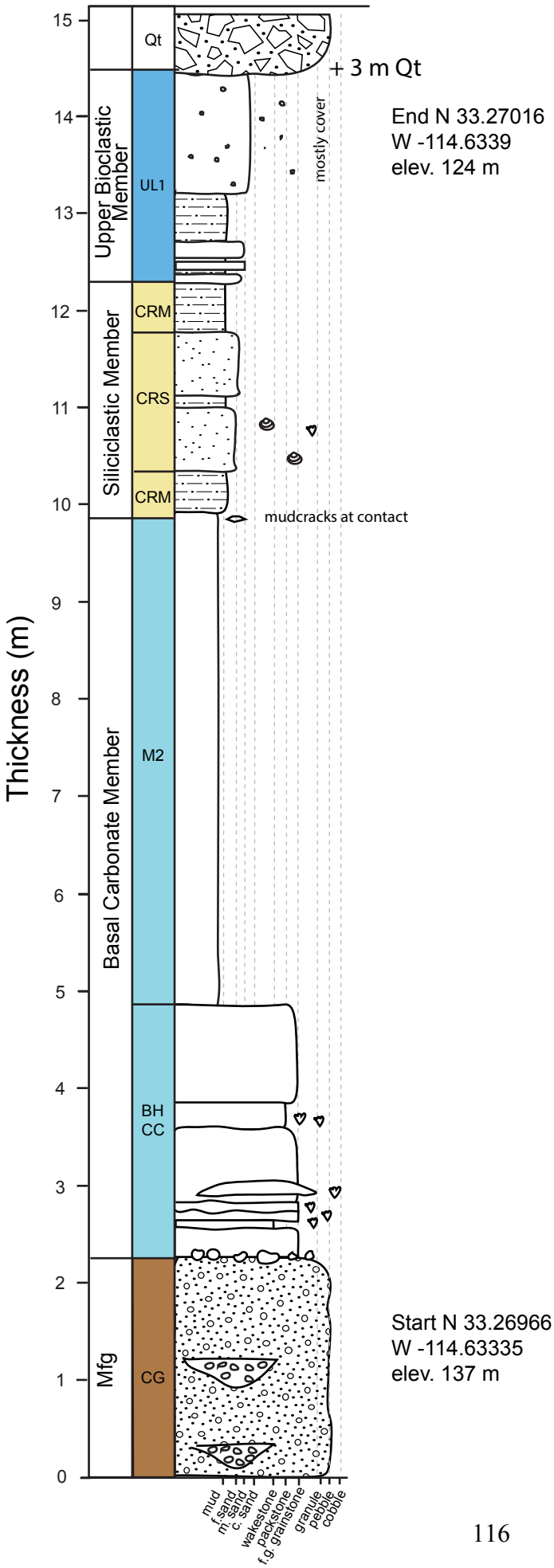

End N 33.27016
W -114.6339
elev. 124 m

Start N 33.26966
W -114.63335
elev. 137 m

Section 53

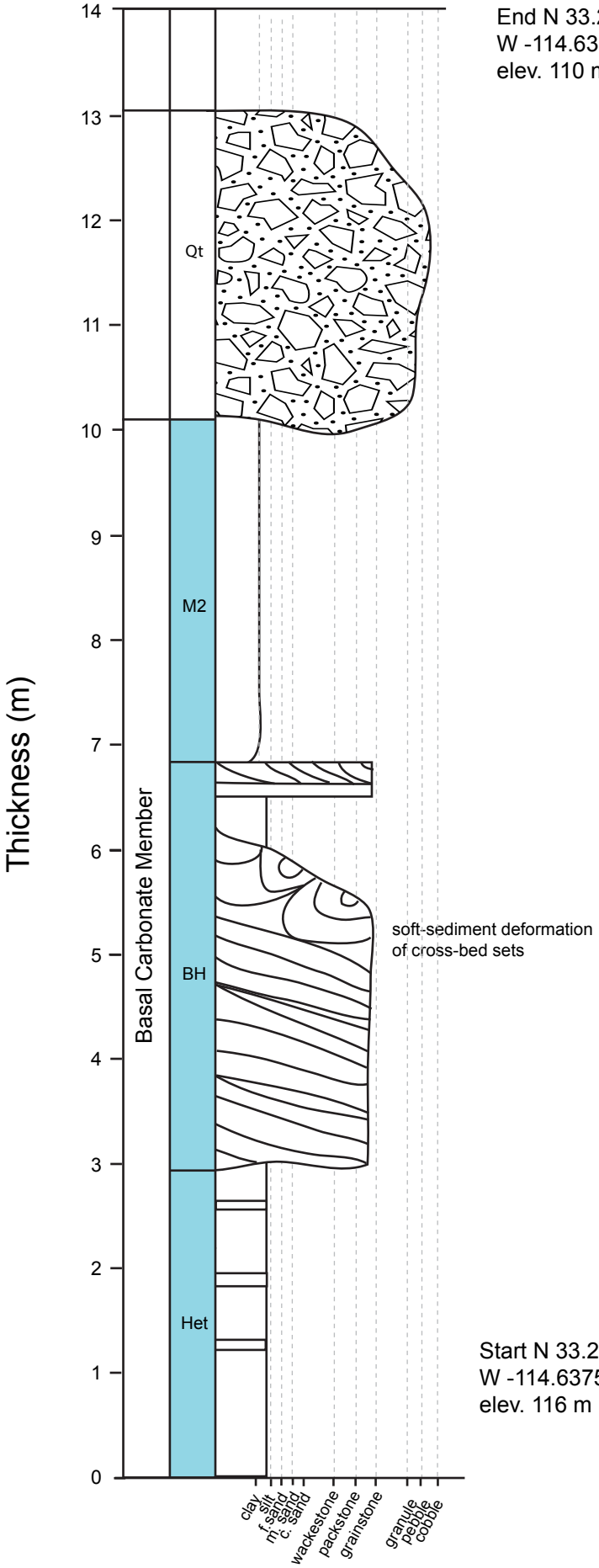

End N 33.26969
W -114.63767
elev. 110 m

Start N 33.26978
W -114.63752
elev. 116 m (bottom of wash, not accurate?)

Section 54

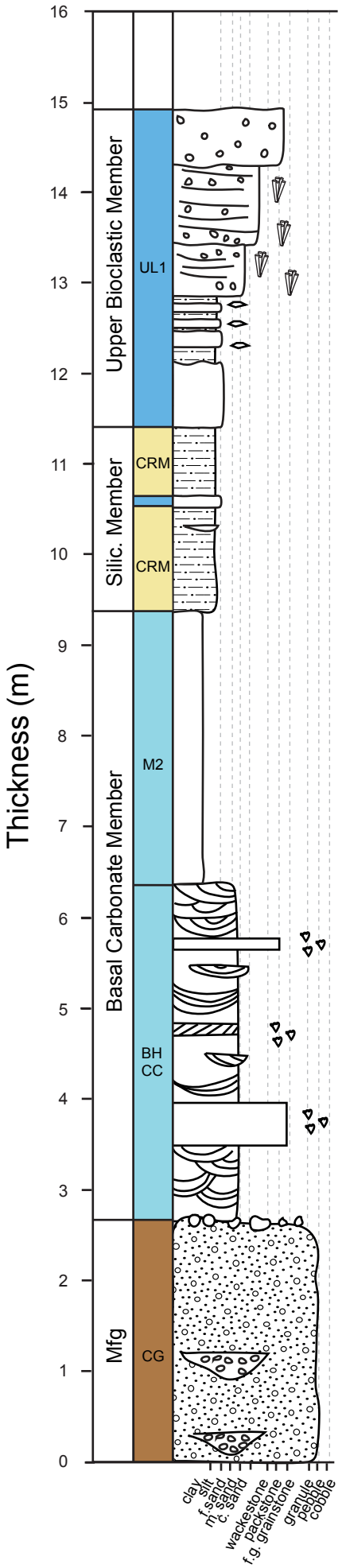
End N 33.27016
W -114.6339
elev. 124 m
Thickness (m)
16
15
14
13
12
11
10
9
8
7
6
5
4
3
2
1
0
Upper Bioclastic Member
Silic. Member
Basal Carbonate Member
Mfg
UL1
CRM
CRM
M2
BH
CC
CG
clay
silt
f. sand
m. sand
c. sand
wackestone
packstone
f.g. grainstone
granule
pebble
cobble
Start N 33.26966
W -114.63335
elev. 137 m

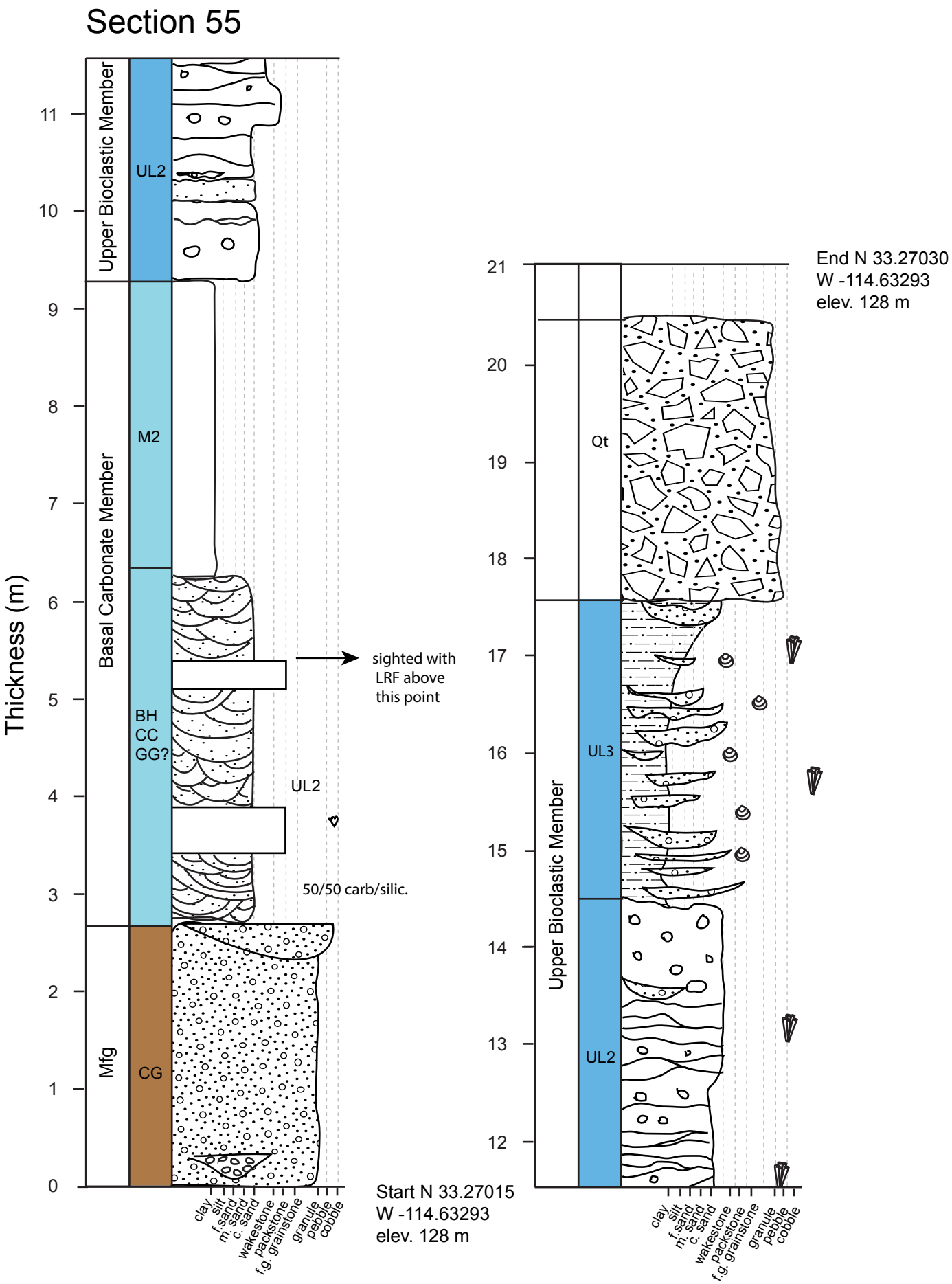
Section 55
Thickness (m)
0
1
2
3
4
5
6
7
8
9
10
11
12
13
14
15
16
17
18
19
20
21
Upper Bioclastic Member
Basal Carbonate Member
Mfg
UL2
M2
BH
CC
GG?
CG
Qt
UL3
UL2
sighted with
LRF above
this point
50/50 carb/silic.
Start N 33.27015
W -114.63293
elev. 128 m
End N 33.27030
W -114.63293
elev. 128 m
clay
silt
f. sand
m. sand
c. sand
wakestone
packstone
f.g. grainstone
granule
pebble
cobble

Section 56

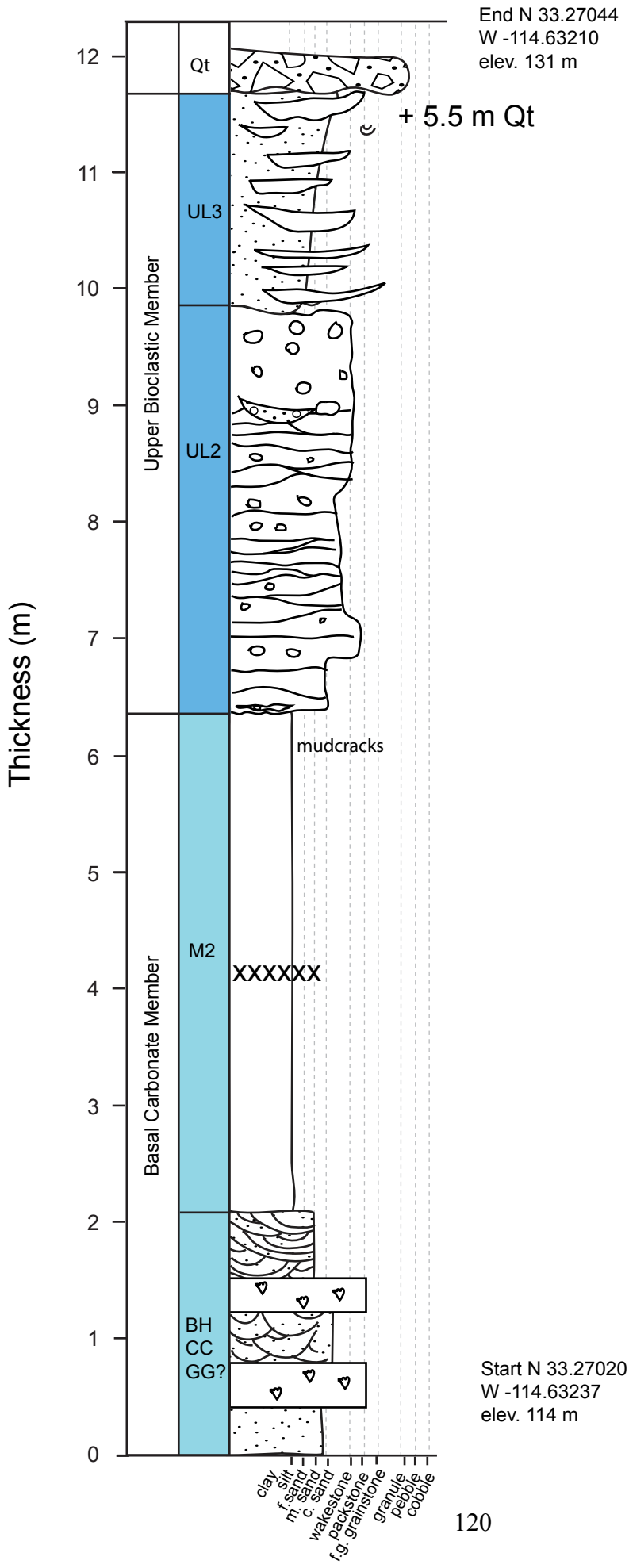
End N 33.27044
W -114.63210
elev. 131 m
+ 5.5 m Qt
Qt
UL3
UL2
Upper Bioclastic Member
Basal Carbonate Member
M2
BH
CC
GG?
mudcracks
XXXXXX
Thickness (m)
0
1
2
3
4
5
6
7
8
9
10
11
12
clay
silt
f. sand
m. c. sand
wakestone
packstone
f.g. grainstone
granule
pebble
cobble
Start N 33.27020
W -114.63237
elev. 114 m

Section 57

End N 33.29341
W -114.62395
elev. 149 m

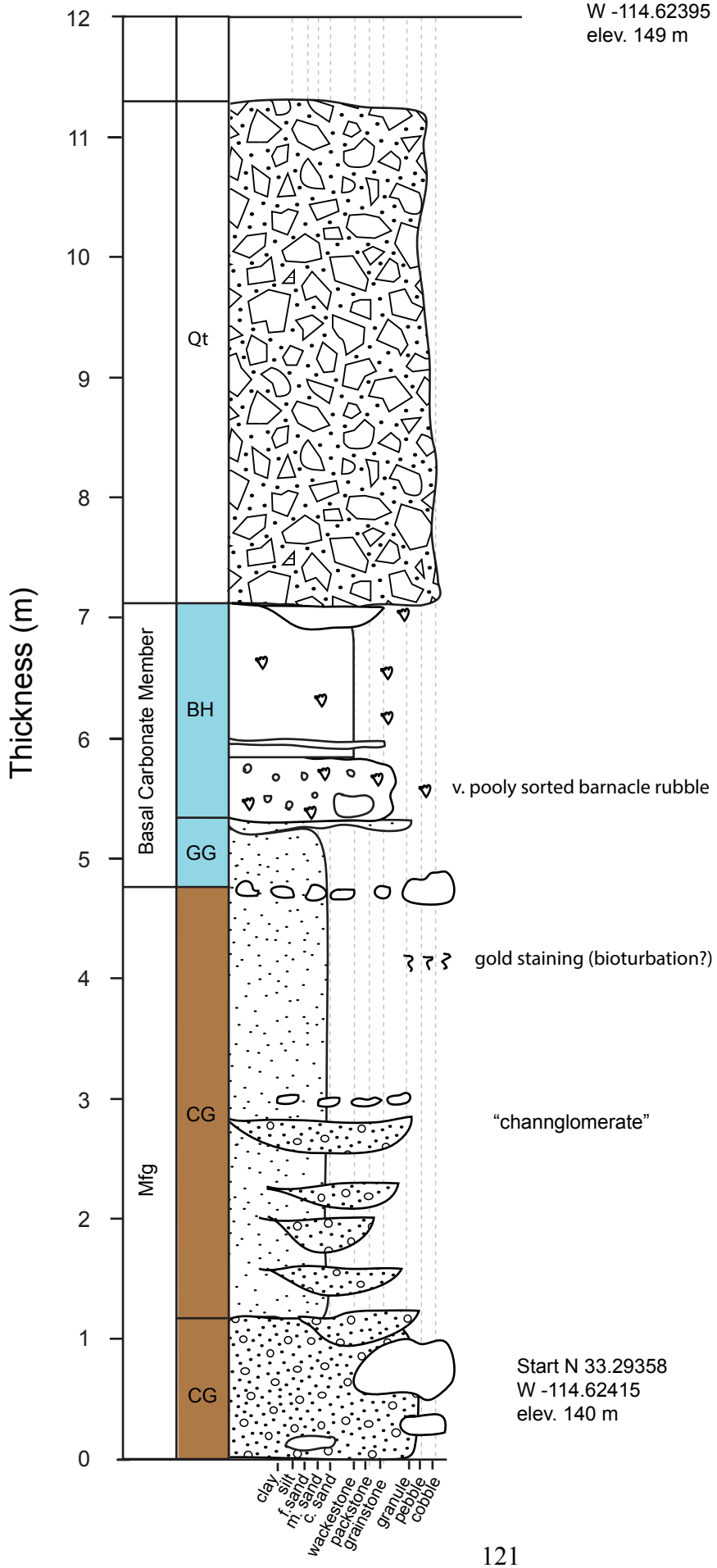

Start N 33.29358
W -114.62415
elev. 140 m

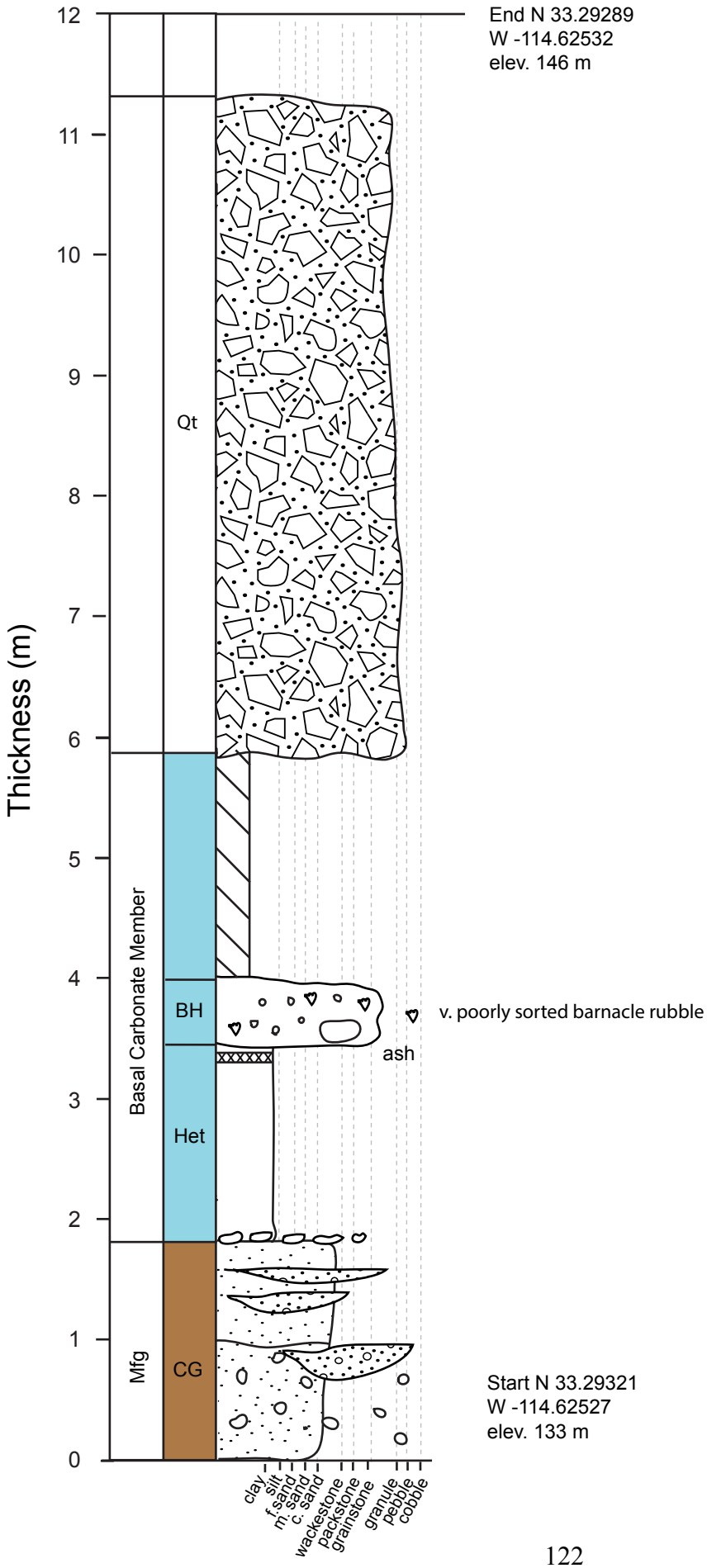
Section 58
End N 33.29289
W -114.62532
elev. 146 m
Thickness (m)
12
11
10
9
8
7
6
5
4
3
2
1
0
Qt
Basal Carbonate Member
BH
Het
Mfg
CG
v. poorly sorted barnacle rubble
ash
Start N 33.29321
W -114.62527
elev. 133 m
clay
silt
f. sand
m. sand
c. sand
wackestone
packstone
grainstone
granule
pebble
cobble

Section 59

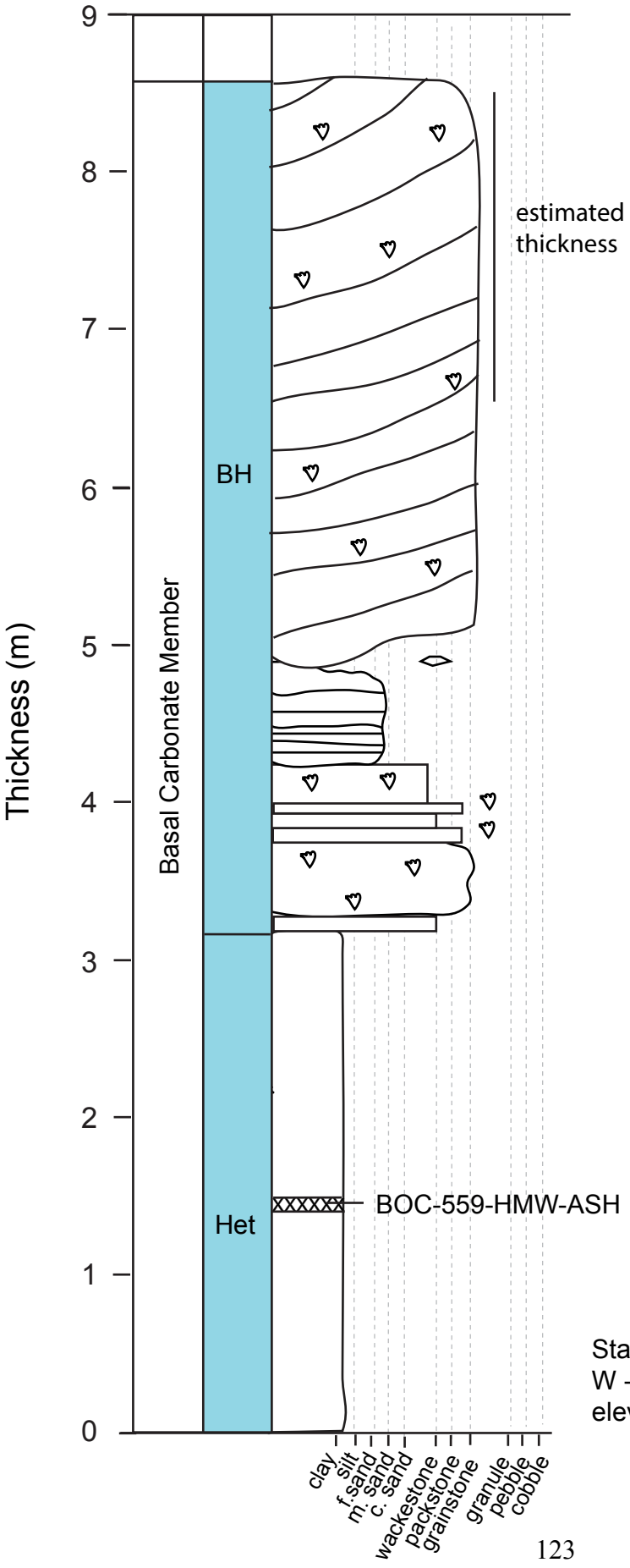

Start N 33.29329
W -114.62659
elev. 147 m

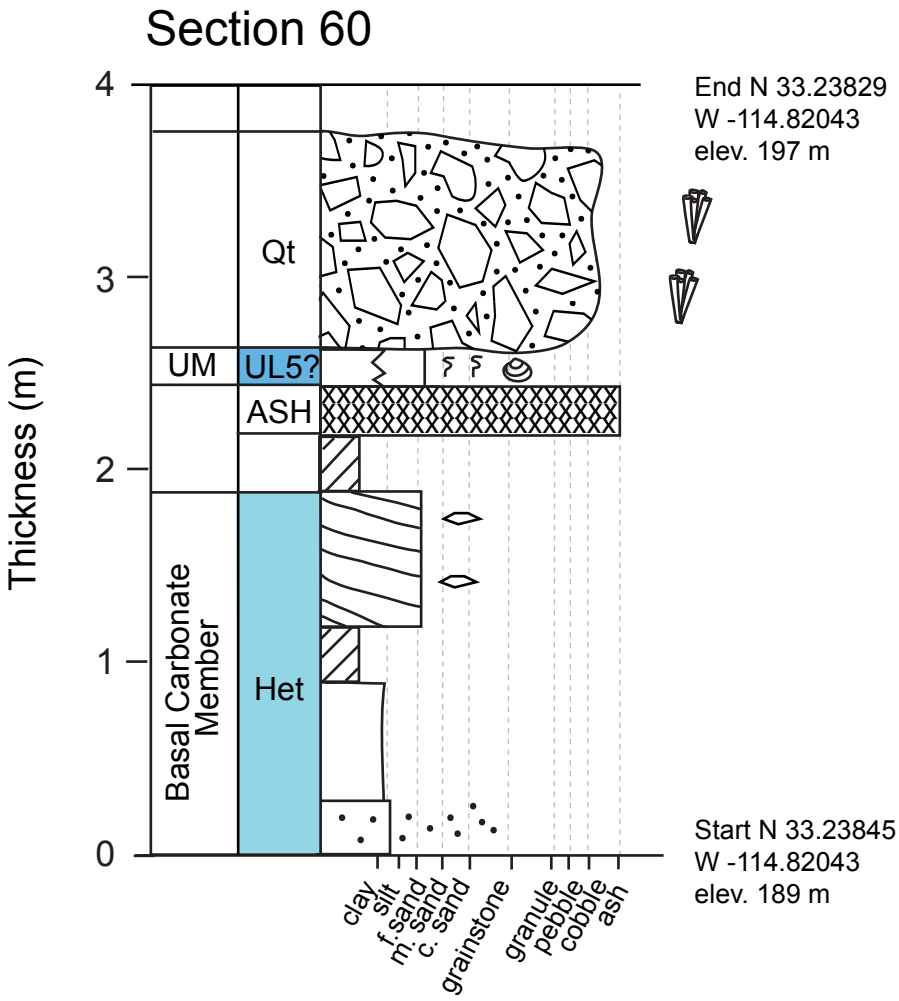
Section 60
Thickness (m)
4
3
2
1
0
Qt
UM
UL5?
ASH
Basal Carbonate Member
Het
End N 33.23829
W -114.82043
elev. 197 m
Start N 33.23845
W -114.82043
elev. 189 m
clay
silt
f. sand
m. sand
c. sand
grainstone
granule
pebble
cobble
ash

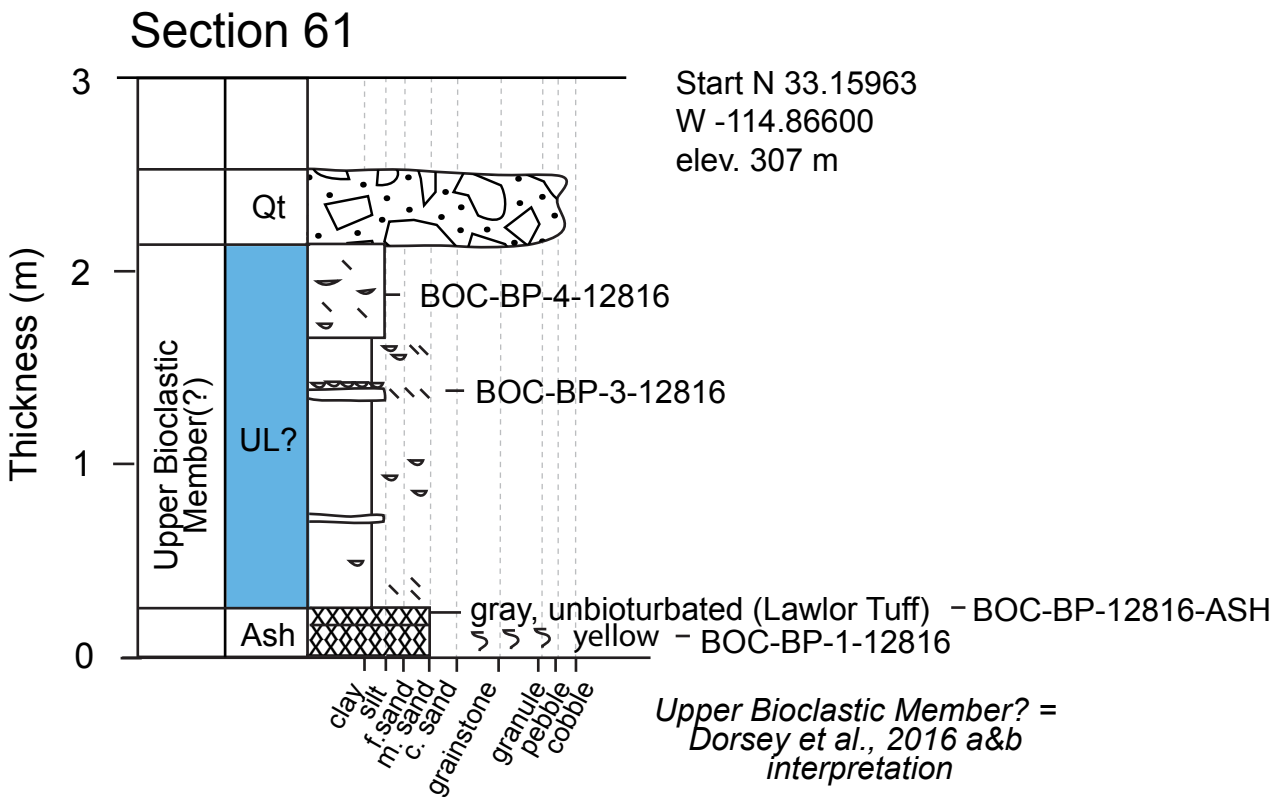
Section 61
Start N 33.15963
W -114.86600
elev. 307 m
Thickness (m)
3
2
1
0
Qt
Upper Bioclastic Member(?)
UL?
Ash
BOC-BP-4-12816
BOC-BP-3-12816
gray, unbioturbated (Lawlor Tuff)
BOC-BP-12816-ASH
yellow
BOC-BP-1-12816
clay
silt
f. sand
m. sand
c. sand
grainstone
granule
pebble
cobble
Upper Bioclastic Member? =
Dorsey et al., 2016 a&b
interpretation

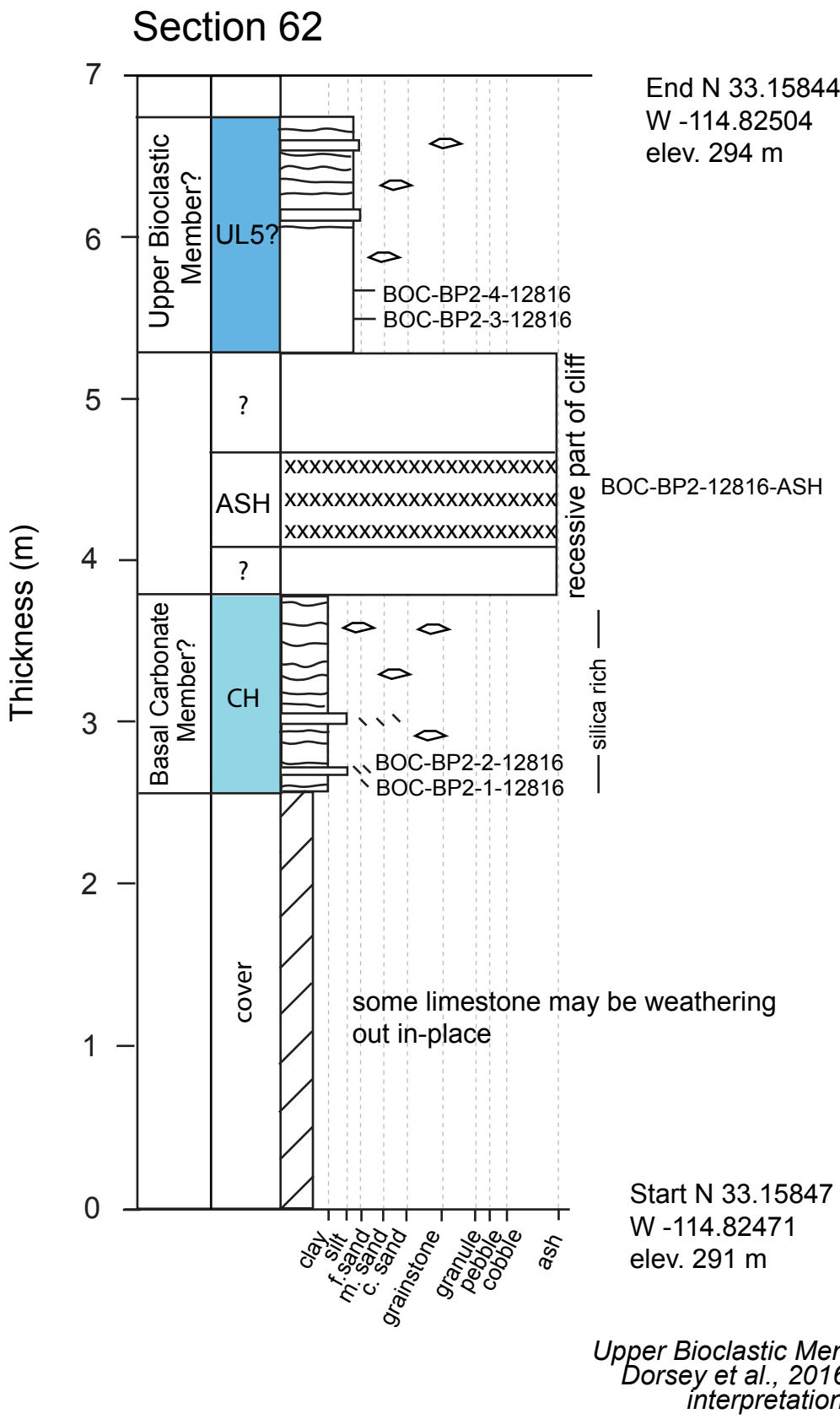
Section 62
Thickness (m)
7
6
5
4
3
2
1
0
Upper Bioclastic Member?
UL5?
?
ASH
?
Basal Carbonate Member?
CH
cover
BOC-BP2-4-12816
BOC-BP2-3-12816
BOC-BP2-12816-ASH
recessive part of cliff
silica rich
BOC-BP2-2-12816
BOC-BP2-1-12816
some limestone may be weathering out in-place
clay
silt
f. sand
m. sand
c. sand
grainstone
granule
pebble
cobble
ash
End N 33.15844
W -114.82504
elev. 294 m
Start N 33.15847
W -114.82471
elev. 291 m
Upper Bioclastic Member? = Dorsey et al., 2016 a&b interpretation

Section 63

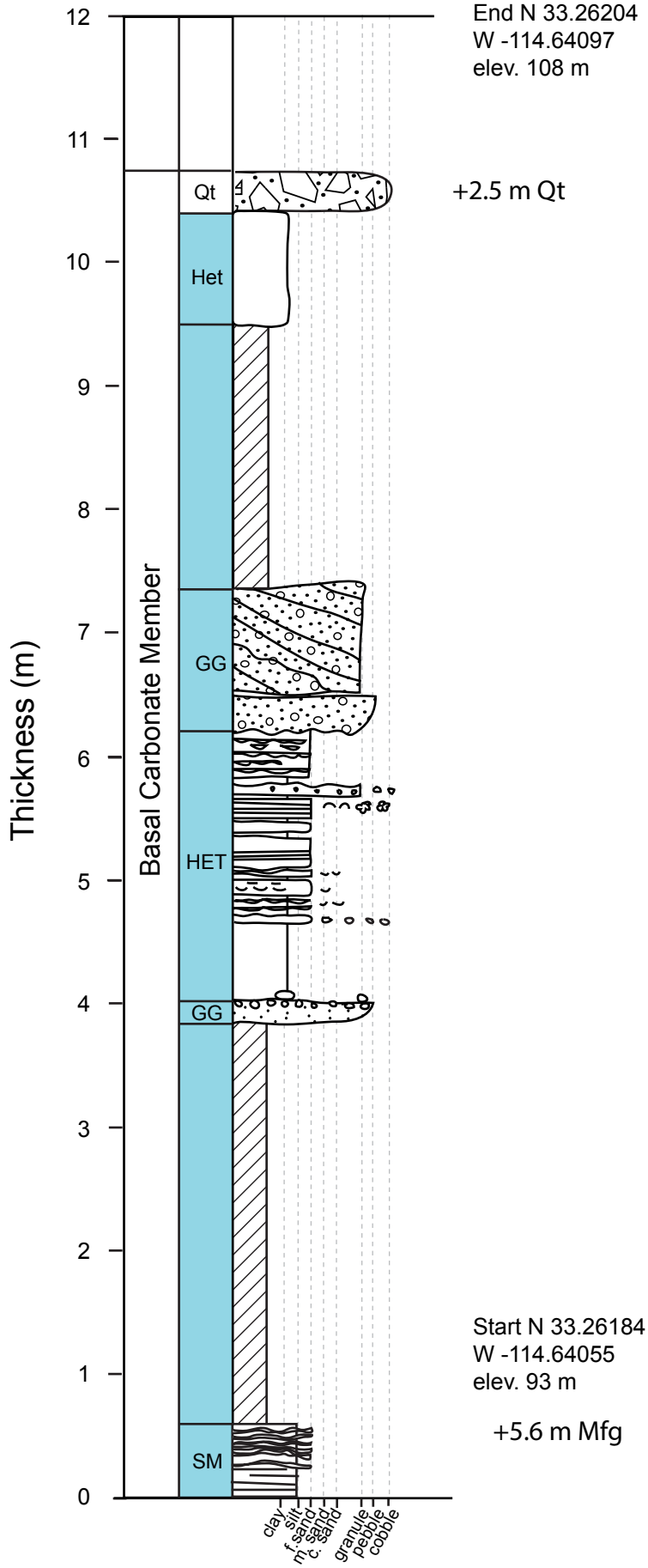
End N 33.26204
W -114.64097
elev. 108 m
+2.5 m Qt
Start N 33.26184
W -114.64055
elev. 93 m
+5.6 m Mfg
Thickness (m)
Basal Carbonate Member
Qt
Het
GG
HET
GG
SM
12
11
10
9
8
7
6
5
4
3
2
1
0
clay
silt
f sand
m. sand
c. sand
granule
pebble
cobble

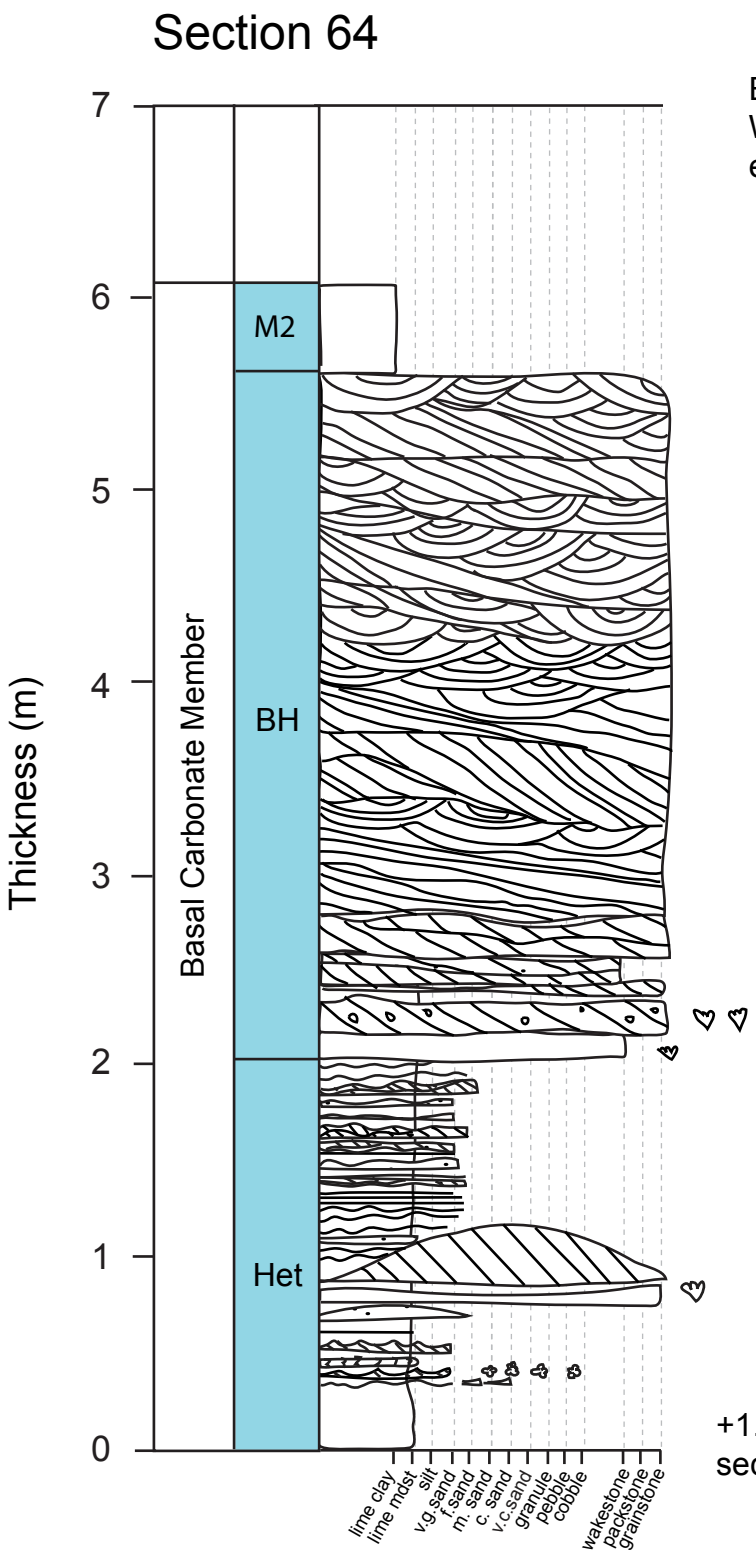
Section 64
End N 33.26786
W -114.64061
elev. 104 m
Thickness (m)
Basal Carbonate Member
M2
BH
Het
0
1
2
3
4
5
6
7
lime clay
lime mdst
silt
v.g.sand
f.sand
m. sand
c. sand
v.c.sand
granule
pebble
cobble
wakestone
packstone
grainstone
+1.4 m Marl 1
section starts 1.4 m above wash
Start N 33.26966
W -114.639480
elev. 93 m

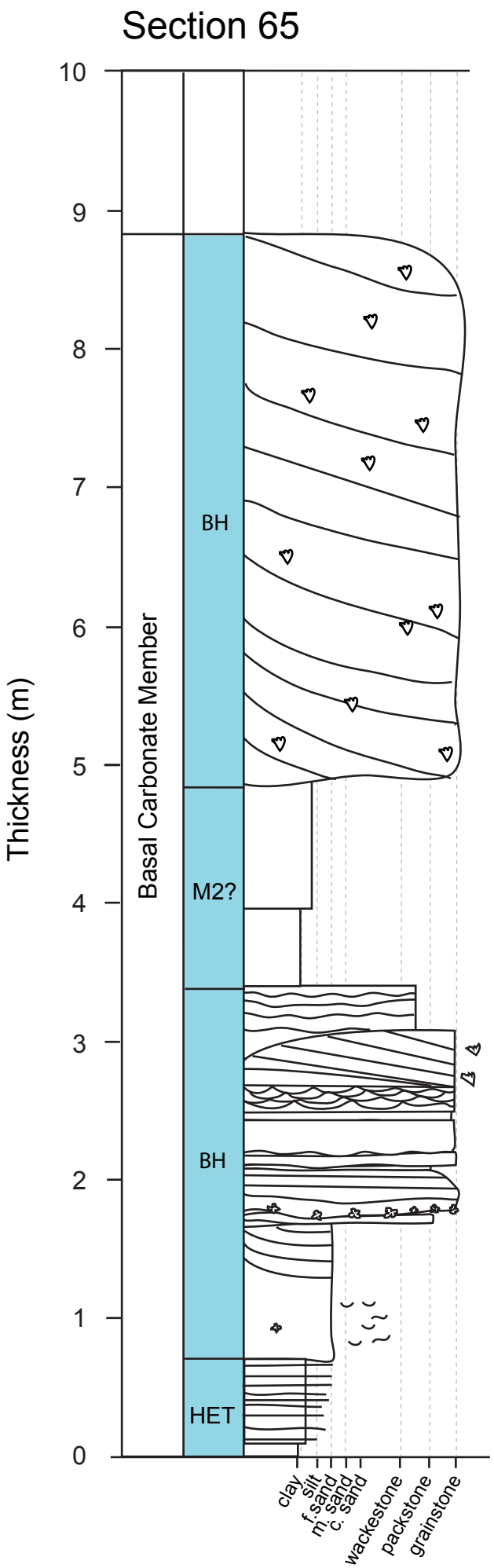
Section 65
End N 33.26204
W -114.64097
elev. 108 m
Start N 33.26184
W -114.64055
elev. 93 m
Thickness (m)
Basal Carbonate Member
BH
M2?
BH
HET
clay
silt
f. sand
m. sand
c. sand
wackestone
packstone
grainstone

Section 66

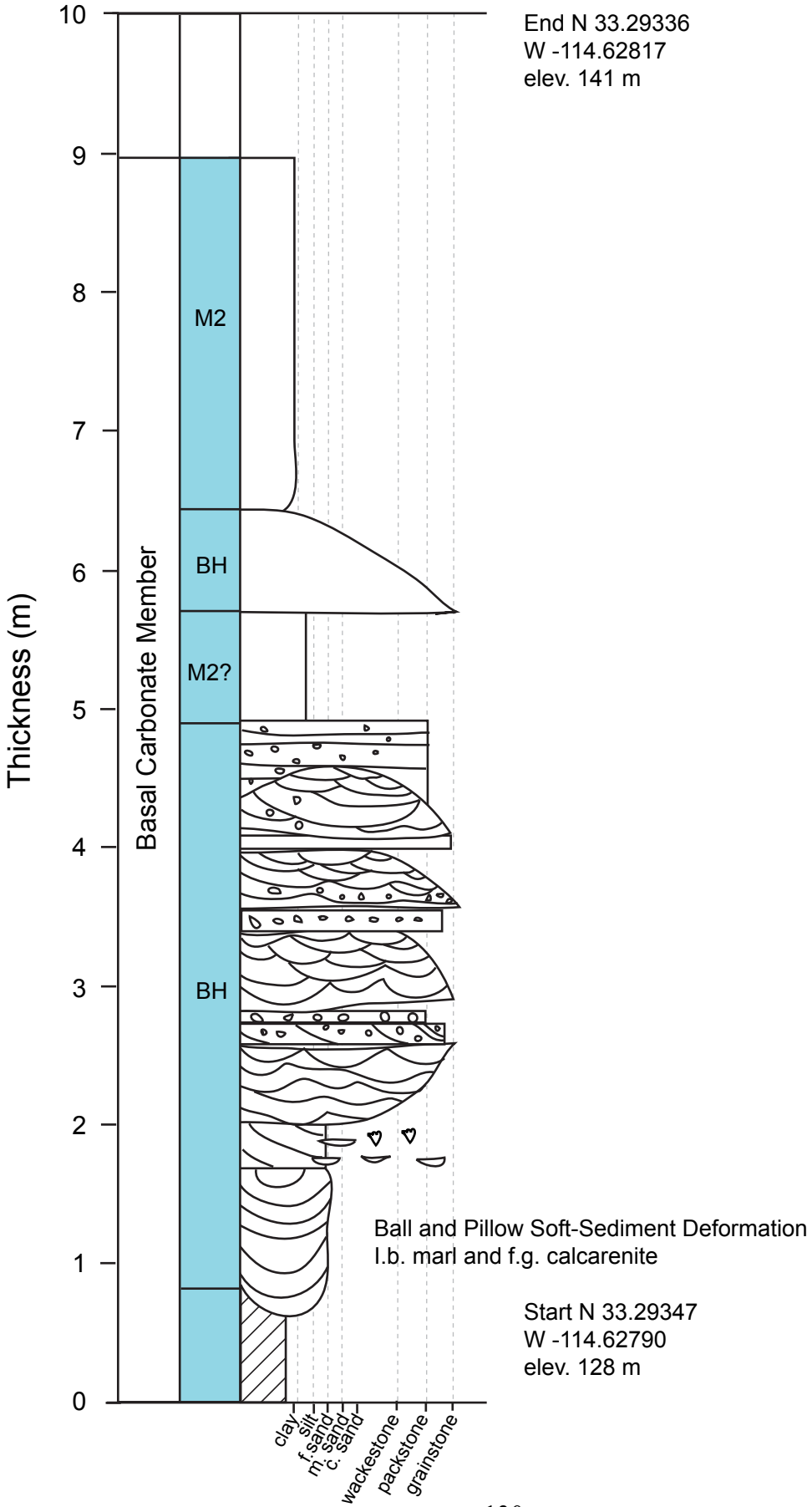
End N 33.29336
W -114.62817
elev. 141 m
Thickness (m)
Basal Carbonate Member
M2
BH
M2?
BH
Ball and Pillow Soft-Sediment Deformation
l.b. marl and f.g. calcarenite
Start N 33.29347
W -114.62790
elev. 128 m
clay
silt
f. sand
m. sand
c. sand
wackestone
packstone
grainstone

Section 67

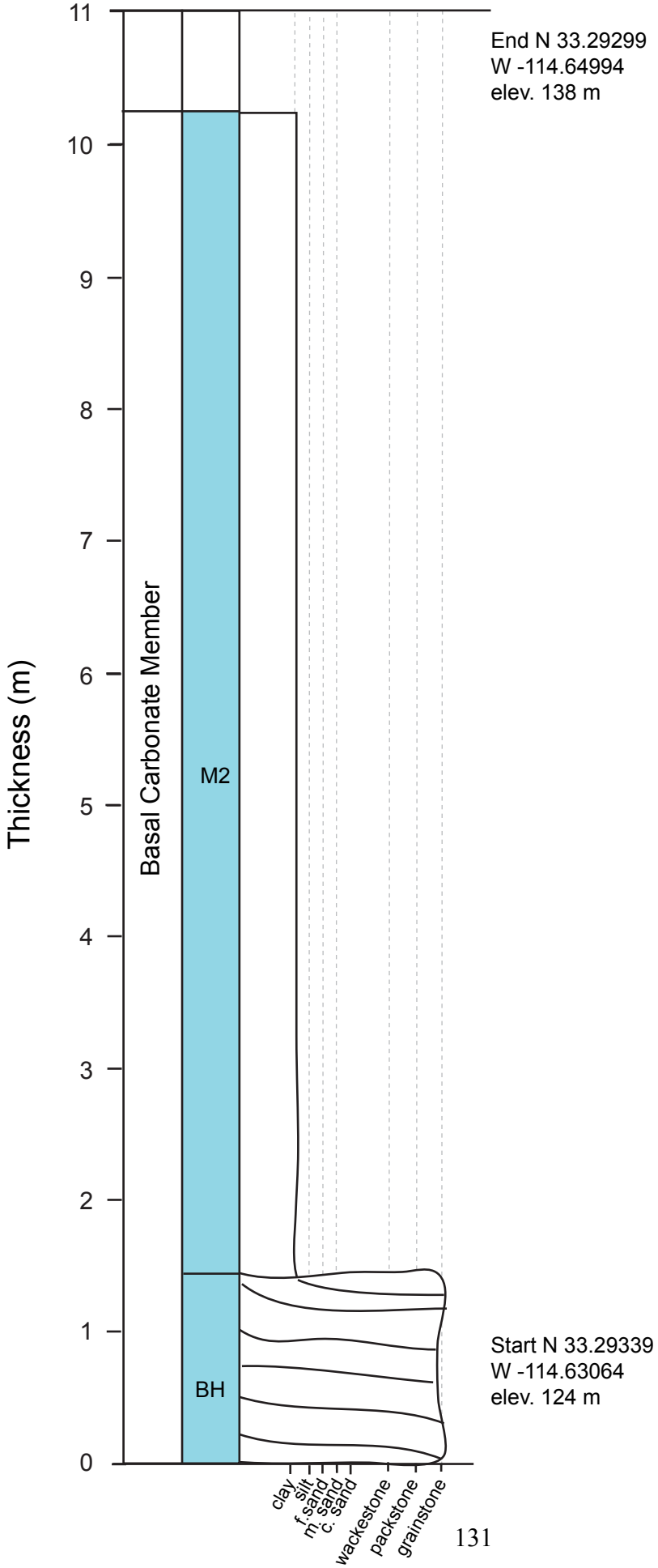
Thickness (m)
11
10
9
8
7
6
5
4
3
2
1
0
Basal Carbonate Member
M2
BH
End N 33.29299
W -114.64994
elev. 138 m
Start N 33.29339
W -114.63064
elev. 124 m
clay
silt
f. sand
m. sand
c. sand
wackestone
packstone
grainstone

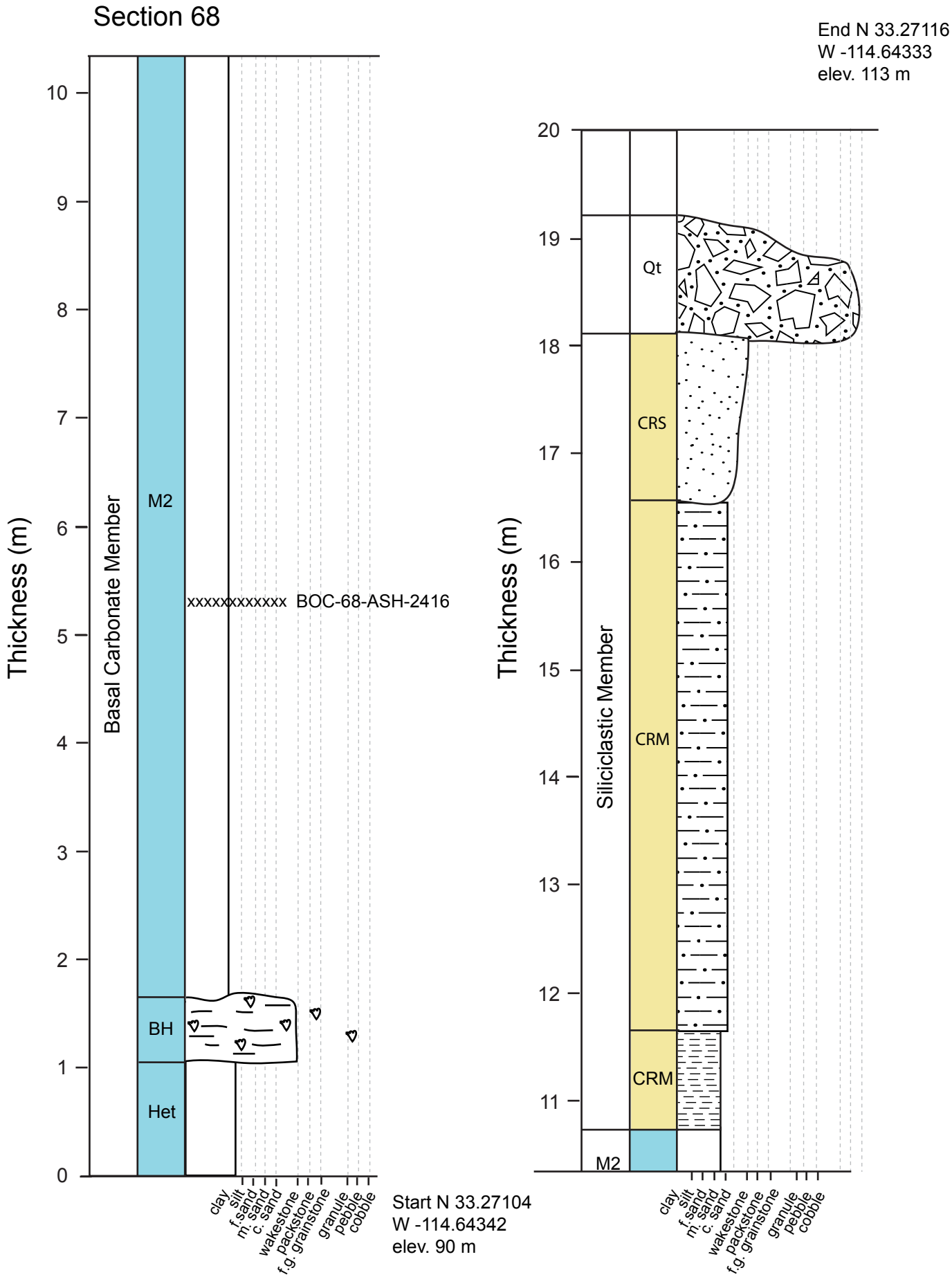
Section 68
End N 33.27116
W -114.64333
elev. 113 m
Thickness (m)
Basal Carbonate Member
M2
BH
Het
xxxxxxxxxxxx BOC-68-ASH-2416
Start N 33.27104
W -114.64342
elev. 90 m
Siliciclastic Member
Qt
CRS
CRM
CRM
M2
clay
silt
f.sand
m. sand
c. sand
wakestone
packstone
f.g. grainstone
granule
pebble
cobble

APPENDIX D

BOUSE FORMATION MEASURED SECTION DATA

All elevations start at wash bottom
Elevation = section starts at wash bottom
Elevation (x) = section starts x meters above wash bottom

Section Name	Latitude	Longitude	Elevation (m)	Thickness (m)
1	33.255500	-114.640378	96 (1.25)	29.5
2	33.255550	-114.631090	108	12.0
3	33.258060	-114.641780	99 (10)	23.4
4	33.255180	-114.642780	86 (4.5)	16.1
5	33.255780	-114.633060	107	14.5
6	33.263690	-114.635790	108 (75 cm)	15.7
7	33.263310	-114.636000	106	12
8	33.263150	-114.636440	100	13.5
9	33.264250	-114.634850	106	23.7
10	33.263020	-114.635310	105	9.0
11	33.257610	-114.641420	92 (15.62)	9.5
12	33.262860	-114.636690	102	11.5
13	33.263220	-114.634780	107	20.3
14	33.260410	-114.634300	106	24.4
15	33.260160	-114.637410	99 (9.4)	1.4
16	33.259200	-114.639020	95	12.7
17	33.247690	-114.629070	136	38.0
18	33.254040	-114.632500	110 (22)	37.5
19	33.252990	-114.633376	129 (5)	12.5
20	33.252070	-114.643890	92 (23)	40.3
21	33.250110	-114.640460	114 (9.6)	10.4
22	33.250090	-114.639850	119 (7.1)	11.6
23	33.246260	-114.623600	231	5.1
24	33.262630	-114.639560	95 (60 cm)	22.0
25	33.256940	-114.640250	93 (2.5)	27.6
26	33.258870	-114.645380	92 (8.25)	14.5
27	33.259532	-114.647969	81 (4.35)	13.8
28	33.260350	-114.642840	91 (2.45)	15.8
29	33.260220	-114.644910	86 (3.6)	4.2
30	33.259650	-114.649610	85 (3)	13

31	33.272090	114.647040	80	8.0
32	33.273200	-114.653520	73	14.1
33	33.290740	-114.636390	107	20.4
34	33.299630	-114.628970	116	17.4
35	33.258370	-114.729890	79	3.7
36	33.255470	-114.751300	111	3.1
37	33.269260	-114.635560	117	12.2
38	33.269650	-114.636630	97	12
39	33.269950	-114.638200	100	12.6
40	33.263770	-114.635500	107	23.0
41	33.269680	-114.640040	110	8.2
42	33.269670	-114.641430	94	6.5
43	33.270030	-114.642160	96	2.9
44	33.268330	-114.633480	115	4.1
45	33.268470	-114.632740	119	4.1
46	33.268510	-114.632450	120 (1.2)	5.5
47	33.245900	-114.806080	170	5.5
48	33.244290	-114.807250	178	5.4
49	33.268530	114.631770	114	4.7
50	33.269240	114.635170	110 (7)	10.3
51	33.264500	114.634400	108 (1)	18.4
52	33.269660	-114.633350	137	18.0
53	33.269780	-114.637520	116	13.0
54	33.269960	-114.633060	115	14.9
55	33.270150	114.632780	109 (1)	20.4
56	33.270200	-114.632370	114 (3.2)	17.5
57	33.293580	-114.624150	140	11.3
58	33.293210	-114.625270	133	11.2
59	33.293290	114.626590	147	8.6
60	33.238290	-114.820830	189 (6.7)	3.9
61	33.253550	-114.631300	117	12.5
62	33.158470	-114.824710	291 (2.5)	6.7
63	33.261840	-114.640550	93 (5.6)	13.2
64	33.269660	-114.639480	93 (1.4)	6.1
65	33.293330	-114.627460	130	8.8
66	33.293470	-114.627900	128	9.0
67	33.293390	114.630640	124	10.4
68	33.271040	-114.643420	90	19.1

APPENDIX E

FUTURE WORK

Questions that I would advise the next process-oriented sedimentologist working on the Bouse Formation to explore:

1. How does the effect of tidal currents on sedimentation change from one side of the basin to the other? There are differences in the sedimentology between east and west localities. While 'tidal' can be inferred from the base of the basal carbonate unit basin-wide, differences from each side of the basin suggest different environments or perhaps non-uniform tidal currents. Perhaps some sort of rotary tidal wave influenced sedimentation one side to the other?
2. Are the Colorado River siliciclastic deposits indeed essentially 'non-tidal'? I can speculate that these siliciclastic deposits don't show many obvious signs of tidal influence, however, I have spent limited time in the siliciclastic unit.
3. Are there any long-term cycles (e.g. Milankovitch cycles) recorded in the upper lime mudstone (Marl 2) unit? There is some regularity to the deposits with alternations of fissile lime mud to more resistant lime mud at intervals of ~50 cm that could record climate various over long-term sedimentation intervals.
4. How do storms contribute to sedimentation? There is sufficient evidence for a storm influence on sedimentation (e.g. pebble beds), and perhaps storms are playing a larger role on sedimentation than we noticed.
5. What is the nature of the soft-sediment deformation of the basal carbonate member? Does the mixed nature of deposits contribute to the apparent propensity for soft-sediment deformation? Does similar deformation occur in either carbonate or siliciclastic environments, or are there fundamental differences in mixed settings?
6. Is there a shoaling and periodic exposure of beds in the upper part of the basal carbonate member just prior to deposition of the green claystone? Stratigraphically it doesn't make sense, but there is evidence for emergence (e.g. mudcracks, or syneresis?) in the lime-mudstone units just prior to arrival of CR green claystone (see Plate 5, i).

REFERENCES CITED

Chapter Two

Ainsworth, R.B., Hasiotis, S.T., Amos, K.J., Krapf, C.B., Payenberg, T.H., Sandstrom, M.L., Vakarelov, B.K., and Lang, S.C., 2012, Tidal signatures in an intracratonic playa lake: Geology, v. 40, p. 607–610, doi:10.1130/G32993.1.

Archer, A.W., and Johnson, T.W., 1997, Modelling of cyclic tidal rhythmites (Carboniferous of Indiana and Kansas, Precambrian of Utah, USA) as a basis for reconstruction of intertidal positioning and palaeotidal regimes: Sedimentology, v. 44, p. 991–1010, doi:10.1111/j.1365-3091.1997.tb02174.x.

Archer, A.W., 1998, Hierarchy of controls on cyclic rhythmite deposition: Carboniferous basins of eastern and mid continental U.S.A., in Alexander, C.R., et al., eds., Tidalites: Processes and products: SEPM (Society for Sedimentary Geology) Special Publication 61, p. 59–68, doi:10.2110/pec.98.61.0059.

Brand, U., and Veizer, J., 1980, Chemical diagenesis of a multicomponent carbonate system: 1. Trace elements: Journal of Sedimentary Research, v. 50, p. 1219–1236, doi:10.1306/212F7BB7-2B24-11D7-8648000102C1865D.

Bright, J., Cohen, A.S., Dettman, D.L., Pearthree, P.A., Dorsey, R.J., and Homan, M.B., 2016, Did a Catastrophic Lake Splillover Integrate the Late Miocene Early Pliocene Colorado River and the Gulf of California?: Microfaunal and Stable Isotope Evidence from Blythe Basin, California-Arizona, USA: Palaios, v. 31, p. 81–91, doi:10.2110/palo.2015.035.

Buising, A. V., 1990, The Bouse Formation and bracketing units, southeastern California and western Arizona: Implications for the evolution of the Proto-Gulf of California and the lower Colorado River: Journal of Geophysical Research: Solid Earth (1978–2012), v. 95, p. 20111–20132.

Crossey, L. C., Karlstrom, K.E., Dorsey, R., Pearce, J., Wan, E., Beard, L.S., Asmerom, Y., Polyak, V., Crow, R.S., Cohen, A., Bright, J., and Huth, J., 2015, The importance of groundwater in propagating downward integration of the 6–5 Ma Colorado River System: Geochemistry of springs, travertines and lacustrine carbonates of the Grand Canyon region over the past 12 million years: Geosphere, v. 11, no. 3, p. 660–682, doi:10.1130/GES01073.1.

Crow, R., House, K., Karlstrom, K., Heizler, M., Polyak, V., Asmerom, Y., Pearthree, P., O'Connell, B., Crossey, L., Champion, D., Beard, S., Dorsey, R.J., and McDougall, K., 2016, Deciphering lower Colorado River integration through geochronologic studies of the Bouse Formation: Preliminary results and future directions: Geological Society of America Abstracts with Programs, v. 48, no. 7, doi:10.1130/abs/2016AM-286483.

Crow, R., Karlstrom, K., Darling, A., Crossey, L., Polyak, V., Granger, D., Asmerom, Y., and Schmandt, B., 2014, Steady incision of Grand Canyon at the million year timeframe: A case for mantle-driven differential uplift: Earth and Planetary Science Letters, v. 397, p. 159–173, doi:10.1016/j.epsl.2014.04.020.

Dalrymple, R.W., 2010, Tidal depositional systems, in James, N.P., and Dalrymple, R.W., eds., Facies Models, 4, GEOText6: Geological Association of Canada, p. 199–208.

Dalrymple, R.W., and Choi, K., 2007, Morphologic and facies trends through the fluvial–marine transition in tide-dominated depositional systems: A schematic framework for environmental and sequence stratigraphic interpretation: Earth-Science Reviews, v. 81, p. 135–174, doi:10.1016/j.earscirev.2006.10.002.

Davis, R.A., Jr., 2012, Tidal signatures and their preservation potential in stratigraphic sequences: Principles of tidal sedimentology: Dordrecht, Springer, p. 35–55, doi:10.1007/978-94-007-0123-6_3.

De Boer, P.L., Oost, A.P., and Visser, M.J., 1989, The diurnal inequality of the tide as a parameter for recognizing tidal influences: Journal of Sedimentary Research, v. 59, p. 912–921.

Eisma, D., de Boer, P.L., Cadée, G.C., Dijkema, K., Philippart, C.J.M., and Ridderinkhof, H., 1998, Intertidal deposits: River mouths, tidal flats and coastal lagoons: Boca Raton, Florida, CRC Press, 544 p.

Fraser, G., Thompson, T., Kvale, E., Carlson, C., Fishbaugh, D., Graver, B., Holbrook, J., Kairo, S., Kohler, C., and Malone, A., 1991, Sediments and sedimentary structures of a barred, nontidal coastline, southern shore of Lake Michigan: Journal of Coastal Research, v. 7, p. 1113–1124.

Homan, M.B., 2014, Sedimentology and Stratigraphy of the Miocene-Pliocene Bouse Formation near Cibola, Arizona and Milpitas Wash, California: Implications for the Early Evolution of the Colorado River: University of Oregon, 116 p.

vS Hood, A., Planavsky, N. J., Wallace, M. W., Wang, X., Bellefroid, E. J., Gueguen, B., and Cole, D.B., 2016, Integrated geochemical-petrographic insights from component-selective D238U of Cryogenian marine carbonates: Geology, p. G38533. 38531.

House, P.K., Pearthree, P.A., and Perkins, M.E., 2008, Stratigraphic evidence for the role of lake spillover in the inception of the lower Colorado River in southern Nevada and western Arizona: Geological Society of America. Special Paper, v. 439, p. 335–353.

Hovikoski, J., Räsänen, M., Gingras, M., Roddaz, M., Brusset, S., Hermoza, W., Pittman, L.R., and Lertola, K., 2005, Miocene semidiurnal tidal rhythmites in Madre de Dios, Peru: Geology, v. 33, p. 177–180, doi:10.1130/G21102.1.

Karlstrom, K., Coblentz, D., Dueker, K., Ouimet, W., Kirby, E., Van Wijk, J., Schmandt, B., Kelley, S., Lazear, G., and Crossey, L., 2012, Mantle-driven dynamic uplift of the Rocky Mountains and Colorado Plateau and its surface response: Toward a unified hypothesis: Lithosphere, v. 4, p. 3–22, doi:10.1130/L150.1.

Kvale, E.P., Cutright, J., Bilodeau, D., Archer, A., Johnson, H.R., and Pickett, B., 1995, Analysis of modern tides and implications for ancient tidalites: Continental Shelf Research, v. 15, p. 1921–1943, doi:10.1016/0278-4343(95)00001-H.

Kvale, E.P., Johnson, H.W., Sonett, C.P., Archer, A.W., and Zawistoski, A., 1999, Calculating lunar retreat rates using tidal rhythmites: Journal of Sedimentary Research, v. 69, p. 1154–1168, doi:10.2110/jsr.69.1154.

Longhitano, S.G., 2010, The record of tidal cycles in mixed silici–bioclastic deposits: Examples from small Plio–Pleistocene peripheral basins of the microtidal Central Mediterranean Sea: Sedimentology, v. 58, p. 691–719, doi:10.1111/j.1365-3091.2010.01179.x.

Longhitano, S.G., Mellere, D., Steel, R.J., and Ainsworth, R.B., 2012, Tidal depositional systems in the rock record: A review and new insights: Sedimentary Geology, v. 279, p. 2–22, doi:10.1016/j.sedgeo.2012.03.024.

McDougall, K., 2008, Late Neogene marine incursions and the ancestral Gulf of California: Geological Society of America. Special Paper, v. 439, p. 355–373.

McDougall, K., and Martínez, A.Y.M., 2014, Evidence for a marine incursion along the lower Colorado River corridor: Geosphere, v. 10, p. 842–869, doi:10.1130/GES00975.1.

Nio, S.-D., and Yang, C.-S., 1991, Diagnostic attributes of clastic tidal deposits: A review, in Smith, D.G., et al., eds., Clastic tidal sedimentology: Canadian Society of Petroleum Geologists Memoir 16, p. 3–28.

D. Nummedal, D.J.P. Swift, 1987, Transgressive stratigraphy at sequence-bounding unconformities: some principles derived from Holocene and Cretaceous examples ,in: D. Nummedal, O.H. Pilkey, J.D. Howard (Eds.), Sea-Level Fluctuation and Coastal Evolution, SEPM Special Publication, vol. 41, pp. 241–260

Sherrod, D. R., and Tosdal, R. M., 1991, Geologic setting and Tertiary structural evolution of southwestern Arizona and southeastern California: Journal of Geophysical Research: Solid Earth (1978–2012), v. 96, p. 12407–12423.

Spencer, J.E., and Patchett, P.J., 1997, Sr isotope evidence for a lacustrine origin for the upper Miocene to Pliocene Bouse Formation, lower Colorado River trough, and implications for timing of Colorado Plateau uplift: Geological Society of America Bulletin, v. 109, p. 767–778, doi:10.1130/0016-7606(1997)109<0767:SIEFAL>2.3.CO;2.

Spencer, J.E., Pearthree, P.A., and House, P.K., 2008, An evaluation of the evolution of the latest Miocene to earliest Pliocene Bouse lake system in the lower Colorado River valley, southwestern USA: Geological Society of America. Special Paper, v. 439, p. 375–390.

Spencer, J.E., Patchett, P.J., Pearthree, P.A., House, P.K., Sarna-Wojcicki, A.M., Wan, E., Roskowski, J.A., and Faulds, J.E., 2013, Review and analysis of the age and origin of the Pliocene Bouse Formation, lower Colorado River Valley, southwestern USA: Geosphere, v. 9, p. 444–459, doi:10.1130/GES00896.1.

Turak, J., 2000, Re-evaluation of the MiocenePliocene depositional history of the Bouse Formation, Colorado River trough, southern Basin and Range (CA, NV, and AZ)[MS thesis]: Laramie, University of Wyoming, 96 p.

Williams, G.E., 1989, Late Precambrian tidal rhythmites in South Australia and the history of the Earth's rotation: Journal of the Geological Society, v. 146, p. 97–111, doi:10.1144/gsjgs.146.1.0097.

Williams, G.E., 2000, Geological constraints on the Precambrian history of Earth's rotation and the Moon's orbit: Reviews of Geophysics, v. 38, p. 37–59, doi:10.1029/1999RG900016.

Chapter Three

Ainsworth, R.B., Hasiotis, S.T., Amos, K.J., Krapf, C.B., Payenberg, T.H., Sandstrom, M.L., Vakarelov, B.K., and Lang, S.C., 2012, Tidal signatures in an intracratonic playa lake: Geology, v. 40, p. 607–610, doi:10.1130/G32993.1.

Anastas, A. S., Dalrymple, R. W., James, N. P., and Nelson, C. S., 1997, Cross-stratified calcarenites from New Zealand: subaqueous dunes in a cool-water, Oligo-Miocene seaway: Sedimentology, v. 44, no. 5, p. 869-891.

Bartley, J. M., and Glazner, A. F., 1991, En echelon Miocene rifting in the southwestern United States and model for vertical-axis rotation in continental extension: Geology, v. 19, no. 12, p. 1165-1168.

Bennett, S.E.K., Darin, M.H., Dorsey, R.J., Skinner, L.A., Umhoefer, P.J., and Oskin, M.E., 2016, Animated tectonic reconstruction of the Lower Colorado River region: implications for Late Miocene to Present deformation. In: Reynolds, R.E.

(Ed.), 2016 Desert Symposium Field Guide and Proceedings, California State University Desert Studies Center, Zzyzx, CA, p. 73-86.

Boothroyd, J. C., 1985, Tidal inlets and tidal deltas, Coastal sedimentary environments, Springer, p. 445-532.

Bose, P. K., Mazumder, R., and Sarkar, S., 1997, Tidal sandwaves and related storm deposits in the transgressive Protoproterozoic Chaibasa Formation, India: Precambrian Research, v. 84, no. 1, p. 63-81.

Buising, A. V., 1990, The Bouse Formation and bracketing units, southeastern California and western Arizona: Implications for the evolution of the Proto-Gulf of California and the lower Colorado River: Journal of Geophysical Research: Solid Earth (1978–2012), v. 95, no. B12, p. 20111-20132.

Catuneanu, O., Abreu, V., Bhattacharya, J., Blum, M., Dalrymple, R., Eriksson, P., Fielding, C. R., Fisher, W., Galloway, W., and Gibling, M., 2009, Towards the standardization of sequence stratigraphy: Earth-Science Reviews, v. 92, no. 1, p. 1-33.

Chan, M. A., Kvale, E. P., Archer, A. W., and Sonett, C. P., 1994, Oldest direct evidence of lunar-solar tidal forcing encoded in sedimentary rhythmites, Proterozoic Big Cottonwood Formation, central Utah: Geology, v. 22, no. 9, p. 791-794.

Chiarella, D., and Longhitano, S., Sediments segregation rate as tool for discriminating depositional environments in ancient mixed (silici-/bioclastic) shallow-water marine system (Pliocene, Southern Apennines, Italy)[abstract], *in* Proceedings Abstracts2009, p. 469.

Chiarella, D., 2011, Sedimentology of Pliocene-Pleistocene mixed (lithoclastic-bioclastic) deposits in southern Italy (Lucanian Apennine and Calabrian Arc): depositional processes and palaeogeographic frameworks: Unpubl. Doctoral dissertation, University of Basilicata, Potenza, Italy.

Chiarella, D., and Longhitano, S. G., 2012, Distinguishing Depositional Environments In Shallow-Water Mixed, Bio-Siliciclastic Deposits On the Basis Of The Degree Of Heterolithic Segregation (Gelasian, Southern Italy): Journal of Sedimentary Research, v. 82, no. 12, p. 969-990.

Dalrymple, R. W., Knight, R., Zaitlin, B. A., and Middleton, G. V., 1990, Dynamics and facies model of a macrotidal sand-bar complex, Cobequid Bay—Salmon River Estuary (Bay of Fundy): Sedimentology, v. 37, no. 4, p. 577-612.

Dalrymple, R. W., Makino, Y., and Zaitlin, B. A., 1991, Temporal and spatial patterns of rhythmite deposition on mud flats in the macrotidal Cobequid Bay-Salmon River estuary, Bay of Fundy, Canada.

Davis, G. A., and Lister, G., 1988, Detachment faulting in continental extension; perspectives from the southwestern US Cordillera: Geological Society of America Special Papers, v. 218, p. 133-160.

Davis, R.A., Jr., 2012, Tidal signatures and their preservation potential in stratigraphic sequences: Principles of tidal sedimentology: Dordrecht, Springer, p. 35–55, doi:10.1007/978-94-007-0123-6_3.

De Boer, P. L., Oost, A. P., and Visser, M. J., 1989, The diurnal inequality of the tide as a parameter for recognizing tidal influences: Journal of Sedimentary Research, v. 59, no. 6, p. 912-921.

De Vries Klein, G., 1977, Clastic tidal facies, Continuing Education Publication Co, 149 p.

Deynoux, M., Duringer, P., Khatib, R., and (Miller, 2005 #578)Villeneuve, M., 1993, Laterally and vertically accreted tidal deposits in the Upper Proterozoic Madina—Kouta basin, southeastern Senegal, West Africa: Sedimentary geology, v. 84, no. 1-4, p. 179-188.

Di Stefano, A., and Longhitano, S. G., 2009, Tectonics and sedimentation of the Lower and Middle Pleistocene mixed siliciclastic/bioclastic sedimentary successions of the Ionian Peloritani Mts (NE Sicily, Southern Italy): the onset of opening of the Messina Strait: Central European Journal of Geosciences, v. 1, no. 1, p. 33-62.

Dorsey, R. J., and Becker, U., 1995, Evolution of a large Miocene growth structure in the upper plate of the Whipple detachment fault, northeastern Whipple Mountains, California: Basin Research, v. 7, no. 2, p. 151-163.

Dorsey, R. J., Fluette, A., McDougall, K., Housen, B. A., Janecke, S. U., Axen, G. J., and Shirvell, C. R., 2007, Chronology of Miocene–Pliocene deposits at Split Mountain Gorge, southern California: A record of regional tectonics and Colorado River evolution: Geology, v. 35, no. 1, p. 57-60.

Dorsey, R. J., Housen, B. A., Janecke, S. U., Fanning, C. M., and Spears, A. L., 2011, Stratigraphic record of basin development within the San Andreas fault system: Late Cenozoic Fish Creek–Vallecito basin, southern California: Geological Society of America Bulletin, v. 123, no. 5-6, p. 771-793.

Dorsey, R.J., O'Connell, B., Homan, M., and Howard, K.A., 2016a, Upper limestone of the southern Bouse Formation: evidence for unsteady origins of the Colorado River. In:Reynolds, R.E. (Ed.), 2016 Desert Symposium Field Guide and Proceedings, California State University Desert Studies Center, Zzyzx, CA, p. 145-153.

Dorsey, R.J., McDougall, K., O'Connell, B., Howard, K., Homan., M., Kaufmann, A., 2016b, Punctuated Sediment Discharge during the Early Evolution of the Colorado River: Evidence from Regional Stratigraphy and Sedimentology: Geological Society of America Abstracts with Programs, v. 48, no. 7.

Eisma, D., de Boer, P.L., Cadée, G.C., Dijkema, K., Philippart, C.J.M., and Ridderinkhof, H., 1998, Intertidal deposits: River mouths, tidal flats and coastal lagoons: Boca Raton, Florida, CRC Press, 544 p.

Eriksson, K. A., and Simpson, E. L., 2000, Quantifying the oldest tidal record: the 3.2 Ga Moodies Group, Barberton greenstone belt, South Africa: Geology, v. 28, no. 9, p. 831-834.

Eriksson, K., and Simpson, E., 2004, Precambrian tidalites: recognition and significance: The Precambrian Earth: Tempos and Events, v. 12, p. 631-641.

Fitzgerald, D. M., and Nummedal, D., 1983, Response characteristics of an ebb-dominated tidal inlet channel: Journal of Sedimentary Research, v. 53, no. 3.

Glazner, A. F., Walker, J. D., Bartley, J. M., and Fletcher, J. M., 2002, Cenozoic evolution of the Mojave block of southern California: Geologic evolution of the Mojave Desert and southwestern Basin and Range: Geological Society of America Memoir, v. 195, p. 19-41.

Gootee, B.F., Pearthree, P.A., House, P.K., Youberg, A., O'Connell, B., Bright, J. 2016a, A sequence-stratigraphic interpretation of the upper bioclastic unit capping the Bouse Formation in the Cibola Area, Arizona and California. In: Reynolds, R.E. (Ed.), 2016 Desert Symposium Field Guide and Proceedings, California State University Desert Studies Center, Zzyzx, CA, p. 154-159.

Gootee, B.F., Pearthree, P., House., P.K., O'Connell, B., Bright, J., A sequence stratigraphic interpretation of the Upper Bioclastic Unit Capping the Bouse Formation in the Cibola Area, Arizona and California: Geological Society of America Abstracts with Programs, v. 48, no. 7.

Homan, M. B., 2014, Sedimentology and Stratigraphy of the Miocene-Pliocene Bouse Formation near Cibola, Arizona and Milpitas Wash, California: Implications for the Early Evolution of the Colorado River: University of Oregon.

House, P. K., Pearthree, P. A., and Perkins, M. E., 2008, Stratigraphic evidence for the role of lake spillover in the inception of the lower Colorado River in southern Nevada and western Arizona: Geological Society of America Special Papers, v. 439, p. 335-353.

Howard, K. A., and Miller, D. M., 1992, Late Cenozoic faulting at the boundary between the Mojave and Sonoran blocks: Bristol Lake area, California: Deformation

associated with the Neogene, eastern California shear zone, southeastern California and southwestern Arizona, p. 92-91.

Jachens, R., and Howard, K., 1992, Bristol Lake basin—A deep sedimentary basin along the Bristol–Danby trough, Mojave Desert: Old Routes to the Colorado, p. 92-92.

Kreisa, R. D., and Moila, R. J., 1986, Sigmoidal tidal bundles and other tide-generated sedimentary structures of the Curtis Formation, Utah: Geological Society of America Bulletin, v. 97, no. 4, p. 381-387.

Laporte, L. F., 1971, Paleozoic carbonate facies of the central Appalachian shelf: Journal of Sedimentary Research, v. 41, no. 3.

Larsonneur, C., 1975, Tidal deposits, Mont Saint-Michel Bay, France, Tidal deposits, Springer, p. 21-30.

Lisiecki, L. E., and Raymo, M. E., 2005, A Pliocene‐Pleistocene stack of 57 globally distributed benthic δ18O records: Paleoceanography, v. 20, no. 1.

Longhitano, S. G., 2011, The record of tidal cycles in mixed silici–bioclastic deposits: examples from small Plio–Pleistocene peripheral basins of the microtidal Central Mediterranean Sea: Sedimentology, v. 58, no. 3, p. 691-719.

Longhitano, S.G., Mellere, D., Steel, R.J., and Ainsworth, R.B., 2012, Tidal depositional systems in the rock record: A review and new insights: Sedimentary Geology, v. 279, p. 2–22, doi:10.1016/j.sedgeo.2012.03.024.

Longhitano, S. G., Chiarella, D., and Muto, F., 2014, Three-dimensional to two-dimensional cross-strata transition in the lower Pleistocene Catanzaro tidal strait transgressive succession (southern Italy): Sedimentology, v. 61, no. 7, p. 2136-2171.

Mazumder, R., 2004, Implications of lunar orbital periodicity from the Chaibasa tidal rhythmite (India) of late Paleoproterozoic age: Geology, v. 32, no. 10, p. 841-844.

McDougall, K., 2008, Late Neogene marine incursions and the ancestral Gulf of California: Geological Society of America Special Papers, v. 439, p. 355-373.

McDougall, K., and Martínez, A. Y. M., 2014, Evidence for a marine incursion along the lower Colorado River corridor: Geosphere, p. GES00975. 00971.

McDougall, K., and Martínez, A. Y. M., 2016a, Bouse Formation along the lower Colorado River corridor: tracking the transition from marine estuary to saline lake In: Reynolds, R.E. (Ed.), 2016 Desert Symposium Field Guide and Proceedings, California State University Desert Studies Center, Zzyzx, CA, p. 140-144.

McDougall, K., and Martínez, A. Y. M., 2016b, Bouse Formation along the lower Colorado River corridor: transition from marine estuary to saline lake: Geological Society of America Abstracts with Programs, v. 48, no. 7, doi:10.1130/abs/2016AM-286483.

Miller, K. G., Kominz, M. A., Browning, J. V., Wright, J. D., Mountain, G. S., Katz, M. E., Sugarman, P. J., Cramer, B. S., Christie-Blick, N., and Pekar, S. F., 2005, The Phanerozoic record of global sea-level change: science, v. 310, no. 5752, p. 1293-1298.

Mueller, W., Corcoran, P., and Donaldson, J., 2002, Sedimentology of a tide-and wave-influenced high-energy Archaean coastline: the Jackson Lake Formation, Slave Province, Canada: Precambrian Sedimentary Environments–A Modern Approach to Ancient Depositional Systems, v. 3, p. 153-182.

Nielson, J. E., and Beratan, K. K., 1995, Stratigraphic and structural synthesis of a Miocene extensional terrane, southeast California and west-central Arizona: Geological Society of America Bulletin, v. 107, no. 2, p. 241-252.

Nio, S.D., and Yang, C.S., 1991, Diagnostic attributes of clastic tidal deposits: A review, in Smith, D.G., et al., eds., Clastic tidal sedimentology: Canadian Society of Petroleum Geologists Memoir 16, p. 3–28.

O'Connell, B., Dorsey, R.J., Humphreys, E.D., in press, Tidal Rhythmites in the Southern Bouse Formation as Evidence for Post-Miocene Uplift of the Lower Colorado River Corridor.

Posamentier, H. W., and Allen, G. P., 1999, Siliciclastic sequence stratigraphy: concepts and applications, SEPM (Society for Sedimentary Geology) Tulsa.

Prager, E. J., Southard, J. B., and Vivoni-Gallart, E. R., 1996, Experiments on the entrainment threshold of well-sorted and poorly sorted carbonate sands: Sedimentology, v. 43, no. 1, p. 33-40.

Pugh, D., 1987, Tides, surges and mean sea-level: a handbook for engineers and scientists, 472 pp, John Wiley, Chichester, UK.

Raymo, M. E., Hearty, P., De Conto, R., O'Leary, M. J., Dowsett, H., Robinson, M., and Mitrovica, J., 2009, PLIOMAX: Pliocene maximum sea level project: Pages news, v. 17, no. 2.

Richard, S. M., 1993, Palinspastic reconstruction of southeastern California and southwestern Arizona for the middle Miocene: Tectonics, v. 12, no. 4, p. 830-854.

Ricketts, J. W., Girty, G. H., Sainsbury, J. S., Muela, K. K., Sutton, L. A., Biggs, M. A., and Voyles, E. M., 2011, Episodic Growth of the Chocolate Mountains Anticlinorium Recorded By the Neogene Bear Canyon Conglomerate, Southeastern California, USA: Journal of Sedimentary Research, v. 81, no. 12, p. 859-873.

Shelef, E., and Oskin, M., 2010, Deformation processes adjacent to active faults: Examples from eastern California: Journal of Geophysical Research: Solid Earth, v. 115, no. B5.

Sherrod, D. R., and Tosdal, R. M., 1991, Geologic setting and Tertiary structural evolution of southwestern Arizona and southeastern California: Journal of Geophysical Research: Solid Earth (1978–2012), v. 96, no. B7, p. 12407-12423.

Spencer, J. E., and Reynolds, S. J., 1989, Middle Tertiary tectonics of Arizona and adjacent areas: Geologic evolution of Arizona: Arizona Geological Society Digest, v. 17, p. 539-574.

Spencer, J. E., Pearthree, P. A., and House, P. K., 2008, An evaluation of the evolution of the latest Miocene to earliest Pliocene Bouse lake system in the lower Colorado River valley, southwestern USA: Geological Society of America Special Papers, v. 439, p. 375-390.

Spencer, J. E., Patchett, P. J., Pearthree, P. A., House, P. K., Sarna-Wojcicki, A. M., Wan, E., Roskowski, J. A., and Faulds, J. E., 2013, Review and analysis of the age and origin of the Pliocene Bouse Formation, lower Colorado River Valley, southwestern USA: Geosphere, v. 9, no. 3, p. 444-459.

Sztano, O., and Boer, P. L., 1995, Basin dimensions and morphology as controls on amplification of tidal motions (the Early Miocene North Hungarian Bay): Sedimentology, v. 42, no. 4, p. 665-682.

Tape, C. H., Cowan, C. A., and Runkel, A. C., 2003, Tidal-bundle sequences in the Jordan Sandstone (Upper Cambrian), southeastern Minnesota, USA: evidence for tides along inboard shorelines of the Sauk epicontinental sea: Journal of Sedimentary Research, v. 73, no. 3, p. 354-366.

Tessier, B., Archer, A., Laniere, W., and Feldman, H., 2009, Comparison of ancient tidal rhythmites (Carboniferous of Kansas and Indiana, USA) with modern analogues: Tidal Signatures in Modern and Ancient Sediments (Special Publication 24 of the IAS), v. 28, p. 259.

Van Wagoner, J. C., Mitchum, R., Campion, K., and Rahmanian, V., 1990, Siliciclastic sequence stratigraphy in well logs, cores, and outcrops: concepts for high-resolution correlation of time and facies.

Visser, M., 1980, Neap-spring cycles reflected in Holocene subtidal large-scale bedform deposits: a preliminary note: Geology, v. 8, no. 11, p. 543-546.

Williams, G. E., 1989, Late Precambrian tidal rhythmites in South Australia and the history of the Earth's rotation: Journal of the Geological Society, v. 146, no. 1, p. 97-111.

Williams, G. E., 2000, Geological constraints on the Precambrian history of Earth's rotation and the Moon's orbit: Reviews of Geophysics, v. 38, no. 1, p. 37-59.

Appendix A

Adkins, R.M., and Eriksson, K.A., 1998, Rhythmic sedimentation in a mid-Pennsylvanian delta front succession, Four Corners Formation (Breathitt Group), east- ern Kentucky: A near complete record of daily, semi-monthly and monthly tidal periodicities, in Alexander, C.B., et al., eds., Tidalites: Processes and products: SEPM (Society for Sedimentary Geology) Special Publication 61, p. 85–94.

Archer, A. W., 1994, Extraction of sedimentological information via computer-based image analyses of gray shales in carboniferous coal-bearing sections of Indiana and Kansas, USA: Mathematical geology, v. 26, no. 1, p. 47-65.

Archer, 1995, Modeling of cyclic tidal rhythmites based on a range of diurnal to semidiurnal tidal-station data: Marine Geology, v. 123, no. 1, p. 1-10.

Beran, J., 1994, Statistics for long-memory processes: Chapman and Hall, New York, CRC press, 144 pp.

Boothroyd, J. C., 1985, Tidal inlets and tidal deltas, in Davis, R.A., ed., Coastal sedimentary environments: New York, Springer, p. 445-532.

Bose, P. K., Mazumder, R., and Sarkar, S., 1997, Tidal sandwaves and related storm deposits in the transgressive Protoproterozoic Chaibasa Formation, India: Precambrian Research, v. 84, no. 1, p. 63-81.

Chan, M. A., Kvale, E. P., Archer, A. W., and Sonett, C. P., 1994, Oldest direct evidence of lunar-solar tidal forcing encoded in sedimentary rhythmites, Proterozoic Big Cottonwood Formation, central Utah: Geology, v. 22, no. 9, p. 791-794.

De Boer, P. L., Oost, A. P., and Visser, M. J., 1989, The diurnal inequality of the tide as a parameter for recognizing tidal influences: Journal of Sedimentary Research, v. 59, no. 6, p. 912-921.

Deynoux, M., Duringer, P., Khatib, R., and Villeneuve, M., 1993, Laterally and vertically accreted tidal deposits in the Upper Proterozoic Madina—Kouta basin, southeastern Senegal, West Africa: Sedimentary geology, v. 84, no. 1-4, p. 179-188.

Eriksson, K., and Simpson, E., 2004, Precambrian tidalites: recognition and significance: The Precambrian Earth: Tempos and Events, v. 12, p. 631-641.

Eriksson, K. A., and Simpson, E. L., 2000, Quantifying the oldest tidal record: the 3.2 Ga Moodies Group, Barberton greenstone belt, South Africa: Geology, v. 28, no. 9, p. 831-834.

FitzGerald, D. M., and Nummedal, D., 1983, Response characteristics of an ebb-dominated tidal inlet channel: Journal of Sedimentary Research, v. 53, no. 3.

Granger, C. W., and Joyeux, R., 1980, An introduction to long-memory time series models and fractional differencing: Journal of time series analysis, v. 1, no. 1, p. 15-29.

Kreisa, R. D., and Moila, R. J., 1986, Sigmoidal tidal bundles and other tide-generated sedimentary structures of the Curtis Formation, Utah: Geological Society of America Bulletin, v. 97, no. 4, p. 381-387.

Kvale, E.P. 2006, The origin of neap-spring tidal cycles: Marine Geology, v. 235, no.1, p. 5-18

Longhitano, S. G., 2011, The record of tidal cycles in mixed silici–bioclastic deposits: examples from small Plio–Pleistocene peripheral basins of the microtidal Central Mediterranean Sea: Sedimentology, v. 58, no. 3, p. 691-719.

Marinone, S.G., 1997, Tidal residual currents in the Gulf of California: Is the M2 tidal constituent sufficient to induce them?, J. Geophys. Res., v. 102, p. 611-8623.

Mazumder, R., 2004, Implications of lunar orbital periodicity from the Chaibasa tidal rhythmite (India) of late Paleoproterozoic age: Geology, v. 32, no. 10, p. 841-844.

Mueller, W., Corcoran, P., and Donaldson, J., 2002, Sedimentology of a tide-and wave-influenced high-energy Archaean coastline: the Jackson Lake Formation, Slave Province, Canada: Precambrian Sedimentary Environments–A Modern Approach to Ancient Depositional Systems, v. 3, p. 153-182.

Tape, C. H., Cowan, C. A., and Runkel, A. C., 2003, Tidal-bundle sequences in the Jordan Sandstone (Upper Cambrian), southeastern Minnesota, USA: evidence for tides along inboard shorelines of the Sauk epicontinental sea: Journal of Sedimentary Research, v. 73, no. 3, p. 354-366.

Visser, M., 1980, Neap-spring cycles reflected in Holocene subtidal large-scale bedform deposits: a preliminary note: Geology, v. 8, no. 11, p. 543-546.

Williams, G. E., 1989, Late Precambrian tidal rhythmites in South Australia and the history of the Earth's rotation: Journal of the Geological Society, v. 146, no. 1, p. 97-111.

Williams, G. E., 2000, Geological constraints on the Precambrian history of Earth's rotation and the Moon's orbit: Reviews of Geophysics, v. 38, no. 1, p. 37-59.